# The nature of kinematic structures in the Galactic disc

Kushniruk, Iryna

2020

*Document Version:*
Publisher's PDF, also known as Version of record

# The nature of kinematic structures in the Galactic disc

IRYNA KUSHNIRUK
DEPT. OF ASTRONOMY AND THEORETICAL PHYSICS | LUND UNIVERSITY 2020

Printed by Media-Tryck, Lund 2020 NORDIC SWAN ECOLABEL 3041 0903

Faculty of Science
Department of Astronomy
and Theoretical Physics

ISBN 978-91-7895-482-7

# The nature of kinematic structures in the Galactic disc

Iryna Kushniruk


LUND
UNIVERSITY

Thesis for the degree of Doctor of Philosophy

Thesis advisors: Dr. Thomas Bensby, Prof. Sofia Feltzing
Faculty opponent: Dr. Ricardo Schiavon

To be presented, with the permission of the Faculty of Science of Lund University, for public criticism in the Lundmark lecture hall (Lundmarksalen) at the Department of Astronomy and Theoretical Physics on Friday 6th of November 2020 at 09:00.

| Organization | Document name |
|---|---|
| LUND UNIVERSITY<br>Department of Astronomy and Theoretical Physics<br>Box 43<br>SE-221 00 Lund, Sweden | DOCTORAL DISSERTATION |
| | Date of issue<br>06 November 2020 |
| | Sponsoring organization |
| Author(s)<br>Iryna Kushniruk | |


Title and subtitle

The nature of kinematic structures in the Galactic disc


Abstract

The velocity distribution of stars in the Galactic disc is complex and consists of a vast number of kinematic structures, that is, stars that share similar velocity components. The reasons why some stars move together may be different and are related to dynamical processes connected to the Galaxy, both internal as well as external ones, such as resonances with the Galactic bar or the Galactic spiral arm structure, dissolution of open clusters, or merger events with other galaxies. Therefore, studies of kinematic structures of the Galactic disc may provide information about the formation and evolution history of the Milky Way.

In this thesis we focus on detecting and chemo-dynamical characterisation of kinematic structures of the Galactic disc using the most recent and up-to-date astrometric, spectroscopic, and photometric surveys. In Paper I we studied kinematic structures in the solar neighbourhood with the wavelet transform method. In Paper II and Paper III we studied origin of the Arcturus stream and HR 1614 moving group respectively by studying chemo-dynamical properties of the structures.

The result of Paper I is the detection of old and well-known kinematic groups together with three new velocity structures. The results of Paper II and Paper III show that both the Arcturus and the HR 1614 structures are composed of thin and thick disc stars and are not dissolved open clusters or accreted stellar populations. We conclude that the origin of kinematic structures is complex and might be a combination of several dynamical processes such as resonances and phase mixing.



Key words:

Galaxy: evolution, Galaxy: solar neighbourhood, Stars: kinematics and dynamics

Classification system and/or index termes (if any):

| Supplementary bibliographical information: | | Language<br>English |
|---|---|---|
| ISSN and key title: | | ISBN<br>978-91-7895-482-7 (print)<br>978-91-7895-483-4 (pdf) |
| Recipient's notes | Number of pages<br>116 | Price |
| | Security classification | |

# The nature of kinematic structures in the Galactic disc

Iryna Kushniruk


LUND
UNIVERSITY

**Faculty Opponent**

Dr. Ricardo Schiavon
Liverpool John Moores University
Liverpool, United Kingdom

**Evaluation Committee**

Dr. Giacomo Beccari
European Southern Observatory
Garching, Germany

Dr. Paola Di Matteo
Observatoire de Paris-Meudon
Paris, France

Dr. Lise Christensen
University of Copenhagen
Copenhagen, Denmark

**Cover:** The pattern is created of the velocity distribution of nearby stars in the radial and azimuthal directions. These structures were revealed by applying a wavelet transform to stars from the *Gaia* DR2 catalogue.



Faculty of Science , Department of Astronomy and Theoretical Physics
ISBN: 978-91-7895-482-7 (print)
ISBN: 978-91-7895-483-4 (pdf)

Printed in Sweden by Media-Tryck, Lund University, Lund 2020

*Dedicated to my Koala & Whales*

# Contents

# List of publications

This thesis is based on the following publications:

1 **Kinematic structures of the solar neighbourhood revealed by *Gaia* DR1/TGAS and RAVE**

**I. Kushniruk**, T. Schirmer, T. Bensby (2017)
Astronomy & Astrophysics, vol. 608, A73 (19 p.)

2 **Disentangling the Arcturus stream**

**I. Kushniruk**, T. Bensby (2019)
Astronomy & Astrophysics, vol. 631, A47 (18 p.)

3 **The HR 1614 moving group is not a dissolving cluster**

**I. Kushniruk**, T. Bensby, S. Feltzing, C. Sahlholdt, L. Casagrande, D. Feuillet (2020)
Astronomy & Astrophysics, vol. 638, A154 (11 p.)

# Popular summary

How galaxies form and evolve is one of the fundamental questions of modern astrophysics. The information encrypted in the properties of stars such as elemental abundances, stellar ages, and orbital parameters are useful for characterising stellar populations and testing hypotheses of galaxy formation. The Milky Way plays a key role in this aspect as it provides a unique possibility to study individual stars in a detail that is not possible to do for stars in other galaxies. Although significant progress has been made in understanding the structure and evolution of the Milky Way, many pieces of information are still lacking before we can disentangle the complete history of the Galaxy.

Our current view on the Milky Way is that it is a barred spiral galaxy with a complex structure of different stellar populations. The Galactic bulge, the bar, the thin and thick discs, and the stellar halo are its major large-scale stellar components. The stars associated with each component differ on average in their chemical and kinematic properties, although the properties are often overlapping, making it difficult to distinguish them and fully characterise their properties. In addition, it has been found that the Milky Way contains a complex plethora of kinematic structures. These are groups of stars that for some reason share a common motion, meaning that they form overdensities in velocity space.

Although the origin of many kinematic groups are unknown and some widely debated, many of the known kinematic structures can be explained with one or several of the following hypotheses: dissolving star clusters; dynamical resonances between stars and the Galactic bar and/or spiral arms; extragalactic origin via merger events; or phase mixing due to galactic accretion events.

Therefore, one of the approaches to try to understand the detailed structure of the Milky Way has been to search for and characterise such kinematic structures. A combination of observations such as the kinematic properties of stars in the groups with their elemental abundances and ages serves as a test bed for the-

oretical models of the kinematic structures. Nowadays, when we have access to high-precision astrometric data for billions of stars and detailed elemental abundances for hundred of thousands of stars, we have a golden opportunity to trace and characterise many old an uncertain, and also previously unknown, kinematic structures in the Milky Way.

The aim of this thesis is to search for kinematic structures in the Milky Way's disc and to study in detail the properties and the origin of some selected groups using large-scale astrometric and spectroscopic surveys. Our results have allowed us to discover a few new structures and confirm already known structures. Using advanced statistical methods, we detected dozens of kinematic groups in the solar neighbourhood and in the inner and outer parts of the Galactic disc. We also revised the origin of the Arcturus and the HR 1614 moving groups. In both cases we suggest that the groups were formed under the influence of a combination of dynamical processes caused by, for example, past accretion events, the Galactic bar, and the spiral arms, affecting the motions of the stars, forcing them to move together in space.

# Populärvetenskaplig sammanfattning

Hur galaxer bildas och utvecklas är en av de mest grundläggande frågorna i modern astrofysik. Informationen som finns krypterad i stjärnors egenskaper såsom kemisk sammansättning, ålder, och parametrar för omloppsbanor i galaxen är viktiga för att karakterisera stjärnpopulationer och testa hypoteser om hur galaxer bildas. Ur denna aspekt spelar Vintergatan en nyckelroll eftersom det ger oss en unik möjlighet att studera individuella stjärnor detalj, vilket inte är möjligt att göra för stjärnor i avlägsna galaxer. Även om det har gjorts betydande framsteg när det gäller att förstå Vintergatans struktur och utveckling, saknas det fortfarande många bitar innan vi har en komplett bild av dess historia.

Den mest aktuella bild vi har av Vintergatan är att det är en stavspiralgalax innehållande en komplex struktur av olika stjärnpopulationer. Den galaktiska bulgen, staven, de tunna och tjocka skivorna, och halon är de viktigaste storskaliga komponenterna. Stjärnorna som kan associeras med de olika komponenterna skiljer sig i allmänhet åt i sina kemiska och kinematiska egenskaper, men kan även överlappa vilket gör det svårt att särskilja dem och fullständigt karakterisera deras egenskaper. Det har dessutom visat sig att Vintergatan innehåller en mängd kinematiska strukturer. Dessa är grupper av stjärnor som av någon anledning har liknande rörelser, vilket gör att de bildar grupperingar i hastighetsrummet.

Även om ursprunget till många kinematiska strukturer är okänt och vissa debatteras, så kan de flesta antagligen förklaras med en eller flera av följande hypoteser: upplösning av stjärnhopar; resonanser mellan stjärnor och den galaktiska staven eller de galaktiska spiralarmarna; extragalaktiskt ursprung via kollisioner med andra galaxer; fasblandning på grund av att andra galaxer kolliderat och slagits samman med Vintergatan.

Därför har en av metoderna för att förstå Vintergatans detaljerade struktur

varit att söka efter, och karakterisera, sådana kinematiska strukturer. Genom att kombinera de kinematiska egenskaperna hos stjärnorna i grupperna med deras grundämnessammansättningar och åldrar så kan man skapa en testbädd för dynamiska modeller av hastighetsstrukturen i Vintergatan. Numera har vi tillgång till astrometrisk högprecisionsdata för miljarder stjärnor och detaljerade kemiska sammansättningar för hundratusentals stjärnor. Detta ger oss ett gyllene tillfälle att spåra och karakterisera många gamla, och kanske osäkra, och även tidigare okända, kinematiska strukturer i Vintergatan.

Syftet med denna avhandling är att söka efter kinematiska strukturer i Vintergatans skiva och att i detalj studera deras egenskaper och ursprung med hjälp av data från storskaliga astrometriska och spektroskopiska undersökningar. Vi har upptäckt några nya grupper och bekräftat redan kända strukturer. Med hjälp av avancerade statistiska metoder upptäckte vi dussintals kinematiska grupper i solens närhet och i de inre och yttre delarna av den galaktiska skivan. För Arcturusströmmen och HR 1614, som är två kinematiska grupper, så reviderade vi deras ursprung och förslår att de bildats genom dynamisk påverkan av vintergatans stav och spiralarmar, och tidigare kollisioner mellan vintergatan och andra galaxer som har påverkat hastighetsstrukturen. Därav har stjärnorna tvingats in i grupperingar som rör sig med liknande hastigheter.

# Chapter 1

# Introduction

Today we know that the Milky Way is a barred spiral galaxy which has a complex stellar structure and consists of three major components: the Galactic bulge, the disc, and the stellar halo. Each structural component has its own formation history, which has led to significant differences in their kinematic, chemical, and morphological properties (e.g. Bland-Hawthorn & Gerhard 2016).

The Galactic bulge has a boxy/peanut shape and contains the Galactic bar (e.g. Portail et al. 2017). The metallicity[1] distribution of bulge stars is wide and may have up to five peaks including that it may consist of multiple stellar populations (e.g. Ness et al. 2013; Bensby et al. 2017). Today it is commonly thought that a large fraction of the Galactic bulge stars formed from disc material (e.g. Portail et al. 2017).

The Galactic disc has two components known as the thin and the thick discs, and there are at least four different ways to define them. The disc can be split into two sequences by morphology, kinematics, chemical composition, or ages of the stars (e.g. Martig et al. 2016). The first notion about the thick disc comes from Gilmore & Reid (1983), who defined it morphologically. They found that the vertical density distribution of stars in the Galactic disc had to be fitted with two exponential functions, rather than one, with different scale-heights. In terms of chemical composition and age the thin disc is metal-rich, $\alpha$-poor[2], and old, while the opposite holds for the thick disc (e.g. Haywood et al. 2013; Bensby et al. 2014).

[1] In astronomy the term 'metals' usually refers to all elements heavier than helium. However, here the term 'metallicity' refers to the amount of iron in a star.

[2] By $\alpha$ we mean elements which are produced in stars by adding helium nuclei, for example Si, Mg, Ca, and Ti.

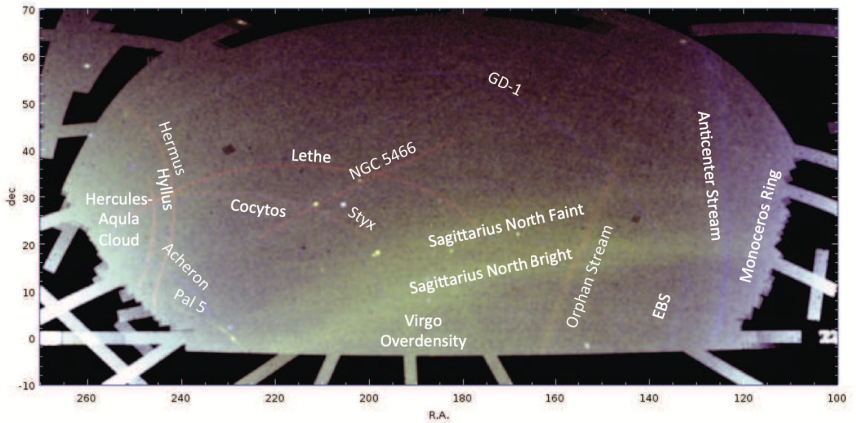


Figure 1.1: Stellar streams across the northern sky as seen with the Sloan Digital Sky Survey. The figure is taken from Grillmair & Carlin (2016) and is reprinted by permission from Springer Nature.

Similar properties of the high- and low-$\alpha$ sequences are observed not just in the solar vicinity, but across a wide range of Galactocentric radii (e.g. Bensby et al. 2011; Hayden et al. 2015; Queiroz et al. 2020).

The stellar halo is a spheroidal component which contains just about one percent of the total stellar mass of the Milky Way. Even though its stellar density is very low, it is an important part of the Galaxy that can help us to trace the merger history of the Milky Way. Our Galaxy is surrounded by satellite dwarf galaxies, and thus, occasionally undergoes tidal interactions. The Sagittarius stream, discovered by Ibata et al. (1994), is undeniable evidence of an ongoing merger event. Today we know that the stellar halo has a complex structure and has formed through multiple mergers. Figure 1.1 shows the large number of stellar streams that were discovered with the Sloan Digital Sky Survey (York et al. 2000) including the Sagittarius stream. Among the most recent discoveries of accreted stellar populations are the remnants of the Gaia-Enceladus-Sausage and Gaia-Sequoia dwarf galaxies that probably merged with the Milky Way about ten billion years ago (Belokurov et al. 2018; Helmi et al. 2018; Myeong et al. 2019). Smaller halo streams can be found in the solar vicinity. For example, Helmi et al. (1999) showed that up to 500 halo streams cross the solar neighbourhood. Such streams can be traced in velocity spaces. It is therefore important to study velocity distributions of nearby

stars as well.

Due to the dynamical influence of the large-scale internal components of the Milky Way and its neighbouring dwarf galaxies not only the Galactic halo contains stellar streams. The Galactic disc shows a rich structure in velocity space and one of the first evidences that the velocity distribution of disc stars is not smooth is the discovery of the Pleiades and Hyades moving groups in the middle of the 19th century. Further findings such as the moving groups discovered by Olin J. Eggen, also suggested a complex velocity distribution in the solar neighbourhood (e.g. Eggen 1971, 1992, 1998).

Studies of the velocity distribution of the stars in the local Galactic disc were boosted by the data release of the Hipparcos mission, which provided a high-precision catalogue of astrometric measurements for more than 100 000 stars (Perryman et al. 1997). Figure 1.2 shows kinematic structures detected by Dehnen (1998) using Hipparcos data. It shows that the local velocity distribution is much more complex than a Gaussian distribution with the moving groups forming a rich branch-like structure in velocity space (e.g. Skuljan et al. 1999). This was later confirmed by Antoja et al. (2008) who analysed the local velocity distribution using the wavelet transform method. The analyses of stars in these branches showed them to have a wide spread of metallicities, questioning the dissolving open cluster origin for such streams.

Kinematic structures in the Galactic disc is not just a local phenomenon, they are also present outside the solar neighbourhood (e.g. Antoja et al. 2012). Analyses of data from *Gaia* DR2 have revealed a rich structure in the velocity distribution across a wide range of Galacticentric radii (e.g. Gaia Collaboration et al. 2018b). For instance, Antoja et al. (2018) and Ramos et al. (2018) showed that kinematic groups form arches in the radial and azimuthal directions, and form ridge-like structures when exploring groups across the Galactic disc. Figure 1.3 shows an example of the kinematic structures detected with *Gaia* DR2 (Gaia Collaboration et al. 2018b). In addition, Antoja et al. (2018) discovered a phase-space spiral which could be evidence of an ongoing phase mixing induced by the merger event with the Sagittarius dwarf galaxy.

Today there is a variety of numerical models that are able to reproduce the observed velocity distribution in the solar neighbourhood. For example, Hunt et al. (2019) show that phase mixing induced by a combined effect of various transient spiral arms and the Galactic bar can explain the observed velocity distribution. Khanna et al. (2019) show that phase mixing induced by internal as well as external mechanisms can reproduce the ridges and arches observed in the

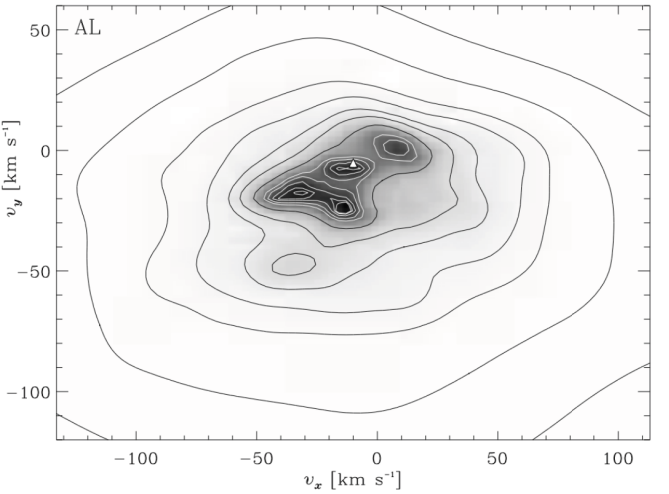


Figure 1.2: Velocity distribution of stars in the solar neighbourhood seen with Hipparcos. $v_x$ and $v_y$ denote radial and azimuthal motion of stars. The figure is adopted from Dehnen (1998). ©AAS. Reproduced with permission.

disc. Velocity structures were reproduced by simulations performed by Laporte et al. (2019), who modelled the interaction of the Milky Way with the Sagittarius dwarf galaxy. Hunt & Bovy (2018) showed that resonances with the bar can also reproduce many structures.

The availability of a wide range of models leads us to the question of how many and which processes have actually contributed to the formation of the today observed velocity distribution of stars in the Galactic disc. To answer these questions we need to detect kinematic structures at high precision and characterise them chemically. Unlike the kinematic and orbital parameters of stars in the Galactic disc which are often influenced by the secular dynamical processes, the stellar chemical composition varies less with time (Freeman & Bland-Hawthorn 2002). Therefore, information about the chemical composition of stars is a long-term parameter which allows us to study if stars within a kinematic group have a common origin (Freeman & Bland-Hawthorn 2002).

This thesis is focused on studying kinematic structures, that is, overdensities in velocity space, as a way to understand the formation and evolution history of the Milky Way. The aim of this thesis is to study velocity distribution of stars with the

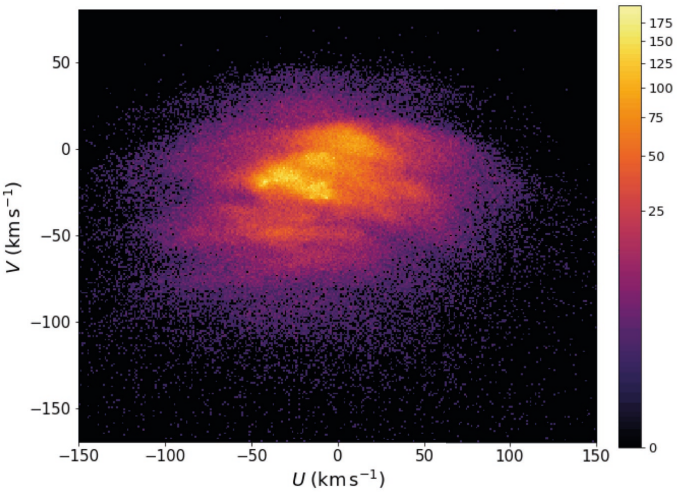


Figure 1.3: Velocity distribution of nearby stars seen with *Gaia* DR2. $U$ and $V$ denote velocities in the radial and azimuthal directions. The figure is adopted from Gaia Collaboration et al. (2018b). ©ESO. Reproduced with permission.

most up-to-date large-scale surveys in order to discover new kinematic structures and study their chemo-kinematic properties in great detail to better understand the structure of the Milky Way.

# Chapter 2

# The origin of kinematic structures

Nowadays there are four main hypotheses that are widely discussed in the literature to explain the origin of kinematic structures seen in the Galactic disc.

## 2.1 Dissolving open clusters

Stars form in clusters from the same interstellar gas cloud. Most star clusters dissolve with time, and this leads to the formation of so-called stellar moving groups. Stars in such groups share similar chemo-dynamical properties, since they have a common origin, but are usually spread all over the sky. The idea of dissolving stellar clusters was the first theory to explain the origin of kinematic structures and was first proposed in Eggen (1965). The stars in such kinematic structures should then be chemically homogeneous and have approximately the same age. A detailed age and elemental abundance analysis of stars in the moving group can tell us if the structure truly is a dissolved stellar cluster or not.

## 2.2 Resonant origin

The presence of large-scale density waves, caused by, for example, the Galactic bar and the spiral arms, influences the movement of stars in the Galactic disc through resonances. The main resonances are called the co-rotation resonance and the inner and outer Lindblad resonances. Stars trapped by these resonances will form overdensities in velocity space.

The co-rotation resonance occurs when the angular velocity of a star, $\Omega$, is equal to the angular velocity of the bar or spiral structure, $\Omega_b$. The Lindblad res-

onance occurs when the orbit's epicyclic frequency, $k$, is a multiple of the forcing frequency encountered by a star[1]. Depending on if the orbit's epicyclic motion overtakes or lags the forcing frequency, the system is in the inner Lindblad resonance and the outer Lindblad resonance, respectively (e.g. Minchev 2016). Stars in the kinematic groups caused by resonances will be from the general disc stellar populations and usually show chemical and kinematic properties similar to what is observed for the Galactic thin and thick discs.

## 2.3 Accretion origin

Numerical simulations of the Milky Way show that our Galaxy may have formed through a great number of merger events (e.g. Renaud et al. 2020). The discovery of the Sagittarius stream (Ibata et al. 1994) and recently debris of the massive Gaia-Enceladus-Sausage galaxy (Belokurov et al. 2018; Helmi et al. 2018) support this picture. In addition to this large-scale merger debris, we have today the possibility to observe dozens of remnants of minor accretion events like the Sequoia galaxy (Myeong et al. 2019) or the Helmi streams (Helmi et al. 1999). Some halo streams are also present even in the solar neighbourhood. Even though they are already strongly phase-mixed, it is possible to find them in velocity space (Helmi et al. 1999).

An additional way to study accreted stellar populations is to examine stellar chemical compositions. Stars in accreted structures were formed outside our Galaxy in gaseous environments such as dwarf galaxies which might have had different chemical enrichment histories and therefore have different elemental abundance pattern from those observed in the Milky Way (e.g. Venn et al. 2004). Hence, it should be possible to trace accreted stellar populations using the chemical compositions and ages of stars.

## 2.4 Phase mixing

The Galactic bar, the spiral structure, and nearby dwarf satellite galaxies can dynamically heat the Galactic disc, causing velocity overdensities. As shown in numerical simulations by Minchev et al. (2009), the result of a merger event that happened about two billion years ago can be seen in the velocity space as a wave with

[1]The epicyclic frequency is the frequency of an orbit's radial motion. The forcing frequency is the frequency at which a star encounters the forcing from the Galactic bar or spiral arms and it can be expressed as $\Omega - \Omega_b$.

streams appearing separated by a fixed step in azimuthal velocity. Later, this idea was confirmed with the discovery of a phase-space spiral, arches, and ridges in various velocity spaces by Antoja et al. (2018). Numerical simulations performed by Antoja et al. (2018) suggest that the Galactic disc was likely perturbed by the passage of the Sagittarius dwarf galaxy and a result of this interaction is the observed velocity distribution. The external perturbation origin of the observed phase-space spiral is also favoured in a number of papers studying the origin of nearby velocity groups (e.g. Laporte et al. 2019; Bland-Hawthorn et al. 2019). However, some studies show that, in addition to external mechanisms, the observed phase-space features can also be successfully reproduced by internal dynamical processes that are related to the Galactic bar and spiral arms (e.g. Khanna et al. 2019; Hunt et al. 2019). Currently there is no unique solution to explain the complexity of the observed velocity distribution.

## 2.5 Examples of kinematic structures with different origins

Visible to the naked eye, the Pleiades and the Hyades moving groups have for a long time been known as classical examples of dissolved open clusters. However, during the past few decades, their pure cluster origins have been questioned. For example, Famaey et al. (2008) investigated if stars in the Pleiades and the Hyades moving groups follow single-age isochrones as can be expected for stars from open clusters. They found that only about half of the stars in these moving groups follow the isochrones with the age of the clusters and suggested that the moving groups could be due to dynamical resonances. A similar result comes from a detailed elemental abundance analysis of stars in the Hyades moving group performed by Pompéia et al. (2011). Because of the large scatter in elemental abundances, they favour a dynamical origin of the Hyades moving group. Numerical simulations of resonances in the Galactic disc performed by Minchev et al. (2010) show that the Pleiades, Hyades, Coma Berenices, and Sirius moving groups could be caused by internal dynamical processes such as resonances with the Galactic bar or the spiral arms.

The origin of the Arcturus and the HR 1614 moving groups, that were discovered by Eggen (1971) and Eggen (1978), respectively, were also originally linked to the dissolving open clusters scenario. Later the Arcturus structure was considered an accreted stellar population due to its low metallicity (e.g. Navarro et al. 2004; Helmi et al. 2006). Studies by Williams et al. (2009) and Bensby et al. (2014) suggested a resonant origin due to the high scatter of elemental abundances in the

structure.

The nature of the Arcturus and the HR 1614 moving groups is investigated in this thesis as well. In Paper II (Kushniruk & Bensby 2019), using the *Gaia* Data Release 2 (DR2) (Gaia Collaboration et al. 2018a), we found no evidence of either the accretion or the dissolving cluster origin and suggested a dynamical origin for the Arcturus structure. In Paper III (Kushniruk et al. 2020) we revise the origin of the HR 1614 moving group and refute the dissolving cluster origin of the structure due to a large spread of metallicities and ages within the group.

The Hercules stream is one of the largest nearby velocity overdensities and it is widely discussed in the literature as a structure caused by dynamical resonances. Some studies link the Hercules stream to the resonances with the Galactic bar (e.g. Dehnen 2000; Antoja et al. 2014; Hunt & Bovy 2018), while others explain it as a combined effect of spiral arms and the Galactic bar (e.g. Chakrabarty 2007; Hunt et al. 2019). These findings also confirm the dynamical origin of the Hercules stream. A detailed analysis of elemental abundances of stars in the Hercules stream performed by Bensby et al. (2007) showed that the group is a mix of stellar populations similar to the thick and thin disc stars. The metallicity and age distributions of the Hercules stream is wide (e.g. Kushniruk et al. 2017, 2020), and its colour-magnitude diagram can be described by a wide range of isochrones (Kushniruk et al. 2020). The studies of the Hercules stream caused a vivid discussion in the literature if the Galactic bar is short and fast (e.g. Antoja et al. 2014), or long and slow (e.g. Hunt & Bovy 2018). Thus, the Hercules stream can be used to trace the length and pattern speed of the Galactic bar and the properties of the spiral structure.

Dynamical resonances is one of the ways to explain ridges and arches in phase-space and the phase-space spiral discovered by Antoja et al. (2018) using the *Gaia* DR2. Various combinations of the Galactic bar and multiple spiral arms can explain the observed phase-space distribution of stars (Hunt et al. 2019; Khanna et al. 2019). As pointed out in Hunt et al. (2019), there is currently no unique solution, there are simply too many models that can successfully reproduce the kinematic structures, including the Hercules stream, in the numerical simulations.

Accreted stellar populations usually have peculiar chemical compositions. For example, Gaia-Enceladus-Sausage stands clearly out in the [$\alpha$/Fe][2] versus [Fe/H] distribution as a population different from the thin and thick disc stars and the

[2]Elemental abundances in stars are usually provided relative to the Sun in the following format: $[X/H] = \log\left(\frac{N(X)}{N(H)}\right)_{\star} - \log\left(\frac{N(X)}{N(H)}\right)_{\odot}$, where X denotes a chemical element. An abundance of a star is shown with $\star$ symbol. Solar abundance is marked with $\odot$ symbol.

*in situ* halo stellar population(Helmi et al. 2018). On the other hand, a chemical composition analysis of the Arcturus stream refuted its extragalactic origin and showed that the structure is a mix of stars from the Galactic thin and thick discs (e.g. Williams et al. 2009; Bensby et al. 2014; Kushniruk & Bensby 2019). Accreted halo populations show relatively low aluminium abundance compared to the majority of stars in the Galaxy (e.g. Koppelman et al. 2019).

Understanding the origin of kinematic structures is a non-trivial task. Complex dynamical processes such as resonances, cluster dissolution, and merger events form the clumpy velocity distribution that we observe today. Even though many numerical models are able to reproduce the observed kinematic features, there is still an ongoing hunt for the unique recipe. The degeneracy of numerical models leads to a number of questions. Which explanation is the true one? Is the observed velocity distribution a result of various dynamical processes? If yes, to what fraction? How can we understand the origin of each individual kinematic structure? The future *Gaia* data releases together with the spectroscopic data from the upcoming surveys such as WEAVE (Dalton et al. 2014) and 4MOST (de Jong et al. 2019) may help to find the true nature of the observed velocity distribution.

# Chapter 3

# Numerical methods and data sets

## 3.1 Velocity-action spaces

In this thesis kinematic structures are described using space velocities, angular momentum components, and actions. We have examined distributions of stars in four different velocity-action spaces: $U-V$, $V-\sqrt{U^2+2V^2}$, $L_z-\sqrt{L_x^2+L_y^2}$, and $L_z-\sqrt{J_r}$ spaces.

The space velocity of a star can be represented by three velocity components $U$, $V$, and $W$, that are defined as follows:

- the radial $U$ velocity component is positive towards the Galactic centre,
- the rotational $V$ velocity component is positive in the direction of the rotation of the Galaxy,
- the vertical $W$ velocity component is positive towards the North Galactic Pole.

Often these velocities are given relative to the local standard of rest (LSR), which is an imaginary point at the distance of the Sun that follows a circular orbit around the Galactic centre with a speed of 220 $\mathrm{km\,s^{-1}}$. In this work the Sun's velocity components relative to the LSR are $(U_\odot, V_\odot, W_\odot) = (11.10, 12.24, 7.25)$ $\mathrm{km\,s^{-1}}$ and were taken from Schönrich et al. (2010).

The angular momentum of a star is a cross product of its position and momentum vectors. The components of the angular momentum in the $X$, $Y$, and

$Z$[1] directions, denoted as $L_x$, $L_y$, and $L_z$, can also be used to search for kinematic structures. Fully conserved quantities in axisymmetric systems are orbital actions and integrals of generalized momenta around closed paths in phase space (Sanders & Binney 2016). In this thesis we study stars using the vertical component of the angular momentum $L_z$, which is the azimuthal action, and the radial action $J_r$, which is a measure of the orbit eccentricity.

In order to quantify the velocity and action components of individual stars, one needs to know the positions, proper motions, distances, and radial velocities of each star. We used the `astropy`[2] (Astropy Collaboration et al. 2013, 2018) and `galpy`[3] (Bovy 2015) packages to perform coordinate transformation and calculate space velocities, angular momenta components, and actions. Actions cannot be derived analytically for many potentials. In this work we used the `MWPotential2014` potential which is provided by `galpy`. To estimate actions of stars we used a `Stäckel fudge` approximation which is already implemented in `galpy`.

Figure 3.1 illustrates the distribution of nearby stars in all four spaces. In all cases the kinematic structures look like clumps except in the angular momentum space, where structures remind us of stripes. Each of the spaces has advantages and disadvantages. Below we discuss the different spaces individually.

### 3.1.1 The $U - V$ space

The analysis of stars in the $U - V$ space is commonly used to search for kinematic structures (e.g. Dehnen 1998; Antoja et al. 2008, 2012). The advantage of the analysis of stars in the $U - V$ space is that it is model independent and there is no need to make any assumptions about the Galactic potential. Studying small volumes in the $U - V$ space at different Galactocentric distances allows us to track sizes and shapes of velocity structures (e.g. Ramos et al. 2018). An example of the distribution of nearby stars in the $U - V$ space is shown in the top left plot of Fig. 3.1. It has a rich structure and one of them is the Hercules stream which is marked in the plot.

[1] $X$, $Y$, and $Z$ are components of the right-handed Cartesian coordinate system. The $X$ axis points towards the Galactic centre, the $Y$ axis defines the direction of Galactic rotation, and the $Z$ axis points towards the Galactic North Pole.

[2] http://www.astropy.org

[3] http://github.com/jobovy/galpy

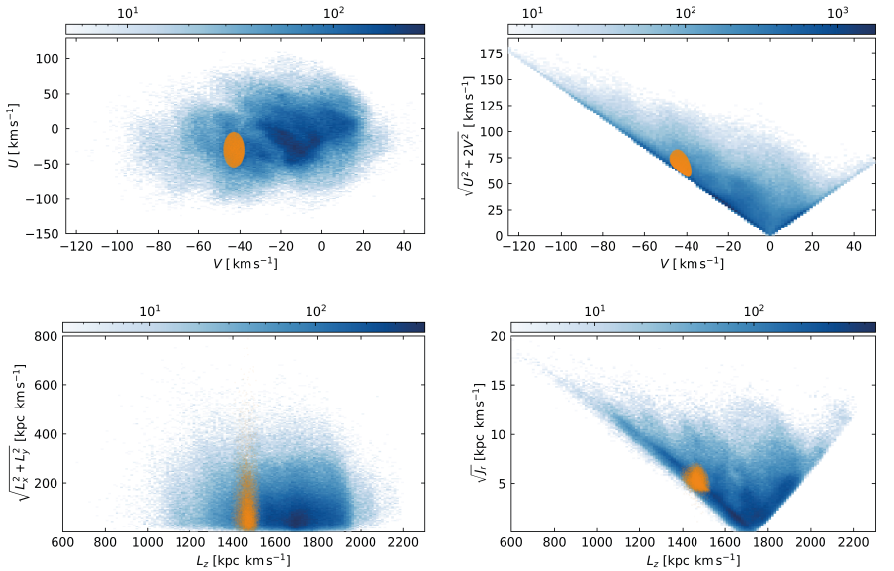


Figure 3.1: Density plots show distributions of nearby stars in different velocity, angular momentum, and action spaces, all based on data from *Gaia* DR2. Stars in the Hercules stream which were selected as an ellipse in the $U - V$ space, are shown with orange colour.

### 3.1.2 The $V - \sqrt{U^2 + 2V^2}$ space

To study stars on planar orbits in axisymmetric potentials in the $V - \sqrt{U^2 + 2V^2}$ space was proposed by Arifyanto & Fuchs (2006). The advantage of this space is that in this case $V$ is proportional to a vertical component of the angular momentum. Since the angular momentum is an integral of motion in axisymmetric potentials, the velocity clumps can be easily recognised among field stars. The second quantity $\sqrt{U^2 + 2V^2}$ is a measure of eccentricity in the Dekker's approximation (Dekker 1976). The disadvantage of this velocity space is that it is applicable only to stars whose orbits are located in the plane of the Galactic disc. The $V - \sqrt{U^2 + 2V^2}$ space has been used in a number of works to search for kinematic structures like the Arcturus stream (e.g. Klement et al. 2008; Zhao et al. 2014). The distribution of nearby stars in the $V - \sqrt{U^2 + 2V^2}$ space is shown in the top right plot of Fig. 3.1 and unlike the $U - V$ space, the $V - \sqrt{U^2 + 2V^2}$

space has a V-shaped structure. The Hercules stream is a clump in this space as well.

### 3.1.3 The $L_z - \sqrt{L_x^2 + L_y^2}$ space

As proposed by Helmi et al. (1999), kinematic structures can be characterised in the $L_z - \sqrt{L_x^2 + L_y^2}$ space, where $L_z$ is a conserved quantity and $\sqrt{L_x^2 + L_y^2}$ is nearly conserved. This method has been used to search for kinematic structures in the Galactic disc and halo (e.g. Helmi et al. 1999; Klement et al. 2008; Zhao et al. 2014). This method suits well to search for large-scale groups that have constant angular momenta across a range of Galactocentric distances since $L_z$ is an integral of motion. The disadvantage of this method is that $\sqrt{L_x^2 + L_y^2}$ is not fully conserved in axisymmetric potentials. An example of the distribution of nearby stars in this space is shown in the bottom left plot of Fig. 3.1. Structures in the $L_z - \sqrt{L_x^2 + L_y^2}$ space look like stripes including the Hercules stream since the quantity on the $Y$ axis is not fully conserved.

### 3.1.4 The $L_z - \sqrt{J_r}$ space

Fully conserved quantities in axisymmetric systems are orbital actions. This fact makes action space advantageous. Following Trick et al. (2019), we examine the $L_z - \sqrt{J_r}$ action space to search for kinematic structures. The radial action, $J_r$, characterises the orbit eccentricity. We take the square root of the radial action as it makes the analysis of the plots more clear. This method suits well for analysis of large stellar volumes and allows us to detect large-scale structures. The illustrative distribution of nearby stars in the $L_z - \sqrt{J_r}$ space is shown on the bottom right plot of Fig. 3.1. The Hercules stream looks like a clump in this space, similarly to the $U - V$ and $V - \sqrt{U^2 + 2V^2}$ spaces.

## 3.2 Wavelet transform

If one makes a plot of stars in the velocity-action spaces defined in Sects. 3.1.1-3.1.4, it is not guaranteed that we will see kinematic structures. The kinematic structures, if present, have to be filtered out from the general background, the field stars. There are different ways to search for overdensities in the different spaces and in this thesis the wavelet transform was chosen as the main method. It

is an advanced statistical tool which allows us to filter the randomly distributed stars from the kinematic structures. Unlike Fourier transform, which transforms time-based signals into frequency-based ones in such a way that time domain is lost, the wavelet transform also provides resolution in time. Infinite functions, like the sine trigonometric function, are used to represent a frequency domain of a signal via Fourier transform. The word "wavelet" means "small wave" and basically denotes a finite function, which allows to characterise a signal in terms of both scale and time via wavelet transform.

According to Starck et al. (1998), the continuous wavelet transform for a real one-dimensional signal $f(x)$ can be defined as follows:

$$w_j(b) = \frac{1}{\sqrt{j}} \int_{-\infty}^{+\infty} f(x)\, \Psi\left(\frac{x-b}{j}\right) dx \tag{3.1}$$

where

- $w_j(b)$ is the wavelet coefficient of the function $f(x)$,
- $\Psi(x)$ is the analysing wavelet,
- $j$ is the scale parameter,
- $b$ is the position of the point.

The original function, $f(x)$, which in our case is the observed velocity distribution of the stars, can be represented by wavelet transform through scaling of the analysing wavelet $\Psi(x)$. The original function $f(x)$ can be represented as the sum over $j$ and $b$ of the following product: $w_j(b) \cdot \Psi\left(\frac{x-b}{j}\right)$. The wavelet coefficients contain information about the location of the kinematic structures, their sizes, and their shapes.

In this thesis we use a discrete wavelet transform with *à trous* algorithm, which means "with holes" in French (Starck & Murtagh 2006). The advantage of this algorithm is that it allows us to avoid the direct computation of the product between the original function $f(x)$ and the analysing wavelet $\Psi(x)$. In order to calculate wavelet coefficients, a relation between the analysing wavelet and the scaling function is used instead (Eq. 1 in Chereul et al. 1999). The method can be easily adopted from 1-D to 2-D spaces, like the $U - V$ space. The discrete wavelet transform is used simply because we analyse velocity spaces presented in a finite number of bins, thus, scaling and translation parameters are finite as well.

The input data in any velocity space is a 2-D binned map of stellar velocities. The bin size has to be smaller than the typical structure size in each velocity space. For example, in the case of the $U - V$ space, the adopted bin size $\Delta$ was set to 1 $\mathrm{km\,s^{-1}}$. The binned data were analysed using the *à trous* algorithm, which decomposed the initial 2-D map into wavelet coefficients via applying filters $(h, g)$ at different scales $j$. A scale parameter $j$, the size of the structure $s$, and the bin size $\Delta$ follow the relation: $s_j = 2^j \times \Delta$ in the *à trous* algorithm. To perform the wavelet transform we used the MR (Multi-resolution) software[4] developed by CEA (Saclay, France) and Nice Observatory (Starck & Murtagh 2006).

Except for the useful information about the kinematic structures such as positions and shapes, the wavelet transform also returns an estimation of the noise that has to be filtered from the output data. This noise comes from the wavelet transform algorithm itself and is called a Poisson noise "a few events" because it follows the Poisson statistics and in the situation when most of the bins of the original velocity map have less than 30 star counts is called the Poisson noise with "a few events" (Starck & Murtagh 2006). The reduction of Poisson noise with "a few events" is done automatically by the MR software (Starck & Murtagh 2006). In addition, the velocity components of individual stars have uncertainties. These uncertainties add noise to the results of the wavelet transform as well.

In order to get robust results, we perform Monte Carlo simulations, assuming that each star can be represented with a Gaussian distribution, where the mean is defined by its velocity and the width by the estimated velocity uncertainty. Then we applied the wavelet transform to every Monte Carlo generated sample and over-plotted the central positions of all detected structures. In that way we could estimate sizes and uncertainties of the detected kinematic groups.

## 3.3 Data sets

To detect and characterise kinematic structures, we examined the above mentioned velocity and action spaces using large samples of stars from a number of large-scale astrometric, spectroscopic, and photometric surveys.

### 3.3.1 Gaia

*Gaia* is an astrometric space mission which was launched in December 2013 and is still ongoing. The aim of the mission is to provide precise astrometric data such

[4] http://www.multiresolutions.com/mr/

as positions, proper motions, photometric measurements, and radial velocities for over one billion targets. The first *Gaia* data release (DR1; Lindegren et al. 2016) contained positions and magnitudes. The combined astrometry of *Gaia* and the *Tycho-2* catalogues (Høg et al. 2000) allowed for an improved astrometric solution and provided parallaxes and proper motions for 2.5 million targets, which is known as the Tycho-*Gaia* astrometric solution (TGAS; Michalik et al. 2015). TGAS data was used in Paper I.

The second *Gaia* data release provided astrometric parameters for more than one billion targets (DR2; Gaia Collaboration et al. 2018a). The parallax and proper motion uncertainty varies from 0.04 to 0.7 $\mu$as and 0.06 to 1.2 $\mu$as for bright and faint targets respectively. *Gaia* DR2 data was used in Papers II and III.

### 3.3.2 StarHorse

`StarHorse` is a Bayesian isochrone-fitting code (Queiroz et al. 2018) which was applied to the *Gaia* DR2 stars by Anders et al. (2019). The code combines astrometric measurements from *Gaia* DR2 and data from a number of photometric surveys such as 2MASS (Cutri et al. 2003), PanSTARRS-1 (Chambers et al. 2016), and AllWISE (Cutri et al. 2013) to estimate stellar parameters, distances, and extinctions for 265 million *Gaia* objects that are brighter than $G = 18$. The aim of the catalogue is to supplement *Gaia* data with stellar parameters and extinctions for a large number of stars (Anders et al. 2019). We use extinctions, reddening, and distances provided by the `StarHorse` code in Paper III.

### 3.3.3 RAVE

The Radial Velocity Experiment (RAVE) is a medium-resolution (R $\sim$ 7 500) spectroscopic survey carried out with the 1.2-meter UK Schmidt Telescope of the Australian Astronomical Observatory (Steinmetz et al. 2006). The RAVE survey provides radial velocities, elemental abundances, and stellar parameters for hundreds of thousands of stars in the Southern hemisphere. In this thesis we use the RAVE data release (DR5; Kunder et al. 2017) which contains 457 588 unique targets in Paper I.

### 3.3.4 GALAH

The GALactic Archaeology with HERMES (GALAH) is a high-resolution (R $\sim$ 28 000) large spectroscopic survey that uses the High Efficiency and Resolution Multi-Element Spectrograph (HERMES) with the 3.9-meter Anglo-Australian

Telescope of the Australian Astronomical Observatory (De Silva et al. 2015; Martell et al. 2017). The main goal of the GALAH survey is to study formation and evolution of the Galactic disc. The survey provides optical observations of 342 682 stars in the Southern hemisphere. Elemental abundances and stellar parameters of the GALAH targets were estimated using the *Cannon* code (Ness et al. 2015). In this thesis we use data from the second GALAH release (DR2; Buder et al. 2018) in Papers II and III.

### 3.3.5 APOGEE

The Apache Point Observatory Galactic Evolution Experiment (APOGEE) of the Sloan Digital Sky Survey is a near-IR (H-band), high-resolution ($R \sim 23\,000$) and high signal-to-noise spectroscopic survey (Majewski et al. 2017; Wilson et al. 2019). In this work we used data from the fourteenth APOGEE data release (DR14; Abolfathi et al. 2018) and the sixteenth APOGEE data release (DR16; Ahumada et al. 2019). APOGEE DR14 provides elemental abundances and stellar parameters of 277 371 stars in the Northern hemisphere, while APOGEE DR16 covers 437 485 unique stars in both hemispheres. The observations were carried out on the 2.5-meter Sloan Foundation Telescope at Apache Point Observatory and the 2.5-meter du Pont telescope at Las Campanas Observatory with the help of near-infrared spectrographs described in Wilson et al. (2019). The spectra were processed with the APOGEE Stellar Parameter and Chemical Abundance Pipeline (ASPCAP; García Pérez et al. 2016). The advantage of the APOGEE survey is its wide coverage of Galactocentric distances allowing us to study chemical composition of stars in the bulge, disc, and halo of the Milky Way. We analyse data from APOGEE DR14 in Paper II and data from APOGEE DR16 in Paper III.

### 3.3.6 SkyMapper

The SkyMapper is a photometric survey of over 285 million object with the 1.35-meter optical telescope at Siding Spring Observatory (Keller et al. 2007). Its main aim is to survey the southern sky complementing the Sloan Digital Sky Survey in the Northern hemisphere. In this thesis we use the photometric metallicities by Casagrande et al. (2019) in Paper III.

### 3.3.7 Distance estimates

The calculation of velocities, angular momenta, and actions requires knowledge of distances to stars. Thus, the availability of accurate distance estimates is one of

the important aspects of this work. In this context it is important to note that the inverted parallax is a biased estimate of stellar distances (e.g. McMillan 2018).

Widely used distances to *Gaia* DR2 stars are the estimates provided to all *Gaia* stars by Bailer-Jones et al. (2018), who used stellar parallaxes and the expected distribution of all *Gaia* stars as a prior. In Paper II we used only stars in the *Gaia* DR2 catalogue that had available radial velocity measurements, with distances from McMillan (2018). These are distances for the radial velocity sample only and were estimated using parallaxes and $G_{RVS}$ magnitudes, that help to better account for selection effects. The estimates provided by McMillan (2018) and Bailer-Jones et al. (2018) diverge at larger distances (see Fig. 1 in McMillan 2018).

In Paper III we used magnitudes and colours corrected for extinction and reddening, and also distance estimates from the `StarHorse` code. The motivation to use distances provided by the `StarHorse` code was to use the all necessary data from the same catalogue to reduce the uncertainties of the analysis. According to Anders et al. (2019) these distances are not more precise than the ones by Bailer-Jones et al. (2018), but more accurate at large distances.

# Chapter 4

# This work

## 4.1 Searching for kinematic structures in the solar neighbourhood

This section is a summary of Paper I, where we studied the velocity distribution of nearby stars using the TGAS and RAVE catalogues.

As discussed in Chapter 2, the origin of kinematic structures is connected to various internal and external dynamical mechanisms, and to better understand what causes the overdensities in velocity space, it is important to have an understanding of how many kinematic structures there are in the Galactic disc. Therefore, when the TGAS catalogue became available, we decided to study the velocity distribution of stars in the Milky Way disc to search for such velocity structures. To calculate the space velocity components, astrometric data from TGAS were combined with radial velocities from RAVE. The benefit of this work was the astrometric precision that TGAS provided and the relatively high number of stars compared to what was available in previous studies that searched for kinematic structures. The stellar sample consisted of roughly 50 000 stars and was split into four subsamples to better understand the nature of the groups:

- the solar neighbourhood subsample: stars with distances from the Sun less than 300 pc,
- the beyond the solar neighbourhood subsample: stars with distances from the Sun larger than 300 pc,
- the chemically defined thin disc subsample: [Mg/Fe] $< 0.2$,

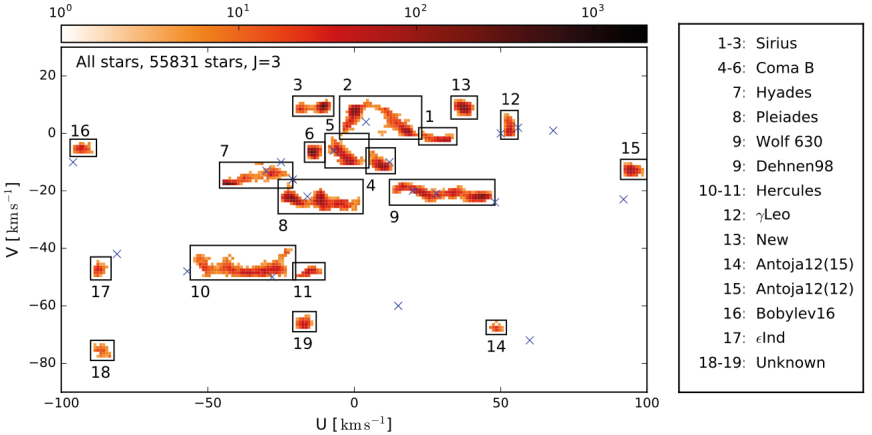


Figure 4.1: Kinematic structures found with wavelet transform applied to TGAS data in the $U - V$ space for scale $J = 3$. Colour map shows structure counts of 2 000 superimposed Monte Carlo simulations. This figure is adopted from Kushniruk et al. (2017). ©ESO. Reproduced with permission.

- the chemically defined thick disc subsample: [Mg/Fe] $> 0.2$.

The thin and thick disc separation criteria were adopted from Wojno et al. (2016), who performed a probabilistic analysis to chemically separate the two discs in the RAVE catalogue. To search for kinematic structures we applied a wavelet transform in the $U - V$ velocity space on the total sample as well as on the four subsamples defined above. We found that scales 2, 3, and 4 were the most suitable scales to search for kinematic structures since they most efficiently cover both small- and large-scale structures (see Sect. 4 in Paper I for more details).

We also performed a convergence test of the results and found that about 1 400 Monte Carlo simulations were needed for the number of detected structures to converge. To reduce the noise that comes from velocity uncertainties we decided to increase to 2 000 Monte Carlo simulations.

Figure 4.1 is the key figure of Paper I and shows the 19 kinematic structures that were found at the $J = 3$ scale. All these groups were detected at the $3\sigma$ significance level. The velocity distribution of nearby stars is clumpy, with most of the groups located around $U \simeq 0\,\mathrm{km\,s^{-1}}$ and negative $V$ velocities. The strongest detections are the Hyades, Pleiades, Coma Berenices, Sirius, and Hercules struc-

tures. We confirmed three groups (groups 14, 15, and 16 in Fig. 4.1) that were recently discovered by Antoja et al. (2012); Bobylev & Bajkova (2016), and found three new groups (number 13, 18, and 19 in Fig. 4.1). Group 13 has a strong detection, while groups 18 and 19 are slightly weaker. We found that Wolf 630 and Dehnen98 are connected and form one elongated structure in the $U - V$ space structure. The results are presented in Tables 1 and 2 in Paper I. These tables list all kinematic structures detected at different scales with the names found in the literature. For scale $J = 3$ we also indicate if the structure is present in any of the four subsamples.

The results of the wavelet transform applied to our four subsamples show that kinematic structures are mainly present in the nearby solar neighbourhood subsample. The thin and thick disc subsamples show that groups consist of mainly thin disc stars with maybe some contamination of thick disc stars. We did not find any group that consists of thin or thick disc stars only. Since RAVE provides elemental abundances for the stars, we also analysed the metallicity distributions and the [Mg/Fe] versus [Fe/H] plane for each of the kinematic structures. This allowed us to check if any of the structures had a peculiar chemical composition. Our results show that all structures are a mixture of thin and thick disc stars, pointing to resonant origins.

## 4.2 The origin of the Arcturus stream

This section is a summary of Paper II, where we investigated the origin of the Arcturus stream.

The Arcturus moving group was first defined in Eggen (1971) as a set of about 50 stars that shared a similar rotational velocity of about $V \simeq -100\,\mathrm{km\,s^{-1}}$. Eggen proposed that the structure was a remnant of a dissolved open cluster since this was the main hypothesis to explain co-moving groups at that time. Later it was found that the group consists of mainly metal-poor ([Fe/H] $\simeq -0.6$) and old ($\simeq 10$ Gyr) stars, and also taking into account its rather high velocity, several studies proposed that the Arcturus moving group was not a dissolved star cluster, but rather an accreted population (e.g. Gilmore et al. 2002; Navarro et al. 2004). A detailed elemental abundance analysis of stars in the Arcturus overdensity showed a wide scatter in abundances and ages, making resonances within the Galactic disc the most favourable hypothesis for its origin (e.g. Williams et al. 2009; Bensby et al. 2014). The nature and origin of the Arcturus stream is, however, still debated. In Paper II we revised the origin of the Arcturus stream with *Gaia* DR2 astrometric

data, distances from the `StarHorse` code, and elemental abundances from the APOGEE and GALAH spectroscopic surveys.

First, we searched for the Arcturus stream in four different velocity-action spaces: the $U-V$, the $V-\sqrt{U^2+2V^2}$, the $L_z-\sqrt{L_x^2+L_y^2}$, and the $L_z-\sqrt{J_r}$ spaces. The choice of velocity and action spaces was based on previous studies of the Arcturus stream. For example, Zhao et al. (2014) clearly detected the group in the $V-\sqrt{U^2+2V^2}$ and Trick et al. (2019) studied structures in angle-action space. This allowed us to compare our results with previous studies. We also examined 66 small subsamples of stars in every space to trace shapes and sizes of kinematic groups at different distances from the Sun. The subsamples were defined in the $R$ versus $\phi$ space[1]. The size of every box is $0.4$ kpc in radial coordinate and $3^\circ$ in azimuthal direction. Figure 1 in Paper II shows the location and sizes of the boxes.

Our analysis revealed dozens of kinematic structures including the Arcturus stream. The observed groups form arches in the $U-V$ space. These arches are observed as clumps in the action and $V-\sqrt{U^2+2V^2}$ spaces and are seen as lines in the angular momentum space. Figure 4.2 shows the kinematic structures detected in the solar neighbourhood box in the $U-V$ space. Kinematic structures can be united into arches, as, for example, proposed in Ramos et al. (2018). We observe kinematic structures at almost every $20-30\,\mathrm{km\,s^{-1}}$ in azimuthal velocity. This is similar to the results of the numerical simulations performed by Minchev et al. (2009), and the results of the analysis of the velocity space performed by, for example, Antoja et al. (2018) and Ramos et al. (2018). These papers explain the observed velocity features as the result of an ongoing phase mixing in the Galactic disc triggered by a major merger event.

The Arcturus stream is observed mainly in the solar neighbourhood and can be seen in all four spaces (see Fig. 6 in Paper II). It is seen as a weak arch in the $U-V$ space and as a clump in the $V-\sqrt{U^2+2V^2}$ space located below $V\simeq-100\,\mathrm{km\,s^{-1}}$, as a stripe in the angular momentum space and as a clump in the action space located at $L_z\simeq1100\,\mathrm{km\,s^{-1}}$. The analysis of the elemental abundances from APOGEE and GALAH spectroscopic surveys of stars in the Arcturus stream and few other nearby groups, known as AF06 and KFR08, showed that all groups are all a mixture of thin and thick disc stars. This result is in agree-

[1] $R$ and $\phi$ are radial and azimuthal components of Galactocentric cylindrical coordinates, where $R$ points towards the Galactic anti-centre, angle $\phi$ follows the direction opposite to the Galactic rotation. The vertical component of cylindrical coordinates is $Z$, which points at the North Galactic Pole.

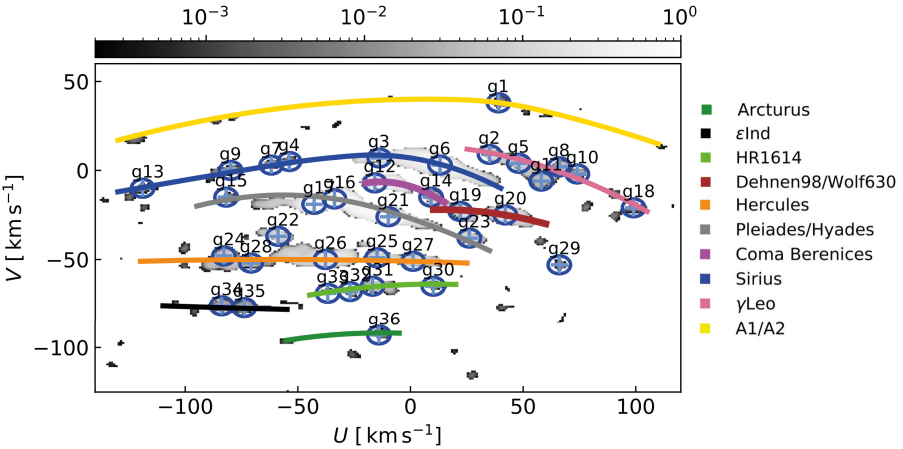


Figure 4.2: Kinematic structures found with wavelet transform applied to *Gaia* DR2 in the $U - V$ space for scale $J = 3$. Colour map shows normalised wavelet coefficients, that is significance of the detected structures. Names of the structures are provided in the legend. This figure is adopted from Kushniruk et al. (2020). ©ESO. Reproduced with permission.

ment with previous studies (e.g. Williams et al. 2009; Bensby et al. 2014).

We also explored how far the Arcturus stream extends from the Galactic mid-plane. Monari et al. (2013) predicts that the structures caused by dynamical resonances should be located in the plane of the Galactic disc. Figure 7 in Paper II shows that while the Hercules stream, which is likely caused by resonances with the Galactic bar (e.g. Dehnen 2000) and is located at low values of $Z$, the Arcturus stream extends farther from the plane.

To summarise, the results of Paper II suggest that the Arcturus stream is part of a phase-space wave. The group has a wide spread of elemental abundances, extends farther from the Galactic plane than the structures caused by dynamical resonances, is present beyond the solar neighbourhood, and is one of the groups that appear in steps of $20 - 30\,\mathrm{km\,s^{-1}}$ in the $V$ velocity.

## 4.3 The origin of the HR 1614 moving group

This section is a summary of Paper III, where we investigated the origin of the HR 1614 moving group.

A group of stars that move with velocities similar to the star HR 1614 was first discovered by Eggen (1978) and was called the HR 1614 moving group. The mean $U$ and $V$ velocity components of the stars in the group are about 0 and $-60\,\mathrm{km\,s^{-1}}$, respectively (e.g. Eggen 1992). The group was studied in detail with Hipparcos data by Feltzing & Holmberg (2000) who proposed a list of group member candidates by examining isochrones of stars. An analysis of the chemical composition of these stars was performed by De Silva et al. (2007) who found that the group has higher than solar metallicity of [Fe/H] $\simeq 0.2$, that its age is about two billion years, and that its chemical composition is homogeneous with very small scatter. These findings suggested a dissolving open cluster origin for the HR 1614 moving group.

While studying velocity-action spaces in Paper II to search for the Arcturus stream we clearly detected an overdensity of stars below the Hercules stream in the $U - V$ space. This is the HR 1614 moving group. We decided to re-investigate the origin of the HR 1614 moving group for several reasons. First, the existence of a two billion year old and metal-rich stellar population in the solar neighbourhood is surprising as most of the nearby moving groups are much younger (e.g. Cantat-Gaudin et al. 2018). Second, Feltzing & Holmberg (2000) did not see the HR 1614 overdensity in the $U - V$ space with Hipparcos data and defined the group by analysing isochrones. Based on previous studies Feltzing & Holmberg (2000) searched for a metal-rich stellar population. This could have influenced the results of the follow-up study by De Silva et al. (2015), who found a chemical homogeneity of the group. Third, the HR 1614 had not yet been analysed with data from large-scale surveys such as *Gaia*, APOGEE, GALAH, `StarHorse`, and SkyMapper.

To select stars in the HR 1614 moving group we used the results of the wavelet transform applied to the velocity distribution of nearby stars in the $U - V$ space from Paper II. Figure 4.2 shows kinematic structures detected in the solar neighbourhood, one of them is the HR 1614 moving group. We selected two samples of stars within the ellipses drawn around the HR 1614 structure and the Hercules structure in the $U - V$ space. The second structure was used for comparison reasons. *Gaia* DR2 data allowed us to select thousands of stars in both groups, which are a much larger stellar samples than what was analysed in previous studies.

To check if HR 1614 is a dissolved open cluster we analysed colour-magnitude diagrams, elemental abundances, and the ages of its stars. We used colours and magnitudes corrected for reddening and extinction as well as distances from the `StarHorse` catalogue. Our analyses revealed that the stars do not follow a single

isochrone and most likely are a mixture of stellar populations. Photometric metallicities from the SkyMapper survey and elemental abundances from APOGEE and GALAH show that the metallicity distribution of the HR 1614 moving group is wide, and the age and [Mg/Fe] versus [Fe/H] distributions show that it consist of both low- and high-$\alpha$ stars, consistent with what is observed for the thin and thick disc stellar populations. The same result was obtained for the Hercules stream, which also is likely to be a structure caused by resonances.

Based on the results of our analysis it is clear that HR 1614 is not a dissolving open cluster. It is also not likely to be an accreted stellar population. The HR 1614 structure consists of a mixture of the thin and thick disc stars similarly as the Hercules stream. We suggest that the group has a structure comparable to the general disc stellar population and could have formed due to resonances with the bar and the spiral structure, or as a result of phase mixing.

# Chapter 5

# Conclusions and future work

Our Galaxy has a complex structure consisting of multiple large-scale components such as the Galactic bulge, disc, and halo that influence each other. In addition, the Milky Way most likely underwent a number of merger events with dwarf galaxies. These factors together affect the motion of the stars, leaving imprints in the velocity distribution of stars that we call kinematic structures.

The main reasons for the clumpy velocity distribution of the Galactic disc are connected to complex dynamical processes. Among them are resonances with the bar and/or spiral structure, dissolving open clusters, phase mixing due to internal or external perturbation, and accretion events. Thus, understanding the origin of kinematic structures is an important tool for Galactic archaeology.

In this thesis we analysed stars in four velocity-action spaces to search for kinematic structures using data from astrometric, spectroscopic, and photometric surveys such as *Gaia*, TGAS, RAVE, APOGEE, GALAH, SkyMapper, and `StarHorse`. This allowed us to reveal new kinematic groups as well as confirm some recently discovered groups as well as old well-known groups. To search for kinematic structures we applied an advanced statistical tool, the wavelet transform. This method is commonly used to search for velocity groups and is advantageous since it does not require any assumptions on the initial velocity distribution of stars. To check the significance of the detected structures we performed Monte Carlo simulations.

The nature and origin of the detected groups were investigated by looking at the chemical composition of the stars in the groups. If the group is a dissolved open cluster, its stars should have similar chemical composition, since they were formed from the same interstellar gas cloud. If the kinematic structure formed

due to resonances or phase mixing, the chemical composition of its stars should be similar to the majority of stars in the Galactic disc. If the group is an accreted stellar population, it is very likely that they will chemically differ from the stars in the Milky Way.

In Paper I we analysed elemental abundances and metallicities of all groups from the RAVE catalogue. In Paper II we analysed the origin of the Arcturus stream by studying elemental abundances of stars in the APOGEE and GALAH surveys. In Paper III we revised origin of the HR 1614 moving group with data from the `StarHorse`, APOGEE, GALAH, and SkyMapper surveys.

The main results of Papers I, II, and III included in this thesis work are summarised in the following bullet points:

- In Paper I we found 19 velocity overdensities in the $U-V$ space in the solar neighbourhood with *Gaia* DR1/TGAS and RAVE surveys. Three groups were detected for the first time.

- In Paper II we found even more groups with *Gaia* DR2 data and studied stellar volumes farther away in the disc of the Milky Way and in four different velocity-action spaces. Some groups are local structures, others extend farther through the disc. There are groups that have constant angular momenta and radial actions across all Galactocentric radii.

- The analysis of elemental abundances of stars in the groups that were detected in Paper I shows that velocity structures are not chemically distinct and are instead, most likely, a mixture of the thin and thick disc stars. This means that the groups were caused by resonances with the Galactic bar or the Galactic spiral arm structure.

- The origin of the Arcturus stream was revised in Paper II. The elemental abundances of the stars in the stream and its kinematic properties show that the Arcturus stream is likely to be composed of thin and thick disc stars and is thus not a dissolved open cluster nor an accreted population.

- The results of Paper III suggest that the HR 1614 moving group is not a dissolved open cluster. Its stars do not follow a single age isochrone and have wide metallicity and age distributions. The group likely formed due to dynamical resonances and/or phase mixing.

Today different research groups can successfully model the observed velocity distribution. Among the most common explanations of the observed velocity

structures are resonances with the Galactic bar, the spiral structure, phase mixing induced by internal and external perturbations, and various combinations of these dynamical mechanisms. In order to find out how many and which particular dynamical mechanisms that have influenced the stellar motions and led to the formation of velocity overdensities, it is important to carry out further studies of the kinematic structures.

The upcoming *Gaia* data releases will provide even more precise astrometry and radial velocities for even larger number of stars. It will allow us to detect even more kinematic structures and trace arches and ridges at a higher precision than ever before. The imminent *Gaia* EDR3 will provide improved parallax, proper motion, and coordinates measurements which will be useful for a detailed investigation of the shapes and positions of kinematic structures in velocity spaces. *Gaia* DR3 will provide radial velocities for stars with estimated atmospheric parameters and will cover fainter targets than *Gaia* DR2. This will allow to detect more groups beyond the solar neighbourhood.

Kinematic structures of the solar neighbourhood form arches in the $U - V$ space. Some structures inside these arches, such as Wolf 630 or Sirius, are known as dissolved stellar clusters. But how do structures within one arch relate to each other is not clear. Do they have a similar chemical composition? Are they dissolved clusters that were later perturbed by the Galactic bar or spiral arms? Also if more groups will be detected at a wider range of Galactocentric radii, it is important to chemically characterise them as well. Astrometric data combined with chemical information from large-scale spectroscopic surveys like the Gaia-ESO survey Gilmore et al. (2012), GALAH (Buder et al. 2018), APOGEE (Majewski et al. 2017), and the upcoming WEAVE (Dalton et al. 2014), and 4MOST (de Jong et al. 2019) surveys, will allow us to further study the chemical properties of these groups. Together with more advanced numerical simulations we will be able to unravel more details about the formation history of the Milky Way.

# References


Abolfathi, B., Aguado, D. S., Aguilar, G., et al. 2018, ApJS, 235, 42

Ahumada, R., Allende Prieto, C., Almeida, A., et al. 2019, arXiv e-prints, arXiv:1912.02905

Anders, F., Khalatyan, A., Chiappini, C., et al. 2019, A&A, 628, A94

Antoja, T., Figueras, F., Fernández, D., & Torra, J. 2008, A&A, 490, 135

Antoja, T., Helmi, A., Bienayme, O., et al. 2012, MNRAS, 426, L1

Antoja, T., Helmi, A., Dehnen, W., et al. 2014, A&A, 563, A60

Antoja, T., Helmi, A., Romero-Gómez, M., et al. 2018, Nature, 561, 360

Arifyanto, M. I. & Fuchs, B. 2006, A&A, 449, 533

Astropy Collaboration, Price-Whelan, A. M., SipHocz, B. M., et al. 2018, aj, 156, 123

Astropy Collaboration, Robitaille, T. P., Tollerud, E. J., et al. 2013, A&A, 558, A33

Bailer-Jones, C. A. L., Rybizki, J., Fouesneau, M., Mantelet, G., & Andrae, R. 2018, AJ, 156, 58

Belokurov, V., Erkal, D., Evans, N. W., Koposov, S. E., & Deason, A. J. 2018, MNRAS, 478, 611

Bensby, T., Alves-Brito, A., Oey, M. S., Yong, D., & Meléndez, J. 2011, ApJ, 735, L46

Bensby, T., Feltzing, S., Gould, A., et al. 2017, A&A, 605, A89

Bensby, T., Feltzing, S., & Oey, M. S. 2014, A&A, 562, A71

Bensby, T., Oey, M. S., Feltzing, S., & Gustafsson, B. 2007, ApJ, 655, L89

Bland-Hawthorn, J. & Gerhard, O. 2016, Annual Review of Astronomy and Astrophysics, 54, 529

Bland-Hawthorn, J., Sharma, S., Tepper-Garcia, T., et al. 2019, MNRAS, 486, 1167

Bobylev, V. V. & Bajkova, A. T. 2016, Astronomy Letters, 42, 90

Bovy, J. 2015, ApJS, 216, 29

Buder, S., Asplund, M., Duong, L., et al. 2018, MNRAS, 478, 4513

Cantat-Gaudin, T., Jordi, C., Vallenari, A., et al. 2018, A&A, 618, A93

Casagrande, L., Wolf, C., Mackey, A. D., et al. 2019, MNRAS, 482, 2770

Chakrabarty, D. 2007, A&A, 467, 145

Chambers, K. C., Magnier, E. A., Metcalfe, N., et al. 2016, arXiv e-prints, arXiv:1612.05560

Chereul, E., Crézé, M., & Bienaymé, O. 1999, A&AS, 135, 5

Cutri, R. M., Skrutskie, M. F., van Dyk, S., et al. 2003, 2MASS All Sky Catalog of point sources.

Cutri, R. M., Wright, E. L., Conrow, T., et al. 2013, Explanatory Supplement to the AllWISE Data Release Products, Explanatory Supplement to the AllWISE Data Release Products

Dalton, G., Trager, S., Abrams, D. C., et al. 2014, in SPIE Conf. Ser., Vol. 9147, 91470L

de Jong, R. S., Agertz, O., Berbel, A. A., et al. 2019, The Messenger, 175, 3

De Silva, G. M., Freeman, K. C., Bland-Hawthorn, J., Asplund, M., & Bessell, M. S. 2007, AJ, 133, 694

De Silva, G. M., Freeman, K. C., Bland-Hawthorn, J., et al. 2015, MNRAS, 449, 2604

Dehnen, W. 1998, AJ, 115, 2384

Dehnen, W. 2000, AJ, 119, 800

Dekker, E. 1976, Phys. Rep., 24, 315

Eggen, O. J. 1965, The Observatory, 85, 191

Eggen, O. J. 1971, PASP, 83, 762

Eggen, O. J. 1978, ApJ, 222, 203

Eggen, O. J. 1992, AJ, 104, 1493

Eggen, O. J. 1998, AJ, 115, 2397

Famaey, B., Siebert, A., & Jorissen, A. 2008, A&A, 483, 453

Feltzing, S. & Holmberg, J. 2000, A&A, 357, 153

Freeman, K. & Bland-Hawthorn, J. 2002, ARA&A, 40, 487

Gaia Collaboration, Brown, A. G. A., Vallenari, A., et al. 2018a, A&A, 616, A1

Gaia Collaboration, Katz, D., Antoja, T., et al. 2018b, A&A, 616, A11

García Pérez, A. E., Allende Prieto, C., Holtzman, J. A., et al. 2016, AJ, 151, 144

Gilmore, G., Randich, S., Asplund, M., et al. 2012, The Messenger, 147, 25

Gilmore, G. & Reid, N. 1983, MNRAS, 202, 1025

Gilmore, G., Wyse, R. F. G., & Norris, J. E. 2002, ApJ, 574, L39

Grillmair, C. J. & Carlin, J. L. 2016, Astrophysics and Space Science Library, Vol. 420, Stellar Streams and Clouds in the Galactic Halo, ed. H. J. Newberg & J. L. Carlin, 87

Hayden, M. R., Bovy, J., Holtzman, J. A., et al. 2015, ApJ, 808, 132

Haywood, M., Di Matteo, P., Lehnert, M. D., Katz, D., & Gómez, A. 2013, A&A, 560, A109

Helmi, A., Babusiaux, C., Koppelman, H. H., et al. 2018, Nature, 563, 85

Helmi, A., Navarro, J. F., Nordström, B., et al. 2006, MNRAS, 365, 1309

Helmi, A., White, S. D. M., de Zeeuw, P. T., & Zhao, H. 1999, Nature, 402, 53

Høg, E., Fabricius, C., Makarov, V. V., et al. 2000, A&A, 355, L27

Hunt, J. A. S. & Bovy, J. 2018, MNRAS, 477, 3945

Hunt, J. A. S., Bub, M. W., Bovy, J., et al. 2019, MNRAS, 490, 1026

Ibata, R. A., Gilmore, G., & Irwin, M. J. 1994, Nature, 370, 194

Keller, S. C., Schmidt, B. P., Bessell, M. S., et al. 2007, PASA, 24, 1

Khanna, S., Sharma, S., Tepper-Garcia, T., et al. 2019, MNRAS, 489, 4962

Klement, R., Fuchs, B., & Rix, H.-W. 2008, ApJ, 685, 261

Koppelman, H. H., Helmi, A., Massari, D., Price-Whelan, A. M., & Starkenburg, T. K. 2019, A&A, 631, L9

Kunder, A., Kordopatis, G., Steinmetz, M., et al. 2017, AJ, 153, 75

Kushniruk, I. & Bensby, T. 2019, A&A, 631, A47

Kushniruk, I., Bensby, T., Feltzing, S., et al. 2020, A&A, 638, A154

Kushniruk, I., Schirmer, T., & Bensby, T. 2017, A&A, 608, A73

Laporte, C. F. P., Minchev, I., Johnston, K. V., & Gómez, F. A. 2019, MNRAS, 485, 3134

Lindegren, L., Lammers, U., Bastian, U., et al. 2016, A&A, 595, A4

Majewski, S. R., Schiavon, R. P., Frinchaboy, P. M., et al. 2017, AJ, 154, 94

Martell, S. L., Sharma, S., Buder, S., et al. 2017, MNRAS, 465, 3203

Martig, M., Minchev, I., Ness, M., Fouesneau, M., & Rix, H.-W. 2016, ApJ, 831, 139

McMillan, P. J. 2018, Research Notes of the American Astronomical Society, 2, 51

Michalik, D., Lindegren, L., & Hobbs, D. 2015, A&A, 574, A115

Minchev, I. 2016, Astronomische Nachrichten, 337, 703

Minchev, I., Boily, C., Siebert, A., & Bienayme, O. 2010, MNRAS, 407, 2122

Minchev, I., Quillen, A. C., Williams, M., et al. 2009, MNRAS, 396, L56

Monari, G., Antoja, T., & Helmi, A. 2013, ArXiv e-prints

Myeong, G. C., Vasiliev, E., Iorio, G., Evans, N. W., & Belokurov, V. 2019, MNRAS, 488, 1235

Navarro, J. F., Helmi, A., & Freeman, K. C. 2004, ApJ, 601, L43

Ness, M., Freeman, K., Athanassoula, E., et al. 2013, MNRAS, 430, 836

Ness, M., Hogg, D. W., Rix, H. W., Ho, A. Y. Q., & Zasowski, G. 2015, ApJ, 808, 16

Perryman, M. A. C., Lindegren, L., Kovalevsky, J., et al. 1997, A&A, 500, 501

Pompéia, L., Masseron, T., Famaey, B., et al. 2011, MNRAS, 415, 1138

Portail, M., Gerhard, O., Wegg, C., & Ness, M. 2017, MNRAS, 465, 1621

Queiroz, A. B. A., Anders, F., Chiappini, C., et al. 2020, A&A, 638, A76

Queiroz, A. B. A., Anders, F., Santiago, B. X., et al. 2018, MNRAS, 476, 2556

Ramos, P., Antoja, T., & Figueras, F. 2018, A&A, 619, A72

Renaud, F., Agertz, O., Read, J. I., et al. 2020, arXiv e-prints, arXiv:2006.06011

Sanders, J. L. & Binney, J. 2016, MNRAS, 457, 2107

Schönrich, R., Binney, J., & Dehnen, W. 2010, MNRAS, 403, 1829

Skuljan, J., Hearnshaw, J. B., & Cottrell, P. L. 1999, MNRAS, 308, 731

Starck, J.-L. & Murtagh, F. 2006, Astronomical Image and Data Analysis (Springer Berlin Heidelberg)

Starck, J.-L., Murtagh, F. D., & Bijaoui, A. 1998, Image Processing and Data Analysis, 297

Steinmetz, M., Zwitter, T., Siebert, A., et al. 2006, AJ, 132, 1645

Trick, W. H., Coronado, J., & Rix, H.-W. 2019, MNRAS, 484, 3291

Venn, K. A., Irwin, M., Shetrone, M. D., et al. 2004, AJ, 128, 1177

Williams, M. E. K., Freeman, K. C., Helmi, A., & RAVE Collaboration. 2009, in IAU Symposium, Vol. 254, The Galaxy Disk in Cosmological Context, ed. J. Andersen, Nordströara, B. m, & J. Bland-Hawthorn, 139–144

Wilson, J. C., Hearty, F. R., Skrutskie, M. F., et al. 2019, PASP, 131, 055001

Wojno, J., Kordopatis, G., Steinmetz, M., et al. 2016, MNRAS, 461, 4246

York, D. G., Adelman, J., Anderson, John E., J., et al. 2000, AJ, 120, 1579

Zhao, J. K., Zhao, G., Chen, Y. Q., et al. 2014, ApJ, 787, 31

# Acknowledgements

I would like to express my sincere and enormous gratitude to my main supervisor Thomas Bensby. Thank you very much for your guidance, regular meetings, discussions, proof-readings, persistence, and support. It has been a pleasure to have such a caring and responsive supervisor like you. I would also like to thank my co-supervisor Sofia Feltzing for valuable advice, discussions, and encouragement.

I want to thank everyone at Lund Observatory for making four years of my PhD amazing. Thank you all for fun talks about science and life at fika, discussions, tips, and help when I most needed it. I thank Thiebaut with whom we worked together on the first paper. I thank Paul for helping me when I had questions about Galactic dynamics. Special thanks go to my dear friends Simona, Madeleine, and Noemi. Louise, Diane, and Alessandra, thank you very much for your support when I was applying for a postdoctoral position. I thank Edita for helping me to get to know everyone when I just started my PhD. I have been lucky to share my office with Daniel who also likes darkness and has never objected when I raised the temperature on the thermostat. Thank you, everyone, for a great time!

I would like to thank my husband Roman. Thank you for your love and patience! I also thank my parents for their encouragement and love.

# Author contributions

The next pages summarize my contribution to each paper included in this thesis.

## Paper I:
## Kinematic structures of the solar neighbourhood revealed by *Gaia* DR1/TGAS and RAVE

**I. Kushniruk**, T. Schirmer, T. Bensby (2017)
Astronomy & Astrophysics, vol. 608, A73 (18 p.)

The project was proposed by TB. IK and TS developed analysis routines that involve the wavelet transform, Monte Carlo simulations, and analysis of metallicity distributions. The results were interpreted by IK. The text of the paper was written mainly by IK, Section 4 was written together with TS, with corrections and suggestions from TB.

## Paper II:
## Disentangling the Arcturus stream

**I. Kushniruk**, T. Bensby (2019)
Astronomy & Astrophysics, vol. 631, A47 (17 p.)

The project was proposed by TB. IK developed routines and codes, ran simulations, analysed and interpreted the results. The text was written by IK with corrections and suggestions from TB.

## Paper III:
## The HR 1614 moving group is not a dissolving cluster

**I. Kushniruk**, T. Bensby, S. Feltzing, C. Sahlholdt, L. Casagrande, D. Feuillet (2020)
Astronomy & Astrophysics, vol. 638, A154 (11 p.)

SF proposed the original idea of the project. IK led the project, developed routines and codes to analyse the data, and interpreted the results. LC and DF

provided data samples that were used to study metallicity and age distributions of HR 1614. CS provided age estimates for SkyMapper stars and Fig. 10. The text was written mainly by IK with suggestions and corrections from TB and SF. Section 2 was written together with DF and LC. Section 3.2.3 was written together with CS.

# Paper I

A&A 608, A73 (2017)
DOI: 10.1051/0004-6361/201731147


Astronomy & Astrophysics

# Kinematic structures of the solar neighbourhood revealed by *Gaia* DR1/TGAS and RAVE

I. Kushniruk[1], T. Schirmer[1,2], and T. Bensby[1]

[1] Lund Observatory, Department of Astronomy and Theoretical Physics, Box 43, 221 00 Lund, Sweden
e-mail: iryna@astro.lu.se
[2] École Normale Supérieure Paris-Saclay, Département de physique, 61 avenue du Président Wilson, 94 235 Cachan Cedex, France

Received 10 May 2017 / Accepted 19 September 2017

**ABSTRACT**

*Context.* The velocity distribution of stars in the solar neighbourhood is inhomogeneous and rich with stellar streams and kinematic structures. These may retain important clues regarding the formation and dynamical history of the Milky Way. However, the nature and origin of many of the streams and structures is unclear, hindering our understanding of how the Milky Way formed and evolved.
*Aims.* We aim to study the velocity distribution of stars of the solar neighbourhood and investigate the properties of individual kinematic structures in order to improve our understanding of their origins.
*Methods.* Using the astrometric data provided by *Gaia* DR1/TGAS and radial velocities from RAVE DR5 we perform a wavelet analysis with the *à trous* algorithm of 55 831 stars that have $U$ and $V$ velocity uncertainties less than 4 km s$^{-1}$. An auto-convolution histogram method is used to filter the output data, and we then run Monte Carlo simulations to verify that the detected structures are real and are not caused by noise due to velocity uncertainties. Additionally we analysed our stellar sample by splitting all stars into a nearby sample (<300 pc) and a distant sample (>300 pc), and two chemically defined samples that to a first degree represent the thin and the thick disks.
*Results.* We detect 19 kinematic structures in the solar neighbourhood in the range of scales 3−16 km s$^{-1}$ at the 3$\sigma$ confidence level. Among them we identified well-known groups (such as Hercules, Sirius, Coma Berenices, Pleiades, and Wolf 630), confirmed recently detected groups (such as Antoja12 and Bobylev16), and detected a new structure at $(U, V) \approx (37, 8)$ km s$^{-1}$. Another three new groups are tentatively detected, but require further confirmation. Some of the detected groups show clear dependence on distance in the sense that they are only present in the nearby sample (<300 pc), and others appear to be correlated with chemistry as they are only present in one of the chemically defined thin and thick disk samples.
*Conclusions.* With the much enlarged stellar sample and much increased precision in distances and proper motions, provided by *Gaia* DR1/TGAS we have shown that the velocity distribution of stars in the solar neighbourhood contains more structures than previously known. A new feature is discovered and three recently detected groups are confirmed at high confidence level. Dividing the sample based on distance and/or metallicity shows that there are variety of structures which form large-scale and small-scale groups; some of them have clear trends on metallicities, others are a mixture of both disk stars. Based on these findings we discuss possible origins of each group.

**Key words.** stars: kinematics and dynamics – Galaxy: formation – Galaxy: evolution – galaxies: kinematics and dynamics

## 1. Introduction

Studies of the velocity distribution of stars in the solar neighbourhood have shown that it contains a plethora of kinematic structures, with stars that have similar space velocities $(U, V, W)$. There are several possible reasons to why different stars have similar kinematic properties: they could be from evaporated open clusters; they could be due to dynamical resonances within the Milky Way; or they could even be remnants of accreted satellite galaxies that merged with the Milky Way billions of years ago. This means that stellar streams retain a lot of information about the various dynamical processes of the Milky Way's past and provide clues to our understanding of the formation of the Galaxy. Mapping the structure and properties of this benchmark galaxy, will also aid our attempts to understand the evolution and formation of large spiral galaxies in general. A detailed characterisation of the kinematic properties together with chemical composition of the stars of such structures is crucial when trying to trace their origins (e.g. Freeman & Bland-Hawthorn 2002).

The release of HIPPARCOS catalogue twenty years ago (ESA 1997) boosted the study of kinematic properties of the solar neighbourhood. For example, Dehnen (1998) studied the distribution of 14 369 kinematically selected stars using a maximum likelihood estimate method and detected 14 features in the $U-V$ plane of Galactic space velocities. The $W$ direction did not appear very rich in structures with only four moving groups detected. The sample was then split based on $(B-V)$ colour index to study the behaviour of young and old stars separately. They found that there are moving groups composed of red stars (supposed to be older), while younger structures were composed of stars with different colours. This was an argument against the theory previously proposed by Eggen (1996), that kinematic structures could be remnants of disrupted open clusters, in which stars are chemically homogeneous. Instead, Dehnen (1998) propose that moving groups that follow eccentric orbits could be formed through resonances with the Galactic bar.

Skuljan et al. (1999) studied a sample of 4597 HIPPARCOS stars and, unlike Dehnen (1998), used radial velocities provided

in HIPPARCOS Input Catalogue (Turon et al. 1992). Skuljan et al. (1999) applied a wavelet analysis method for kinematic group detection, identified the most significant structures in the $U - V$ plane, and found that the velocity distribution has a more complicated structure than simply moving groups and has a larger, branch-like structure.

Later, using a combination of CORAVEL radial velocities (Baranne et al. 1979) and ages, together with *Tycho*-2 astrometry, Famaey et al. (2005) investigated a stellar sample of 5952 stars and found well-known streams like Hercules, Sirius, Hyades and Pleiades. They suggest that stellar groups are of dynamical origin as isochrones of stars associated with the moving groups show a large dispersion of ages. A deeper study of the origin of moving groups provided by Famaey et al. (2008) involved wavelet transform applied to the same data as in Famaey et al. (2005) and checked the theory of kinematic groups being remnants of open clusters. After fitting isochrones inherent for open clusters to stars associated with the Sirius, Hyades and Pleiades streams, Famaey et al. (2008) claimed dynamical origins for these groups, as they did not match.

Antoja et al. (2008) investigated a larger sample of 24 910 stars using wavelet techniques and analysed the age-metallicity distribution of the kinematic branches of Sirius, Hercules, Hyades-Pleiades and Coma Berenices. Each branch showed a wide spread of metallicities, especially Hercules. Sirius group stars were older and peaked at about 400 Myr, compared to Hyades-Pleiades which consist of mainly younger stars.

Zhao et al. (2009) later detected 22 structures by applying a wavelet analysis to a sample of 14 000 dwarf stars from Nordström et al. (2004) and 6 000 giant stars from Famaey et al. (2005). That study provided a comprehensive comparison of the positions of all kinematic structures detected by different authors. Eleven those 22 groups had previously been found in the literature, while the remaining eleven were discovered for the first time.

Antoja et al. (2012) identified 19 structures in the solar neighbourhood by analysing a sample of over 200 000 stars with available RAVE radial velocities and compared their results with those obtained by using the Geneva-Copenhagen survey (Nordström et al. 2004). The latter found 19 structures in the solar neighbourhood from a sample of over 110 000 stars and their findings support the dynamical origin of stellar branches based on age-metallicity distribution from Antoja et al. (2008) and the fact that the main groups are large-scale structures that are detectable even beyond the solar neighbourhood.

An alternative approach (to analyses in the $U - V$ velocity plane) is to search for streams in the plane defined by the integrals of motions. This way of searching for kinematic overdensities is important as one may discover stellar streams of possible resonant or even extra-galactic origin. Stars in associated kinematic over-densities keep the same angular momenta and in the solar neighbourhood behave the same way as moving groups of the cluster disruption origin. Together with the approximation of Keplerian orbits (see Dekker 1976), Arifyanto & Fuchs (2006) and Klement et al. (2008) studied the distribution of stars in $\sqrt{U^2 + 2V^2}$ and $V$ plane as a consequence of the integral of motion approach, first discussed in Helmi et al. (1999). Arifyanto & Fuchs (2006) applied wavelet transform to the thin and thick disk samples that consist of nearby subdwarfs with metallicities [Fe/H] $> -0.6$ and [Fe/H] $\leq -0.6$. They found Pleiades, Hyades, and Hercules in the thin disk and Arcturus stream in the thick disk. Klement et al. (2008) were the first to use the RAVE DR1 archive. Their sample consisted of 7015 stars that allowed them to detect eight groups in the $\sqrt{U^2 + 2V^2}$ and $V$ plane. Later, Zhao et al. (2014) focused on the search for kinematic structures for the thick disk population based on the LAMOST survey (see Zhao et al. 2012). Their stellar sample consisted of 7993 stars. Thus, only a few kinematic structures were detected.

Usually the origin of kinematic structures is studied with help from our knowledge about other components of the Galaxy, but Antoja et al. (2014) did the opposite: assuming that the Hercules stream was caused by resonances of the Galactic bar, they used Hercules to constrain the Galactic bar's pattern speed and the local circular frequency. This paper further demonstrated the importance of the study of kinematic structures, a possible key to a better understanding of the Milky Way formation.

Cross-matching the first astrometric data release of *Gaia* DR1 (Lindegren et al. 2016) and the radial velocities from the RAVE DR5 catalogue (Kunder et al. 2017), we now have access to the most up-to-date and precise astrometric measurements for more than 200 000 stars. This is a substantially larger sample than most samples previously available, and the precision in the data is also much better than before. Recently, using TGAS and RAVE, the kinematics of halo stars was investigated by Helmi et al. (2017), who studied the velocity correlation function and the energy vs. angular momentum space of about 1000 stars with metallicities [M/H] $\leq -1.5$. They found that the distribution of stars in the space defined by integrals of motion has complex kinematic structure and more than half of them follow retrograde orbits. Halo substructure with TGAS and RAVE was also studied in Myeong et al. (2017). The clump of 14 co-moving metal-poor giants was discovered. Based on small spreads of the metallicity within the group, authors explain its origin as being a dissolving remnant of a globular cluster. Liang et al. (2017) applied a wavelet analysis technique to a sample that is a combination of the LAMOST DR3 (Zhao et al. 2012) and the *Gaia* TGAS (Michalik et al. 2015) catalogues. They detected 16 kinematic structures, identifying four potential new stream candidates.

The list of works on kinematic groups could be extended and all of them prove that the velocity distribution in the solar neighbourhood is inhomogeneous and has a complex, branch-like structure. The mechanism of how individual stellar streams were formed remains is unknown. Some of the above-mentioned papers attempts to resolve this question, and as a result there exists a variety of theories, but there is no exact agreement among them even for the well-studied groups, further demonstrating the importance of the study of kinematic structures.

Using the recent TGAS and RAVE data releases, this study focuses on the velocity distribution of stars in the $U - V$ plane to reveal the structures and to further analyse some properties of each structure in terms of distance and chemistry. The paper is organised in the following way: in Sect. 2 we discuss the stellar sample and its properties; Sect. 3 contains an explanation of numerical methods (wavelet analysis) used in this work; Sect. 4 covers the description of input and output maps for the wavelet analysis; all the results including tables and figures of kinematic structures we present in Sect. 5; finally, the summary and discussion of this work are in Sect. 6.

## 2. Stellar sample

To detect stellar structures in velocity space we will perform a wavelet analysis applied for a data sample in the $U-V$ plane (see Sect. 3), where $U, V, W$ are the space velocities of the stars in a right-handed Cartesian coordinate system $(X, Y, Z)$. The $X$ axis

points towards the Galactic centre, while the $Y$ axis defines the direction of Galactic rotation, and the $Z$ axis points towards the Galactic North Pole. The sample should be as large as possible and contain precise measurements of distances, proper motions, and radial velocities, for the calculation of accurate space velocities.

### 2.1. Distances and radial velocities

Since the *Gaia* satellite was launched in 2013 we have been expecting the most precise astrometric measurements for billions of stars in the Milky Way. The first *Gaia* data release (DR1; Lindegren et al. 2016) due to the shortage of observations is still far from the declared precision: for a star with a magnitude $V = 15$ it is expected to obtain positions, proper motions and parallaxes with the precision up to 5–25 $\mu$as (see Michalik et al. 2015). However, adding astrometry from the HIPPARCOS catalogue, TGAS gives astrometric solutions for 2.5 million stars with precise measurements of all required astrometric data (Michalik et al. 2015). According to Gaia Collaboration (2016) it is recommended that a systematic error of 0.3 mas be concidered. Later, Lindegren (2017) states that parallax uncertainties already represent the total uncertainty and additional systematic error could lead to overestimation. Therefore, in this work we used original TGAS data. In order to calculate the three-dimensional (3D) movements of the stars, that is the $U$, $V$, and $W$ space velocities, the TGAS data must be complemented with radial velocities.

The Radial Velocity Experiment (RAVE) is a medium-resolution spectroscopic survey with the primary goal of determining radial velocities and stellar parameters for hundreds of thousands of stars in the Southern Hemisphere using spectra with a resolving power of $R = 7500$ (Steinmetz 2003). The final release of RAVE (DR5) gives precise measurements of radial velocities of 457 588 unique stars (Kunder et al. 2017). Cross-matching RAVE DR5 with TGAS provides us with a sample of 159 299 stars with known coordinates ($\alpha$, $\delta$), proper motions ($\mu_\alpha$, $\mu_\delta$), positive parallaxes ($\pi$), radial velocities ($v_{\rm rad}$), abundances of Mg and Fe and their associated uncertainties for all stars. The RAVE catalogue contains multiple observations for some stars. In those cases, the median value of every parameter was used in this work.

To further expand our sample we also explore the option of including the data releases from the Large sky Area Multi-Object Fibre Spectroscopic Telescope (LAMOST DR2, Luo et al. 2015). This is a Northern hemisphere survey which contains spectra of almost 2 million stars with a resolution of $R = 2000$. The cross-matching of A-, F-, G- and K-type stars in the LAMOST DR2 catalogue with TGAS[1] leaves us a sample of 107 501 stars with positive parallax.

### 2.2. Space velocities and their uncertainties

Space velocities and their uncertainties, which are dependent on the accuracy of the proper motions, the parallaxes, and the radial velocities, were computed according to the equations in (Johnson & Soderblom 1987).

Figure 1 shows the distributions of the uncertainties in the $U$, $V$, and $W$ velocities for 159 299 RAVE stars (top) and 107 501 LAMOST stars (bottom). Each velocity component is indicated with a different colour. About 35% (55 831) of the RAVE stars have velocities with uncertainties smaller than 4 km s$^{-1}$, while only 0.8% (905) LAMOST stars belong to the same region. Such a comparably low accuracy of LAMOST velocities can be explained with high uncertainties of radial velocities, which are one of the main components when computing $\sigma_U$, $\sigma_V$ and $\sigma_W$. Tian et al. (2015) cross-matched LAMOST DR1 with APOGEE and discovered an offset of ~5.7 km s$^{-1}$ of LAMOST radial velocities. Schönrich & Aumer (2017) report that LAMOST line-of-site velocities are underestimated and have to be corrected by 5 km s$^{-1}$. The accuracy of space velocities is crucial for detection of kinematic groups, shown later in the Sect. 4. Taking into account high uncertainties for the LAMOST stars we decided to focus our analysis on the RAVE sample only, which gives us a sample of 159 299 stars.

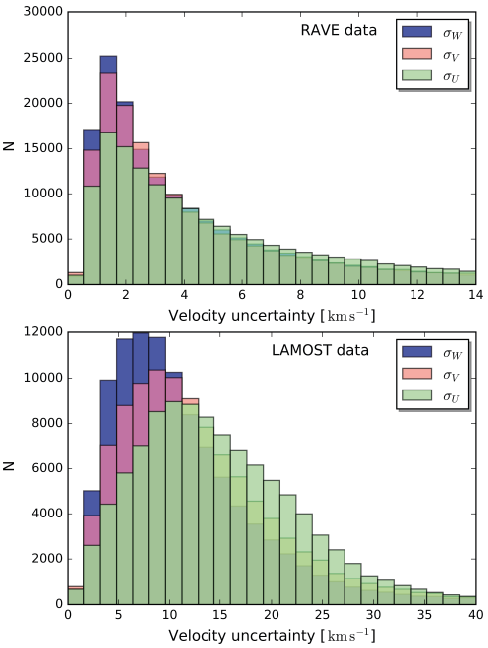


**Fig. 1.** Distribution of the velocity uncertainties, $\sigma_U$ is shown in green, $\sigma_V$ in pink, $\sigma_W$ in blue. *Top*: 159 299 RAVE stars. *Bottom*: 107 501 LAMOST stars.

The spatial distribution of our RAVE-TGAS star sample in the $X - Y$ and $X - Z$ planes is shown in Fig. 2. In this plot we show three distributions: the sample of all 159 299 stars is shown in blue, 55 831 stars with $\sigma_U$, $\sigma_V < 4$ km s$^{-1}$ in green, and the red colour indicates the same stars as the green but with distance limit <300 pc. As is shown in Sect. 4 we focus on the analysis of the last two sub-samples. The precision of the parallax distances provided by TGAS is high enough and additionally the cut on velocity uncertainties ($\sigma_U$ and $\sigma_V$) less than 4 km s$^{-1}$ already cuts stars by parallax too. In Fig. 3 the distribution of parallax-relative uncertainties $\pi_e/\pi$ for the total sample is shown, where $\pi$ is the parallax and $\pi_e$ is its uncertainty. Most stars have uncertainties less than 30%. This cut is necessary to obtain robust positions of kinematic structures.

[1] Using the gaia_tools Python package developed by Jo Bovy that is available at https://github.com/jobovy/gaia_tools

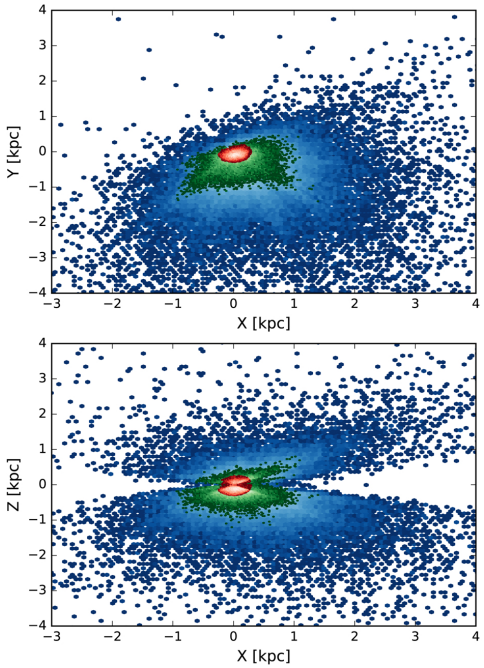


**Fig. 2.** Spatial distribution of RAVE stars in the $X-Y$ (*top*) and $X-Z$ (*bottom*) planes shown as a log-scale density plot. Blue colour shows a sample of 159 299 stars, green colour is for a sample of 55 831 stars with $\sigma_U$ and $\sigma_V < 4$ km s$^{-1}$ and red colour describes the distribution of 31 533 stars associated with the solar neighbourhood ($d < 300$ pc). The lighter shades of each colour show higher numbers of stars in distributions.

Whether or not local standard of rest (LSR) should be included in the space velocities, or not, in the detection analysis for kinematic groups is debatable. In several works the space velocities were not adjusted for the peculiar solar motion (e.g. Skuljan et al. 1999; Antoja et al. 2008, 2012; Zhao et al. 2009), while in some papers it was (e.g. Klement et al. 2008; Zhao et al. 2014). We chose not to correct our space velocities to the LSR as the adopted solar motion relative to the LSR may differ between studies (e.g. Schönrich 2012) and if so, would make direct comparisons of the detected structures more difficult.

## 3. Numerical methods

Different statistical methods have been used to highlight kinematic over-densities: wavelet analysis (e.g. Skuljan et al. 1999; Antoja et al. 2008, 2012; Zhao et al. 2009), maximum likelihood algorithm (e.g. Dehnen 1998; Famaey et al. 2005), and adaptive kernel estimate (e.g. Skuljan et al. 1999). We chose the most efficient technique for our purposes: the wavelet analysis with the *à trous* algorithm (Starck et al. 1998) which gives signal characteristics in terms of location, both in position and scale (size of the structure) simultaneously. The utility of this analysis method applied to the detection of moving groups in the solar

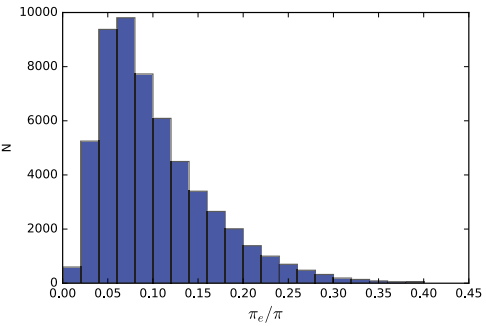


**Fig. 3.** Distribution of parallax relative uncertainties for 55 831 stars with $\sigma_U$ and $\sigma_V < 4.0$ km s$^{-1}$.

neighbourhood has already been demonstrated in several studies (e.g. Chereul et al. 1998; Skuljan et al. 1999; Famaey et al. 2008; Antoja et al. 2008, 2012). The wavelet analysis part of this work is done using MR software[2] developed by CEA (Saclay, France) and Nice Observatory. It is a powerful tool that has been developed since the very beginning of the wavelet era.

The analysis consists of applying a set of filters at different scales to the original data in order to determine wavelet coefficients. Detected structures, which correspond to local maxima in the wavelet space can be either physical (kinematic groups) or "artefacts". The latter can have two origins: (1) The wavelet coefficients contain Poisson noise due to the fact that the stellar sample is finite. Details on the filtering of the Poisson noise can be found in Sect. 3.2; (2) The space velocities of the stars contain significant uncertainties. Details on the verification of the robustness of results are given in Sect. 4.2.

### 3.1. The à trous algorithm

We focused on the wavelet analysis with the *à trous* algorithm because it has an advantage compared to other statistical methods: it does not require any assumptions on the initial stellar distribution. So, the input data correspond only to the original star-count map in the $U-V$ plane. The algorithm implies applying a set of filters at different scales ($s_j = 2^j \times \Delta$) in order to decompose the two-dimensional (2D) signal $c_0(i_x, i_y)$ into a set of wavelet coefficients ($w_1$, ..., $w_n$) that contain the information about kinematic structures. Here, $(i_x, i_y)$ is a position at the input grid, $j$ is the scale index ($j \in [1, p]$), $p$ is the maximum scale and $\Delta$ is the bin size of the input pixel grid which is used to detect structures which have sizes between $s_{j-1}$ and $s_j$ km s$^{-1}$ (for details on the algorithm see Starck & Murtagh 2002).

For one position $(i_x, i_y)$, a positive wavelet coefficient corresponds to an over-density in the velocity space. We followed the documentation provided with the MR software and we used a maximum scale $p$ equal to $\log_2(N-1)$, where $N$, assuming that the input star count map has a size $N \times M$, is the number of pixels in the smaller direction.

[2] http://www.multiresolutions.com/mr/

### 3.2. Image filtering and detection of significant structures

Given that the data sample is finite, wavelet coefficients at each scale except the information about the structures contain also noise which follows Poisson statistics. The procedure to determine if a wavelet coefficient is significant or not depends on the kind of data. First, we determined the multi-resolution support of the resulting image, which is a logical[3] way to store information about the significance of a wavelet coefficient at a given scale $j$ and a position $(i_x, i_y)$. Our data contains a large number of pixels with less than 30 star counts, which is called the case of "few events". In order to remove the Poisson noise in the case of "few events" we used the auto-convolution histogram method (Slezak et al. 1993) which has already been successfully used to detect structures in data with few events such as low-intensity X-ray images (Starck & Pierre 1998).

With the final set of wavelet coefficients we used an algorithm provided with the MR software that groups coefficients into structures that are characterised by the level of confidence $\epsilon$. A structure detected with a $3\sigma$ confidence level corresponds to a 99.86% probability that the structure was not produced by the Poisson noise. Then, the algorithm approximates the shape of the structure by an ellipse, characterised by its centre, its semi-minor axis, its semi-major axis, and the angle between the major axis and the horizontal axis of the input map. These parameters are useful for the estimation of the number of stars belonging to the structure, assuming that all the stars inside the ellipse can be associated with the structure.

## 4. Analysis

### 4.1. Input data

The constraints on velocity uncertainties and the choice of the bin size of the input star-count map are linked. First, the uncertainties have to be simultaneously large enough in order to provide us with as large a sample as possible, and at the same time small enough to take advantage of the high-precision data provided by *Gaia* DR1/TGAS and RAVE. Second, the bin size of the star count map has to be consistent with the space velocity uncertainty of the stars in order to get robust positions of the structures.

This means that the bin size needs to be roughly equal to the average velocity uncertainty of the sample, otherwise the probability that a star falls into a particular bin will be reduced and therefore the precision of the positions of kinematic structures will also decrease. If the bin size is higher than $\sim$5 km s$^{-1}$, the first scale ($J = 1$) would be 10–20 km s$^{-1}$, but from previous studies it has been shown that the typical size of structures is of the order 10 km s$^{-1}$ (e.g. Antoja et al. 2012). Thus, a bin size larger than about 5 km s$^{-1}$ should not be used as too many structures would be lost. With a restriction on $\sigma_U$ and $\sigma_V$ equal to 4 km s$^{-1}$ it should possible to get robust measurements of positions of structures, and that leaves us with a sample of 55 831 stars that have average velocity uncertainties of $\langle\sigma_U\rangle = 1.8$ km s$^{-1}$ and $\langle\sigma_V\rangle = 1.6$ km s$^{-1}$. We then chose a bin size of $\Delta_{\rm bin} = 1$ km s$^{-1}$. With this value the scales of the output images from the wavelet transform will be: $J = 1$ (2–4 km s$^{-1}$), $J = 2$ (4–8 km s$^{-1}$), $J = 3$ (8–16 km s$^{-1}$), $J = 4$ (16–32 km s$^{-1}$), $J = 5$ (32–64 km s$^{-1}$).

[3] If $w_j(i_x, i_y)$ is significant for a given scale $j$ and position $(i_x, i_y)$, then $M_j(i_x, i_y) = 1$, otherwise, $M_j(i_x, i_y) = 0$.

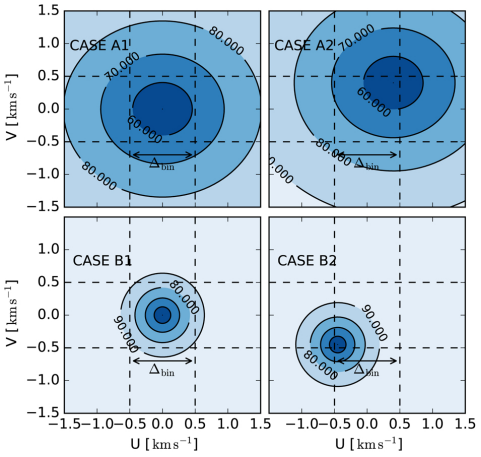


**Fig. 4.** Probability density functions of the location of stars in the $U-V$ plane for different cases and $\Delta_{\rm bin} = 1.0$ km s$^{-1}$. Case A1: the star is located in the centre of a bin and the uncertainty is equal to the average uncertainty of the stars in our sample ($\sigma_U = \langle\sigma_U\rangle = 1.80$ km s$^{-1}$ and $\sigma_V = \langle\sigma_V\rangle = 1.60$ km s$^{-1}$). Case A2: the star is located close to the edge of a bin and the uncertainty is equal to the average uncertainty of the stars in our sample ($\sigma_U = \langle\sigma_U\rangle = 1.80$ km s$^{-1}$ and $\sigma_V = \langle\sigma_V\rangle = 1.60$ km s$^{-1}$). Case B1: the star is located in the centre of a bin and the uncertainty is lower than the average uncertainty of the stars in our sample ($\sigma_U = \langle\sigma_U\rangle = 0.90$ km s$^{-1}$ and $\sigma_V = \langle\sigma_V\rangle = 0.80$ km s$^{-1}$). Case B2: the star is located close to the edge of a bin and the uncertainty is lower than the average uncertainty of the stars in our sample ($\sigma_U = \langle\sigma_U\rangle = 0.90$ km s$^{-1}$ and $\sigma_V = \langle\sigma_V\rangle = 0.80$ km s$^{-1}$). Numbers at each concentric circle show the probability as a percentage for the star to fall inside the circle.

### 4.2. Monte Carlo simulations

The space velocities of the stars have uncertainties that will influence the ability to detect kinematic structures and how robust these detections will be. Figure 4 shows the probability density function of one star to be located in the centre of one bin in the $U-V$ plane (plots on the left-hand side) or at the edge of the bin (plots on the right-hand side) given that the velocity uncertainties are equal to the average uncertainties of the sample (upper plots) or half of the average uncertainties (lower plots). The probability (see numbers at each concentric circle) that a star will fall into different bins is non-zero and consequently, can lead either to structures being "fake detections", or the detection of real physical structures being missed. Hence, we perform Monte Carlo (MC) simulations in order to estimate the robustness of the detected structures.

$N_{\rm MC}$ synthetic samples are generated from the original one by randomly drawing 55 831 new couples $(U, V)$ assuming that the stars have Gaussian velocity distributions, where mean values are positions $(U_i, V_i)$ and the standard deviations are uncertainties $(\sigma_{U_i}, \sigma_{V_i})$, where $i \in [1, N_{\rm stars}]$ refers to the $i$th star in the original sample. Then, the wavelet analysis and the structure detection algorithm are applied to the $N_{\rm MC}$ synthetic stellar samples and the positions of all structures at all scales are stored for each simulated sample.

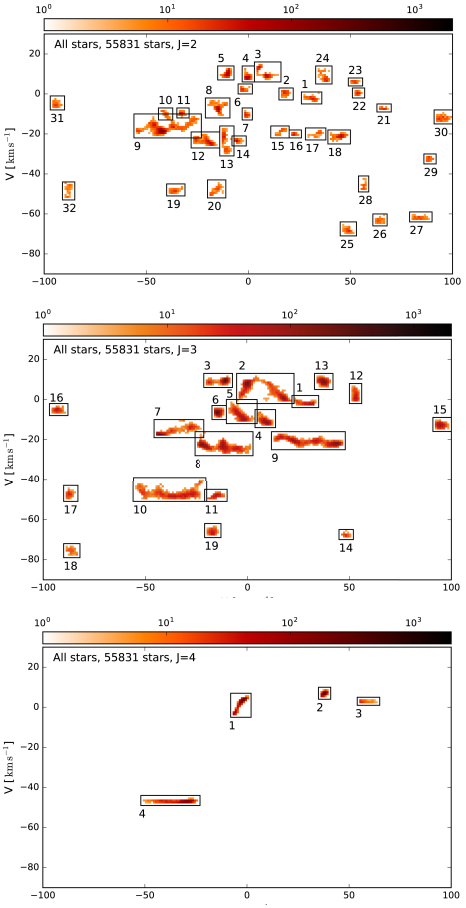


**Fig. 5.** Positions of kinematic stellar structures obtained by wavelet transform applied for $N_{MC} = 2000$ synthetic data samples for levels $J = 2, 3, 4$.

### 4.3. Output data

Following the computations described in Sect. 3 and MC simulations as in Sect. 4.2, the wavelet analysis was applied to these $N_{MC}$ samples giving: (1) $N_{MC}$ sets of wavelet coefficients $\left[\left(w_1^1, w_2^1, ..., w_J^1\right), ..., \left(w_1^{N_{MC}}, w_2^{N_{MC}}, ..., w_J^{N_{MC}}\right)\right]$; (2) the multi-resolution support for $J$ scales and $N_{MC}$ simulations, which gives: $\left[\left(M_1^1, M_2^1, ..., M_J^1\right), ..., \left(M_1^{N_{MC}}, M_2^{N_{MC}}, ..., M_J^{N_{MC}}\right)\right]$; (3) positions of detected structures for $J$ scales and $N_{MC}$ simulations.

The results are presented in two different forms. First as a structure's position count map, in which the positions of the detected structures of each of the 2000 samples are superimposed (see Fig. 5). The detected structures are marked by black boxes. To quantify the "realness" of each group, the fraction of times each group was detected relative to the total number of simulations is calculated.

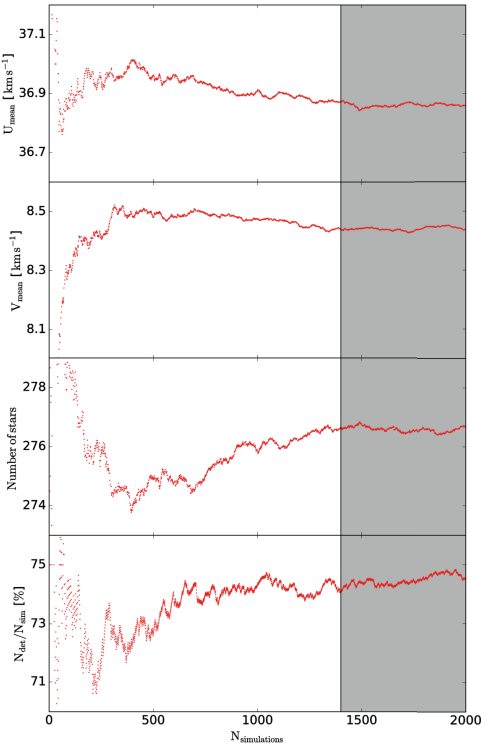


**Fig. 6.** Average position ($U_{mean}$, $V_{mean}$) (1 and 2 pattern *from the top*), estimation of the number of stars (*3 pattern from the top*) and percentage of detection of the moving group 13 from the total sample and $J = 3$ (*bottom pattern*), in function of the number of simulation.

Figure 5 shows the position count map for the detected structures at scales $J = 2$ (4–8 km s$^{-1}$, top plot), $J = 3$ (8–16 km s$^{-1}$, middle plot) and $J = 4$ (16–32 km s$^{-1}$, bottom plot). The highest number of individual structures, shown by black rectangles with individual numbers, is for $J = 2$. However, as can be seen, scale $J = 3$ also includes all significant structures detected at scales $J = 2$ and $J = 4$, and covers smaller and bigger scales.

How many Monte Carlo simulations are needed for the results to converge? To explore this, Fig. 6 shows how the positions for structure number 13 from the $J = 3$ map converge as the number of Monte Carlo simulations increases. We introduce four different estimators: the first two are mean positions of the structure $U_{mean}$ and $V_{mean}$ (calculated based on coordinates $U$ and $V$ of all structures inside the rectangle number 13); The third one is the number of stars inside structure number 13 which was calculated as an averaged number of stars from the total number of Monte Carlo simulations ($N_{MC}$ runs); The last estimator is the percentage of structure detection inside the rectangle. Convergence is reached at around 1400 simulations (marked by grey

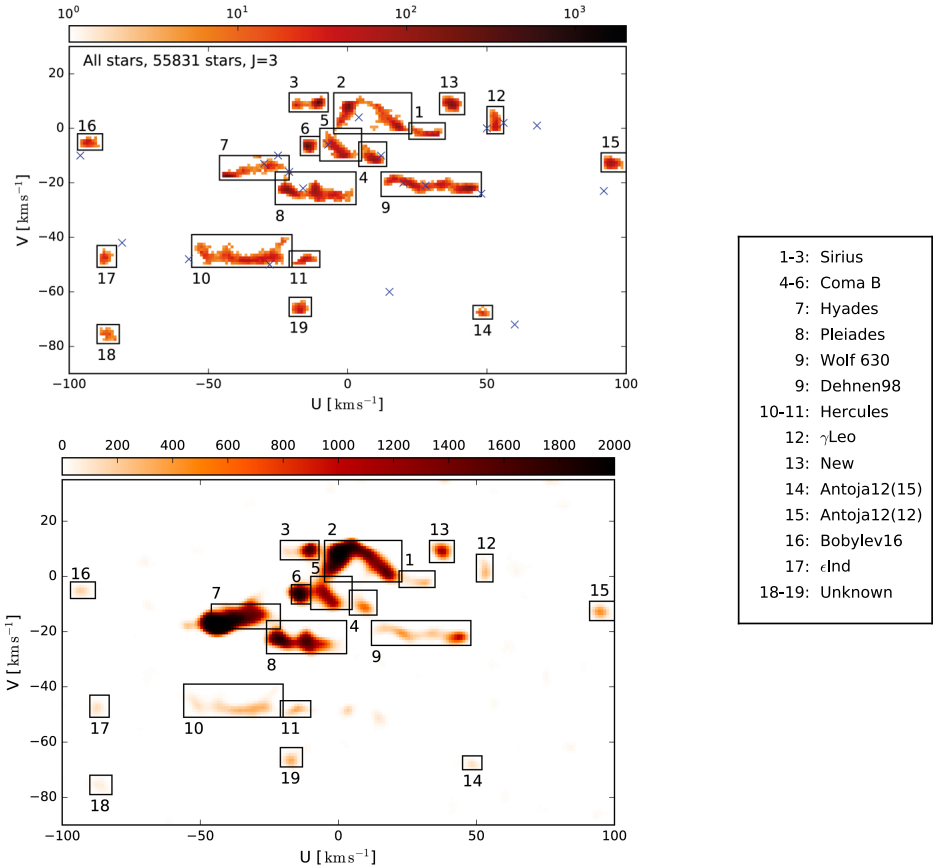


**Fig. 7.** *Top*: positions of kinematic stellar structures obtained by wavelet transform applied for $N_{\rm MC} = 2000$ synthetic data samples for $J = 3$ in the $U - V$ plane. Structure counts are shown with the orange colour. Black boxes embrace region of individual structures. Blue crosses show identification of structures in literature if any. *Bottom*: multi-resolution support count map for $N_{\rm MC} = 2000$ synthetic data samples for $J = 3$ in the $U - V$ plane. Black boxes represent the same structures as in the top plot.

background in Fig. 6). We therefore chose to run 2000 simulations to have confident results.

The position count map is useful for providing positions of structures. However, one cannot decipher whether if the structures are independent, or are connected to other groups. Hence, another way to represent the results is shown in the bottom plot of Fig. 7, and is the multi-resolution support for $N_{\rm MC}$ simulations by displaying the quantity $M_{\rm tot}$ defined as follows:

$$M_{{\rm tot},j}(i_x, i_y) = \sum_{k=1}^{N_{\rm MC}} M_j^k(i_x, i_y) \quad (1)$$

Thus, if $M_{{\rm tot},j}(i_x, i_y) = N_{\rm MC}$, then $w_j(i_x, i_y)$ is significant for all the simulations. Conversely, if $M_{{\rm tot},j}(i_x, i_y) = 0$, then $w_j(i_x, i_y)$ is never significant. We explain in more detail the results that can be gained from Fig. 7 in Sect. 5.

## 5. Results

In this section we present the detected structures in the $U - V$ plane for the following samples: the full TGAS-RAVE sample, the sample split into a nearby and a distant sample, and two chemically defined samples that to a first degree represent the stars belonging to the Galactic thin and thick disks.

### 5.1. Full sample

Figure 5 shows detected structures in the $U - V$ planes for three different scales, $J = 2$ (4–8 km s$^{-1}$): 32 structures, $J = 3$ (8–16 km s$^{-1}$): 19 structures, and $J = 4$ (16–32 km s$^{-1}$): 4 structures. The $J = 3$ structures are listed in Table 1, and the structures from the $J = 2$ and $J = 4$ scales in Table 2. As can be

**Table 1.** $3\sigma$-significant kinematic structures detected for level $J = 3$, 8–16 km s$^{-1}$, $N_{MC} = 2000$.

| $N$ | Name | $U$ | $V$ | $\Delta U$ | $\Delta V$ | $\frac{N_d}{N_{MC}}$,% | $N_*$ | SN | BSN | D | TD |
|---|---|---|---|---|---|---|---|---|---|---|---|
| (1) | (2) | (3) | (4) | (5) | (6) | (7) | (8) | (9) | (10) | (11) | (12) |
| | | 55 831 | | | | | | 31 533 | 24 298 | 36 439 | 11 410 |
| 1 | Sirius | 30 | −3 | 3 | 1 | 31 | 434 | + | | + | + |
| 2 | Sirius | 0 | 8 | 7 | 3 | 154 | 4821 | + | + | + | + |
| 3 | Sirius | −11 | 9 | 3 | 1 | 83 | 879 | + | | + | |
| 4 | Coma B | 9 | −12 | 2 | 2 | 52 | 1102 | | + | | + |
| 5 | Coma B | −2 | −11 | 3 | 3 | 70 | 2753 | + | + | + | |
| 6 | Coma B | −15 | −7 | 1 | 1 | 79 | 673 | + | + | + | |
| 7 | Hyades | −44 | −18 | 6 | 2 | 90 | 2344 | + | | + | |
| 8 | Pleiades | −22 | −23 | 7 | 3 | 170 | 4257 | + | + | + | |
| 9 | Wolf630+Dehnen98 | 43 | −22 | 9 | 2 | 168 | 1777 | + | | + | |
| 10 | Hercules | −38 | −49 | 9 | 3 | 116 | 1451 | + | | + | |
| 11 | Hercules | −16 | −48 | 2 | 1 | 22 | 197 | + | | + | |
| 12 | $\gamma$Leo | 52 | 0 | 1 | 2 | 27 | 96 | + | | + | |
| 13 | New | 37 | 8 | 2 | 2 | 74 | 201 | + | | + | + |
| 14 | Antoja12(15) | 48 | −68 | 1 | 1 | 6 | 8 | + | | + | |
| 15 | Antoja12(12) | 94 | −13 | 1 | 1 | 38 | 10 | + | | + | |
| 16 | Bobylev16 | −94 | −5 | 1 | 1 | 17 | 14 | + | + | + | + |
| 17 | $\epsilon$Ind | −88 | −48 | 2 | 2 | 12 | 24 | + | | | |
| 18 | Unknown | −86 | −76 | 2 | 1 | 8 | 12 | + | | | |
| 19 | Unknown | −18 | −67 | 1 | 1 | 22 | 70 | + | | + | |

**Notes.** Columns 1–8 are for the total sample. Column 1 gives the order of positions of wavelet coefficients for $J = 3$ obtained for 2000 synthetic data samples. Column 2 is the name of the structure if available in literature. Columns 3 and 4 are central positions of kinematic structures in km s$^{-1}$, their uncertainties (standard deviations) are given in Cols. 5 and 6 respectively also in km s$^{-1}$. Column 7 is a percentage showing how many times the structure obtained by MC simulations appears in the wavelet space. The estimated number of stars in each group is given in Col. 8. Columns 9–12 show the presence of the structure in the SN, BSN, D and TD samples for $J = 3$ with + sign. Number of stars of each data sample is indicated in the row 3. Question marks correspond to tentatively new structures with a small detection percentage in MC simulation.

seen, $J = 3$ appears to cover all the detected features, including smaller structures at $J = 2$, as well as larger groups at $J = 4$. Therefore, we will from now on consider $J = 3$ as the main scale since it covers a range around the typical sizes of kinematic structures found in the solar neighbourhood (both small- and large-scale structures), and secondly focus on $J = 2$ and $J = 4$ that cover even smaller and larger structures, respectively.

The top plot of Fig. 7 shows again the detected kinematic structures in the $U - V$ plane for $J = 3$ (as in Fig. 5 middle plot), but now with previously detected structures found in the literature (Eggen 1996; Antoja et al. 2008, 2012; Bobylev & Bajkova 2016) marked with blue crosses. Classical structures such as Sirius (structures number 1–3 in Fig. 7), Coma Berenices (structures 4–6), Hyades (structure 7), Pleiades (structure 8), and Hercules (structures 10–11), and some smaller structures like Wolf 630 (structure 9), Dehnen98 (structure 9), $\gamma$Leo (structure 12) can be easily recognised. They all have a comparably high percentage of detection (Col. 7 in Table 1) and large number of stars (Col. 7 in Table 1). The two structures from Antoja et al. (2012; structures 14 and 15) and one structure from Bobylev & Bajkova (2016; structure 16) are confirmed. We also present evidence for a new structure (number 13) that is detected with 74% significance. Structures 18–19 have low percentages of detection, less than15%, and might be insignificant. In Sect. 5.4 we discuss how our results agree with those from the literature.

The way the detected structures are split into groups is demonstrated with the bottom of Fig. 7 which shows the multi-resolution support obtained for $J = 3$ for all stars and 2000 Monte Carlo simulations. In other words, this is the same plot as the top panel of Fig. 7, but instead of structure counts we show multi-resolution support counts. This representation allows us to see whether structures are bound or separated. Structures 1–3 seem to be connected and thus are united into Sirius stream. Group 5 is bound to structure 2 in the wavelet case. It should not be associated with the Sirius stream as its most significant part is located slightly aside Sirius, but lays on one line with structures 4 and 6, therefore grouping structures 4–6 into the Coma Berenices stream. Groups that have percentage detection higher than 100% (8, 9, 10) show a few distinct peaks in this plot, supporting the statement that these groups consist of a few smaller structures that overlap in the structure count map. Based on that

**Table 2.** Kinematic structures detected in the solar neighbourhood for levels $J = 2$ and $J = 4$, $N_{MC} = 2000$.

| N | Name | $U$ | $V$ | $\Delta U$ | $\Delta V$ | $\frac{N_d}{N_{MC}}$, % | $N_*$ |
|---|---|---|---|---|---|---|---|
| (1) | (2) | (3) | (4) | (5) | (6) | (7) | (8) |
| | | | $J = 2$, 4–8 km s$^{-1}$ | | | | |
| 1 | Sirius | 31 | −3 | 2 | 1 | 12 | 285 |
| 2 | Sirius | 17 | 0 | 1 | 1 | 10 | 377 |
| 3 | Sirius | 8 | 9 | 3 | 2 | 23 | 1105 |
| 4 | Sirius | −1 | 7 | 1 | 1 | 18 | 511 |
| 5 | Sirius | −11 | 9 | 1 | 1 | 23 | 496 |
| 6 | Sirius | −3 | 2 | 1 | 1 | 7 | 459 |
| 7 | Coma B | −2 | −11 | 1 | 1 | 7 | 377 |
| 8 | Coma B | −15 | −8 | 3 | 2 | 26 | 1692 |
| 9 | Hyades | −43 | −19 | 8 | 3 | 108 | 3392 |
| 10 | Hyades | −41 | −11 | 1 | 1 | 5 | 257 |
| 11 | Hyades | −33 | −10 | 1 | 1 | 7 | 243 |
| 12 | Pleiades | −19 | −25 | 3 | 1 | 30 | 1262 |
| 13 | Pleiades | −12 | −22 | 1 | 3 | 20 | 1181 |
| 14 | Pleiades | −6 | −24 | 1 | 1 | 8 | 342 |
| 15 | Wolf 630 | 16 | −18 | 2 | 1 | 6 | 430 |
| 16 | Wolf 630 | 22 | −21 | 1 | 1 | 6 | 153 |
| 17 | Dehnen98 | 34 | −20 | 2 | 1 | 6 | 252 |
| 18 | Dehnen98 | 45 | −22 | 2 | 1 | 10 | 193 |
| 19 | Hercules | −36 | −49 | 2 | 1 | 9 | 178 |
| 20 | Hercules | −19 | −51 | 2 | 2 | 10 | 266 |
| 21 | $\gamma$ Leo | 66 | −8 | 1 | 1 | 5 | 14 |
| 22 | $\gamma$ Leo | 53 | 0 | 1 | 1 | 7 | 40 |
| 23 | $\gamma$ Leo | 52 | 5 | 1 | 1 | 5 | 40 |
| 24 | New | 38 | 6 | 2 | 2 | 12 | 201 |
| 25 | Antoja12(15) | 49 | −69 | 1 | 1 | 9 | 12 |
| 26 | Antoja12(15) | 63 | −64 | 1 | 1 | 7 | 5 |
| 27 | Antoja12(15) | 83 | −62 | 1 | 1 | 9 | 5 |
| 28 | Antoja12(15) | 56 | −48 | 1 | 1 | 5 | 20 |
| 29 | Antoja12(12) | 88 | −32 | 1 | 1 | 6 | 5 |
| 30 | Antoja12(12) | 93 | −13 | 1 | 1 | 14 | 10 |
| 31 | Bobylev16 | −95 | −6 | 1 | 1 | 8 | 11 |
| 32 | $\epsilon$Ind | −89 | −52 | 1 | 2 | 7 | 20 |
| | | | $J = 4$, 16–32 km s$^{-1}$ | | | | |
| 1 | Sirius | −3 | 3 | 2 | 3 | 97 | 1767 |
| 2 | New | 38 | 7 | 1 | 1 | 60 | 106 |
| 3 | $\gamma$Leo | 55 | 2 | 2 | 1 | 8 | 29 |
| 4 | Hercules | −32 | −48 | 7 | 1 | 100 | 437 |

**Notes.** For details see Table 1.

we split group 9 into Wolf 630 (to the left) and Dehnen98 (to the right). Group 11 is a part of the Hercules stream. Structures 12–19 are not connected to other groups.

### 5.2. solar neighbourhood and beyond samples

The detected structures are found in velocity space. Do they depend on the distance from the Sun? We divide the sample into a nearby solar neighbourhood sample with 31 533 stars that have distances $d < 300$ pc (SN), and a sample of stars beyond the solar neighbourhood (BSN), with 24, 298 stars that have $d > 300$ pc (most distant star at 2 kpc). The distance of $d = 300$ pc that was arbitrarily chosen to split the sample is also a reasonable value because it leaves us with almost equal number of stars in both samples. Both samples are then independently analysed in the same way as for the full sample: applying the wavelet transform,

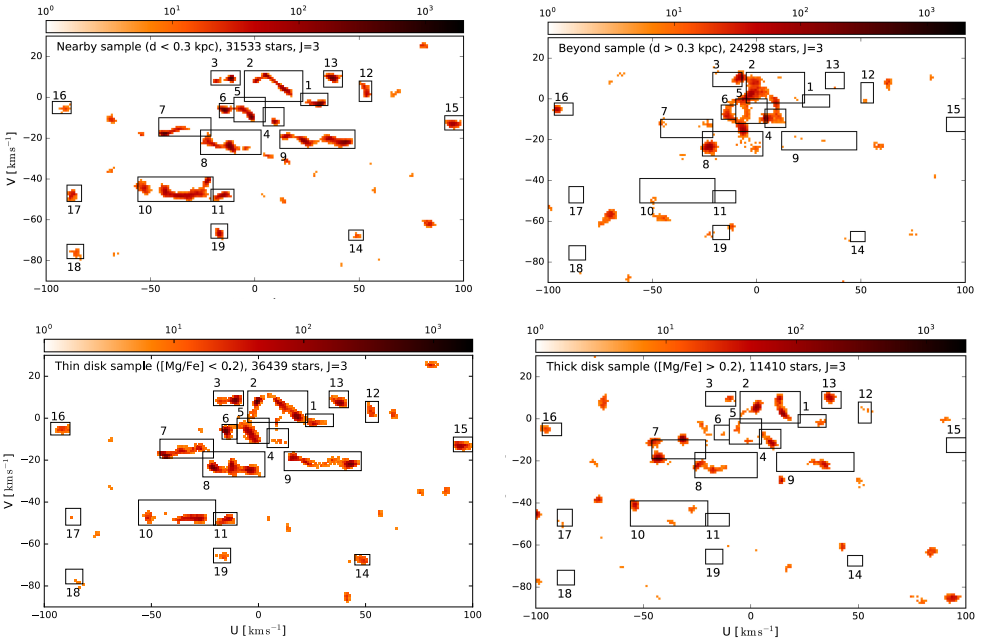


**Fig. 8.** Positions of kinematic stellar structures obtained by wavelet transform applied for $N_{MC}$ = 2000 synthetic data samples for level $J$ = 3. The *top left plot* is for the SN sample (31 533 stars), *top right* is for the BSN sample (24 298 stars), *bottom left* is for the D sample (36 439 stars) and *bottom right* is for the TD sample (11 410 stars). Black boxes indicate regions of detected structures for the total sample and $J$ = 3.

filtering, and structure-detection procedure for 2000 synthetic data samples.

Figure 8 shows the detected structures associated with the SN sample (top left plot), and the BSN sample (top right plot) for the scale $J$ = 3. The rectangles mark the borders for the structures that were detected for the full sample (see Fig. 7). This allows an easier comparison how the shapes on kinematic structures change with the respect to the full sample.

In Table 1 we have indicated "+" signs in Cols. 9 and 10 with if a structure is present in SN and BSN samples. Almost of all of the full sample structures are observed in the SN except two weak Hyades peaks (groups 10, 11). Therefore, the SN results almost completely reproduce the results from the full sample. For the BSN sample that has 7000 less stars than the SN sample, most structures appear to have slightly changed their positions relative to the SN case. A similar result was obtained by Antoja et al. (2012) where the structures detected in distant regions were shifted on the velocity plane. Hence, only 6 of 19 kinematic groups can be recognised: strong Sirius peak 2, all Coma B peaks (4–6), Bobylev16 peak 16, and Pleiades peak 8 are slightly shifted.

In summary, it appears that some kinematic structures are located only in the SN sample as a few significant groups are not detected in the BSN sample at all (groups 1, 3, 7, 9–15, 17–19). These changes in the number of structures, their positions and shapes in the respect to distance, could be due to the different in the number of stars falling into the two samples with the SN sample containing 10 000 more stars than the BSN sample. The technique of wavelet analysis is sensitive to the number of stars in the initial sample; the more stars we have, the more realistic is the picture of structures that we can get. Mean values of velocity uncertainties for two samples are also slightly different and are bigger in the case of the BSN sample: $\langle\sigma_U\rangle_{SN}$ = 1.7, $\langle\sigma_V\rangle_{SN}$ = 1.6 for the SN sample; $\langle\sigma_U\rangle_{BSN}$ = 2.5, $\langle\sigma_V\rangle_{BSN}$ = 2.2 for the BSN sample. Meaning that for the BSN sample, which is at the same time smaller, velocity uncertainties are slightly higher and this can lead to some displacements of the structures. This issue can be investigated further with the availability of the *Gaia* DR2 in April 2018 which will provide precise astrometric parameters for $10^9$ stars and radial velocities for bright stars.

### 5.3. Thin and thick disk structures

Several high-resolution spectroscopic studies of nearby stars have identified and characterised the thin and thick disks as distinct stellar populations, not only in terms of kinematics, but also in terms of elemental abundances and stellar ages (e.g. Reddy et al. 2006; Fuhrmann 2008; Adibekyan et al. 2012; Bensby et al. 2014). The two co-existing and largely overlapping disk populations point to a complex formation history for the Milky Way. A process which is currently not well understood. The question is, can we gain further insights into the nature and origin of this two-disk structure from the kinematic structures seen in the solar neighbourhood?

As shown in Bensby et al. (2014) and Haywood et al. (2013) stellar ages appear to be the best discriminator between the thin and thick disks. However, stellar ages are not available for the stars in our sample. Another way would be to use kinematics, as this is exactly the property that we want to investigate. Another approach which can reveal more features of the kinematic grouping associated with the thin and thick disks is to use their chemical compositions. Several papers have shown that the two disks follow distinct and well separated abundance trends both in the solar neighbourhood (e.g. Bensby et al. 2014; Adibekyan et al. 2012; Fuhrmann 2008) and also further away (Bensby et al. 2011; Hayden et al. 2015). All these studies show that thick disk stars, at a given metallicity, are more $\alpha$-enhanced than thin disk stars.

In this paper we do not perform any spectroscopic analysis of our structures. Instead we separate our stellar sample by magnesium [Mg/Fe] abundances provided by RAVE in order to study our sample in terms of thick (metal-poor) and thin (metal-rich) disks.

In Fig. 9 (see the last plot on the right-hand side on the bottom line) we show [Mg/Fe]-[Fe/H] diagram for the total RAVE sample of 47 849 stars that have RAVE $S/N > 40$. The last limit is needed to obtain abundances with a higher precision (abundance uncertainties less that 0.2 dex, Kunder et al. see 2017). A chemical separation of thick and thin disks with RAVE based on probability density approach has been done in Wojno et al. (2016) and we define a thin disk sample (D) and a thick disk sample (TD) samples according their criteria: thin disk [Mg/Fe] $<$ 0.2, thick disk [Mg/Fe] $>$ 0.2. This separation is shown by the red horizontal line in all plots of Fig. 9. Effective ranges of disk metallicities obtained for a RAVE sample by Wojno et al. (2016) are the following: $-0.27 <$ [Fe/H] $< 0.38$ for an $\alpha$-poor component (thin disk) and $-1.15 <$ [Fe/H] $< -0.05$ for an $\alpha$-enhanced component (thick disk). The metallicity distribution function for the total sample reaches the maximum value at [Fe/H] $\approx -0.1$, which is close to the disk separation values, hence, the total sample represents a mixture of disk populations. In the thin disk sample we have 36 439 stars, and in the thick disk sample there are 11 410 stars. As in the case with SN and BSN samples, we run the same procedure as for the full sample and the SN and BSN samples (i.e. applying the wavelet transform, filtering, and structure detection procedure for 2000 synthetic data samples).

Uncertainties for both [Fe/H] and [Mg/Fe] from RAVE are stated to be around 0.2 dex (see Kunder et al. 2017), which is comparably large to make a clear separation of the two disks. The separation line shown in Fig. 9 is therefore only a first approximation to represent thick and thin disks. Better precision could be achieved with a detailed spectroscopic analysis of stars associated with kinematic structures to investigate which disk population do they belong to.

The bottom panels of Fig. 8 show the structures that were detected by applying wavelet transform to the 2000 synthetic samples associated with thick and thin disks, respectively. The rectangles correspond to the structures detected for the full sample at scale $J = 3$. In Table 1 Cols. 11 and 12 show a clear presence of the structure in T and TD with "+" sign.

Similarly to the SN sample, the thin disk sample (D) contains more stars, so most of the structures detected for the full sample can be recognised. Only groups 17 and 18 appear to be missing. Hyades and Pleiades groups 7 and 8 are more distinct in the D sample, but a few stars are also detected in the TD sample, so they could be a mixture of the two stellar populations. The Hercules stream is almost missing in the TD map, so that is probably constructed mostly of thin disk stars. The same result was obtained by Bensby et al. (2014) and Ramya et al. (2016) from a chemical abundances analysis of stars that belong to the Hercules (for more discussions see Sect. 5.4). Coma Berenices slightly changed its location in the TD case, being more significant in box 4. Groups 11, 12, 14, 15, 17–19 are not seen at all. These groups consist of mostly D stars which points towards their possible origin through the outer Lindblad resonance (OLR; for further explanations see Sect. 5.4).

In Fig. 9 we plot individually for each kinematic structure its [Mg/Fe] – [Fe/H] diagram and its metallicity distribution function which is a [Fe/H] versus a probability density, computed with the kernel density estimation (KDE) method. In each contour plot the positions of individual stars are shown as dots. The numbers in each panel indicate the numbers of the structures as listed in the legend to Fig. 7. The horizontal red line at each density plot corresponds to the [Mg/Fe] = 0.2 showing the approximate separation between the thin and thick disks. Black dashed lines at each histogram show the probability density distribution for the full sample of 47 849 stars with $S/N > 40$. The solid violet histogram at the top of each panel shows a probability density distribution for stars inside the current group. We discuss each structure in detail in the following section.

### 5.4. Individual structures

Each case contains an overview of what is known about each group from the literature and how it compares with the results from the present study. The number in parentheses at the beginning of each paragraph indicates the number of the structure as listed in Table 1 and shown in Figs. 7 and 8.

*Sirius* (1–3): Eggen (1992) studied the properties of the Sirius super-cluster, which is considered as a part of the larger Ursa Major stream. They found that its stars fall into two distinct age groups, 6.3 and 0.2 Gyr, and that its chemical composition differs from the Hyades and Pleiades open clusters, showing heavy element abundances close to solar values. Famaey et al. (2008) tried to reveal the origin of kinematic features including the Sirius stream by probing ages of stars that belong to the Sirius group and the evaporating Ursa Major star cluster. It was shown that only 30% of the stars associated with the stellar stream fall on the same isochrone (300 Myr) as the open cluster, and, as was concluded in Famaey et al. (2008), not all stars of Sirius stream have an origin of being a remnant of an open cluster and favour a dynamical (resonant) origin for the Sirius stream. Later, through modelling of the dynamics of the Milky Way, Minchev et al. (2010) showed that the low-velocity features including the Sirius stream could be reproduced with the OLR of the Galactic bar.

Bovy & Hogg (2010) studied the ages and metallicities of kinematic over-densities of nearby stars from HIPPARCOS ESA (1997) to investigate whether stellar streams consist of stars that belong to the same population, which could indicate that they originated from dissolved open clusters. Their main result was negative for the stellar streams they analysed, including the Sirius stream, and that it should not be associated with the Ursa Major open cluster. To test possible dynamical origins for the stellar streams (such as the OLR of the bar, or the inner Lindblad resonance (ILR) of the spiral structure) Bovy & Hogg (2010) used the Geneva-Copenhagen survey (Holmberg et al. 2009) to compare the metallicities of stellar stream stars to the background population of thin disk stars. Bovy & Hogg (2010) assume that depending on the type of the resonance, orbits of stellar groups are located most of the time inside or outside the solar circle,

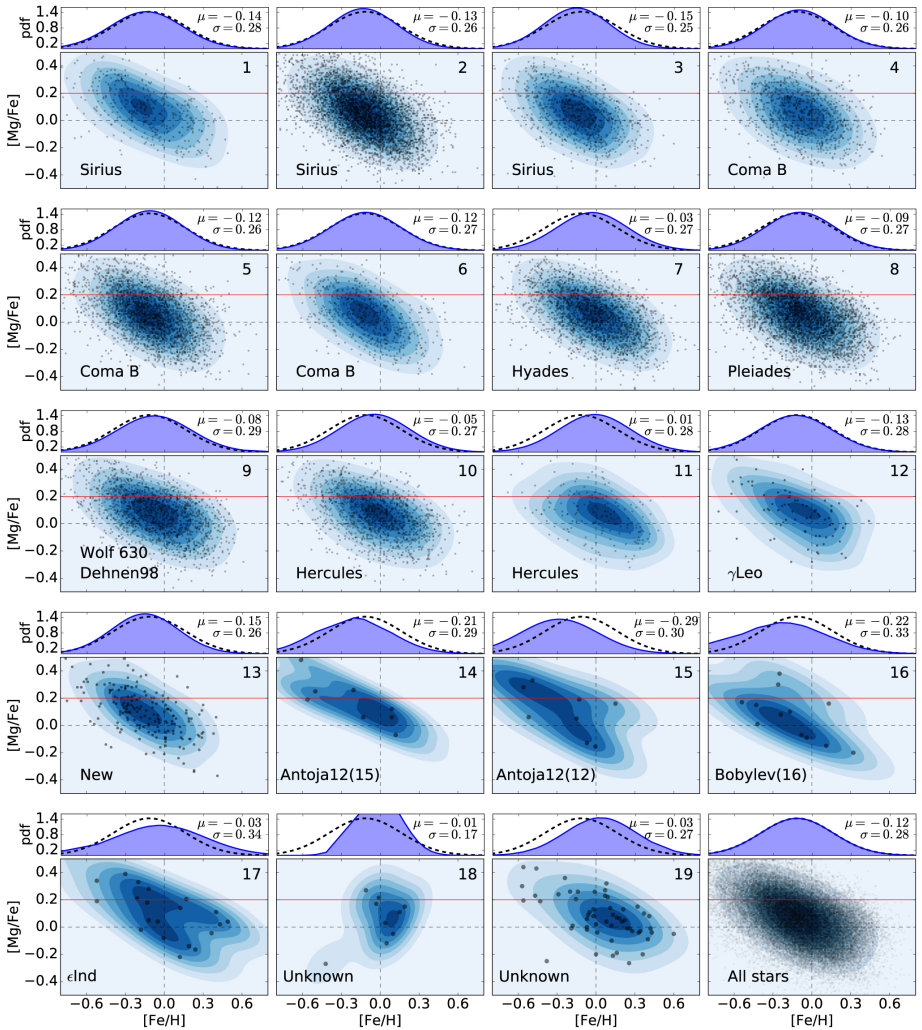


**Fig. 9.** [Mg/Fe]-[Fe/H] diagram for kinematic structures detected for the scale $J = 3$. Numbers on each panel correspond to structures 1–19 as stated in the legend of Fig. 7. The last plot corresponds to the total sample with limits on $S/N > 40$ (47 849 stars). The red line at each density plot corresponds to [Mg/Fe] = 0.2 and divides the total sample into thick (above the line) and thin (below the line) disks. Dashed black lines show [Fe/H] = 0 and [Mg/Fe] = 0. Scatter plots at each density map show positions of individual stars on the diagram. Histograms at the top of each panel show the metallicity distribution for the total sample (black dashed line) and for each group (solid violet distribution). Values of $\mu$ and $\sigma$ represent the violet distribution.

and, consequently, these stars show up the properties of different parts of the Galaxy. Metallicity is one of the main parameters that varies for kinematic groups that come from different parts of the Milky Way due to the existence of a metallicity gradient in the Galaxy. They found "weak evidence" that Sirius stream stars have lower metallicities than the thin disk population and could therefore be related to the ILR of the spiral arms.

We associate the Sirius stream with structures 1–3 (see Fig. 8). Sirius is elongated in both the $U$ and $V$ directions and is detected in all maps, although its shape and location vary from sample to sample. Structure 2 is the most significant sub-stream with more than 4800 stars located inside the "detection box", and 154% of Monte Carlo repeats. As the detection percentage exceeds 100% the structure may consist of a few smaller groups,

**Table 3.** Sirius positions.

| $(U, V)$ [km s$^{-1}$] | Reference |
|---|---|
| (30, −3) | group 1 |
| (0, 8) | group 2 |
| (−11, 9) | group 3 |
| (9, 3) | Dehnen (1998) |
| (15, 1) | Eggen (1992) |
| (10, 3) | Eggen (1996) |
| (7, 4) | Famaey et al. (2005) |
| (5, 2) | Famaey et al. (2008) |
| (10, 3) | Zhao et al. (2009) |
| (9, 4) | Bovy & Hogg (2010) |
| (4, 4) | Antoja et al. (2012) |

such as those detected at the scale $J = 2$ (see Fig. 5) that overlap with each other at the scale $J = 3$. In Table 3 we provide a table of positions of the Sirius stream from this work and from the literature and a blue cross in Fig. 7 corresponds to the Sirius group from Antoja et al. (2012).

Our central peak 2 agrees with all the studies listed. Group 1 has a higher $U$ velocity and group 3 a lower $U$ velocity compared to the central peak but all have approximately the same $V$ velocity, so they could be members of one larger stream. Sirius is a nearby structure, while only stars from group 2 also appear in the distant BSN sample. Most of the stars appear to have chemical compositions comparable to what is observed for the Galactic thin disk stars, but group 2 is still strong in the thick disk sample. So Sirius could be a mixture of stars from both disk populations.

Plots 1–3 in Fig. 9 show the [Mg/Fe] – [Fe/H] diagrams for stars from groups 1–3 that we associate with the Sirius stream and at the top of each panel the metallicity distribution for each individual group is shown (solid violet distribution). The Sirius stream stars appear to have properties similar to the total sample (black dashed histogram) and do not show any particular metallicity trend inherent to the thick or thin disk populations.

Figure 8 also indicates that the Sirius stream is a large-scale structure that is observed in both SN and BSN samples and appears to be a mixture of both disk populations. Since we observe Sirius in both disks, we favour its dynamical origin possibly from the ILR of the spiral arms, but note that our thin/thick disk separation is uncertain due to the rather large errors in the RAVE chemical abundance ratios.

*Coma Berenices* (4–6): Odenkirchen et al. (1998) carried out an astrometric and photometric analysis of the region of the sky where the Coma Berenices open star cluster is located and found that the luminosity function of the core of the cluster decreases, while it increases towards fainter magnitudes in the edges of the cluster. Odenkirchen et al. (1998) assume that there could be a lot of faint, low-mass members of the moving group that were not observed. The proximity of the moving group and the open cluster pointed Odenkirchen et al. (1998) towards the idea that Coma Berenices moving group was formed due to a dissolution of the cluster. Conversely, (Minchev et al. 2010) through modelling of the dynamics of the Milky Way, reproduced a few main stellar streams including Coma Berenices assuming the OLR of the bar and thus, favour resonant mechanism of formation of also this kinematic over-density.

Table 4 lists the detection of the Coma Berenices kinematic over-density in the $U - V$ plane that is available in the literature.

**Table 4.** Coma Berenices positions.

| $(U, V)$ [km s$^{-1}$] | Reference |
|---|---|
| (9, −12) | group 4 |
| (−2, −11) | group 5 |
| (−15, −7) | group 6 |
| (−10, −5) | Dehnen (1998) |
| (−10, −10) | Famaey et al. (2007) |
| $(-11, -7)_d$ | Zhao et al. (2009) dwarf sample |
| $(-13, -6)_g$ | Zhao et al. (2009) giant sample |
| (−7, −6) | Antoja et al. (2012) |
| (−7, −6) | Bobylev & Bajkova (2016) |

In our study Coma Berenices is associated with structures 4–6 (see Fig. 8) and Table 4 shows that the positions we detect are in agreement with results from the other studies.

All three groups 4–6 share similar space velocities. Peak 6 has higher detection percentage in Monte Carlo simulations (79%) than peaks 4 and 5. While group 5 is the biggest and contains over 2700 stars inside the "detection box". The blue cross inside box 5 in Fig. 7 corresponds to the detection of Coma Berenices from Antoja et al. (2012) at (−7, −6) km s$^{-1}$.

Plots 4–6 in Fig. 9 show the [Mg/Fe] – [Fe/H] diagrams and metallicity histograms (at the top of each plot) for groups 4–6. Coma Berenices stream stars show metallicity properties similar to the total sample, and do not show any particular metallicity trend to either the thick or the thin disks. Figure 8 shows a similar result: Coma Berenices unites stars that belong to both thin and thick disk samples with more stars in the thin disk sample. It is a large-scale over-density because it is seen in both distance samples.

As Coma Berenices shares properties similar to the Sirius moving group, both combining stars of different populations, it could also originate from the ILR of the spiral arms, again with the remark that the thin/thick disk separation is uncertain due to the low precision of the RAVE abundances.

*Hyades* (7): Being first discovered by Proctor (1869), the Hyades stream, or Hyades super-cluster, was for a long time considered to be a remnant of the eponymous Hyades open stellar cluster. However, recent studies have shown the opposite. For instance, Famaey et al. (2008) found that only half of the stars of the Hyades stream could originate from the Hyades open cluster as only about 50% of the stars fall onto the same isochrone as would have been expected for an open cluster. They favour the dynamical origin for the Hyades stream.

Later, Pompéia et al. (2011) compared chemical abundances and metallicities of stars belonging to Hyades stream with stars that are members of the Hyades open cluster, which is believed to be chemically homogeneous. It was found that only 2 of the 21 selected Hyades stream stars have similar chemical properties with the open cluster. Furthermore, Pompéia et al. (2011) showed that the Hyades stream stars have a metallicity excess of about 0.06–0.15 dex compared to thin disk stars, which is consistent with an origin caused by the ILR of the spiral arms. They also performed a particle simulation test that supported the same conclusion, showing that the Hyades stream could be reproduced with the 4:1 resonance of the spiral arms.

Another chemical tagging study of the Hyades stream was presented by Tabernero et al. (2012) that further supported the idea of a dynamical origin for the Hyades stream. They analysed

**Table 5.** Hyades positions.

| $(U, V)$ [km s$^{-1}$] | Reference |
|---|---|
| $(-44, -18)$ | group 7 |
| $(-40, -20)$ | Dehnen (1998) |
| $(-35, -18)$ | Famaey et al. (2008) |
| $(-38, -18)_d$ | Zhao et al. (2009) dwarf sample |
| $(-38, -17)_g$ | Zhao et al. (2009) giant sample |
| $(-40, -20)$ | Bovy & Hogg (2010) |
| $(-30, -13)$ | Antoja et al. (2012) |
| $(-30, -15)$ | Bobylev & Bajkova (2016) |

**Table 6.** Pleiades positions.

| $(U, V)$ [km s$^{-1}$] | Reference |
|---|---|
| $(-22, -23)$ | group 8 |
| $(-12, -22)$ | Dehnen (1998) |
| $(-12, -21)$ | Eggen (1996) |
| $(-16, 23)$ | Famaey et al. (2008) |
| $(-12, -23)_d$ | Zhao et al. (2009) dwarf sample |
| $(-15, -23)_g$ | Zhao et al. (2009) giant sample |
| $(-15, -20)$ | Bovy & Hogg (2010) |
| $(-16, -22)$ | Antoja et al. (2012) |
| $(-13, -24)$ | Bobylev & Bajkova (2016) |

stellar spectra of 61 Hyades stream stars and compared the results with a reference star vB 153 that is a verified member of the Hyades open cluster. Only 26 stars were found to have similar parameters with the Hyades open cluster. Tabernero et al. (2012) conclude that the Hyades stream does not completely originate from the Hyades open cluster.

McMillan (2017) used a simple dynamical modelling of the Milky Way to study the origin of the Hyades stream and to check whether it could originate from a Lindblad resonance. The author concluded that Hyades stream has a resonant (dynamical) nature, but that it is not possible to say exactly which resonance due to selection effects associated with the dynamics.

We associate Hyades with group 7 (see Fig. 8). This group contains 2344 stars inside the detection box and has a high Monte Carlo detection of 90%. The blue cross in Fig. 7 marks the detection of Hyades from Antoja et al. (2012). In Table 5 we show positions of Hyades from this work and from the literature.

The [Mg/Fe] – [Fe/H] diagram and the [Fe/H] distribution for structure 7 is shown in Fig. 9. The Hyades stream shows properties that are similar to the full sample. From the analysis of SN/BSN and D/TD sub-samples (see Fig. 8) it is seen that Hyades stream sample mostly consists of nearby stars. It is also more distinct in the thin disk subsample, although the structure is detected in the thick disk subsample too. So, it appears as if the Hyades stream is nearby structure which consists of mixture of disk populations. This does not support the hypothesis for Hyades to be a dissolved open cluster as this theory implies all stars have a solid chemical composition and could have a dynamical origin. Again, the low precision of abundances given in RAVE should be taken into account.

*Pleiades* (8): The Pleiades was the first ever moving group to be discovered. Through observations of Pleiades open cluster, Mädler (1846) found a large number of stars located a few degrees from the cluster that were moving in the same direction (the Pleiades moving group). Its origin has been investigated in several studies. For example, Famaey et al. (2008) conclude that Pleiades moving group has a dynamical (resonant) origin, since only 46% of the moving group's stars fall onto the 100 Myr isochrone, the assumed age for the Pleiades open cluster.

Through galactic dynamics modelling, Minchev et al. (2010) reproduced stellar streams being due to the OLR. However, to be consistent with the number of stars in the Pleiades they assumed that the Milky Way bar was formed 2 Gyr ago. This paper stands against the idea that the Pleiades and the Hyades share a common dynamical origin. Bovy & Hogg (2010) analysed age and metallicity properties of the Pleiades moving group and found that it could not originate through a dissolved Pleiades open cluster as their stellar populations differ. Bovy & Hogg (2010) also compared the metallicity of the Pleiades and Hyades moving groups with the metallicity of the thin disk population and found similar metallicities for the Pleiades and the thin disk stars, while the Hyades shows a higher metallicity than the thin disk. Hence, also Bovy & Hogg (2010) does not support the idea of a common dynamical origin for Pleiades and Hyades.

We detect one large structure that we associate with Pleiades, group 8 in Fig. 8. This group could consist of a few separate groups that overlap since the percentage of detection in Monte Carlo simulations is 170%. Interestingly, at the $J = 2$ scale the Pleiades detection consists of three separate structures, numbers 12–14 (see Fig. 5). Group 8 (in the $J = 3$ scale) is one of the largest groups with about 4200 stars inside the detection box. Table 6 gives the positions for Pleiades stream from this work and from the literature. The blue cross corresponding to Pleiades in Fig. 7 refers to the detection by Antoja et al. (2012).

Plot 8 in Fig. 9 shows the [Mg/Fe] – [Fe/H] diagram as well as the [Fe/H] histogram for the Pleiades stars. The metallicity distribution is almost equal to the full sample. The structure that we associate with the Pleiades does not have any particular distance or abundance dependence as it is observed in both SN/BSN, and both D/TD samples (see Fig. 8). The structure has a higher detection percentage for the thin disk sample, but this could be because the thin disk sample contains three times as many stars than the thick disk sample. The position and the shape of Pleiades group do not vary much between the different sub-samples leading us to the conclusion that it is a large-scale structure, composed of a mixture of different populations of stars. Thus, as it appears to be chemically inhomogeneous; unlike open clusters and moving groups, it could originate from the ILR of the spiral arms and not from the Pleiades open cluster. Again, a better thin/thick disk separation could be achieved with more precise chemical abundances than those provided by RAVE.

*Hercules* (10–11): Being the largest and the most elongated structure in the $U$ direction, the origin of the Hercules stream has been investigated by many authors. For example, Dehnen (2000) favour a hypothesis that Hercules stream is a dynamical feature caused by the Galactic bar resonances (the OLR). Chakrabarty (2007) showed that a combined dynamical effect of spiral arms and a Galactic bar can explain main kinematic structures including the Hercules. Bensby et al. (2007) performed a detailed chemical characterisation of its stars. They favour a dynamical origin through the Galactic bar as the Hercules stream stars appeared to be a mixture of thick and thin disk stars. Also Bovy & Hogg (2010) investigated whether or not moving groups consist of a homogeneous population of stars; the result was

**Table 7.** Hercules stream positions.

| $(U, V)$ [km s$^{-1}$] | Reference |
|---|---|
| $(-38, -49)$ | group 10 |
| $(-16, -48)$ | group 11 |
| $(-30, -50)$ | Eggen (1996) |
| $(-42, -51)$ | Famaey et al. (2005) |
| $(-35, -51)$ | Famaey et al. (2008) |
| $(-32, -48)_d$ | Zhao et al. (2009) dwarf sample |
| $(-35, -51)_g$ | Zhao et al. (2009) giant sample |
| $(-20, -33)$ | Bovy & Hogg (2010) |
| $(-57, -48)_I$ | Antoja et al. (2012) |
| $(-28, -50)_{II}$ | Antoja et al. (2012) |
| $(-57, -48)_I$ | Bobylev & Bajkova (2016) |
| $(-35, -50)_{II}$ | Bobylev & Bajkova (2016) |

**Notes.** [(†)] *I* and *II* mark sub-streams found in the structure.

negative and they further found indications that Hercules stream stars have a higher average metallicity than the local thin disk, and concluded that it could be a structure caused by the OLR of the Galactic bar. Later, Bensby et al. (2014) re-examined the chemical composition of the Hercules stream and found that it mainly consists of stars that chemically can be associated with both the thin and thick disks. Ramya et al. (2016) on the other hand studied 58 Hercules stream red giants and found that they are mostly metal-rich stars from the thin disk. The somewhat discrepant results could be explained by the use of different target-selection methods in the two studies.

Pérez-Villegas et al. (2017) carried out a dynamical modelling of the Hercules stream "in the framework" of a slow bar and compared obtained results with data from the RAVE and LAMOST catalogues. They found that Hercules is more prominent in the Galactic inner disk and should consist, on average, of more metal-rich and older stars compared to the solar negihbourhood.

Hercules is identified as structures 10 and 11 in this study (see Fig. 8). This kinematic structure is the most elongated feature in the $U$ direction and has a detection percentage for group number 10 that exceeds 100%. An explanation of this result is that it appears to consist of a few separate structures that overlap in the Monte Carlo simulations (see the $J = 2$ scale in Fig. 5, where Hercules is detected as the two peaks number 19 and 20. The blue crosses in Fig. 7 (one is inside the Hercules box 10 and another is just outside on the left-hand side) mark the results from Antoja et al. (2012). Table 7 gives the positions of the Hercules stream from this work and from the literature.

The $(U, V)$ velocities of groups 10 and 11 are in agreement with most of the previous studies except Bovy & Hogg (2010), whose position differs from others by about 10 km s$^{-1}$. Antoja et al. (2012) and Bobylev & Bajkova (2016) defined two sub-streams in the Hercules, we have only one centred peak, but the size of the structure covers both of them.

Panels 10 and 11 in Fig. 9 correspond to the Hercules stream and show its metallicity distribution and [Mg/Fe] – [Fe/H] diagram. It appears to contain more metal-rich stars, and is also clearly a thin disk structure located in the nearby sample as it is observed only in the SN sample (see Fig. 8). Our results support recent findings that the Hercules stream mainly belongs to the thin disk population and could be due to the OLR of the Galactic bar.

**Table 8.** Wolf 630 positions.

| $(U, V)$ [km s$^{-1}$] | Reference |
|---|---|
| $(43, -22)$ | group 9 |
| $(23, -33)$ | Eggen (1965) |
| $(28, -21)$ | Antoja et al. (2012) |
| $(29, -21)$ | Bobylev & Bajkova (2016) |

*Wolf 630* (9): Wolf 630 was first identified by Eggen (1965) and its origin is still unclear. Bubar & King (2010) analysed spectra of 34 stars of the Wolf 630 stream and 19 stars were found to be chemically homogeneous. This sub-sample of 19 stars was fitted with a 2.7 Gyr isochrone and a metallicity of [Fe/H] = −0.01. Bubar & King (2010) suggest that the sub-sample of 19 stars could be a remnant of an open cluster since its stars share similar features, but the rest of the sample is inhomogeneous, which makes the origin of Wolf 630 uncertain.

We identify Wolf 630 as the group 9 (see Fig. 8). It has a 168% Monte Carlo detection rate and 1777 stars of our sample can be associated within the group. At the $J = 2$ scale the same region of the $U - V$ plane consists of four individual groups. This could indicate that group 9 consists of at two structures that overlap: Wolf 630 and Dehnen98 (to be discussed below). The result from Antoja et al. (2012) is marked by the blue cross inside structure 9 (see Fig. 7). Table 8 gives positions of Wolf 630 obtained in this work and from the literature.

Our $U$-component differs from other works by at least 10 km s$^{-1}$. This could mean that box 9 corresponds to at least two independent groups and thus its position represents mean coordinates for both groups. Plot 9 in Fig. 9 corresponds to the Wolf 630 stream and shows its metallicity distribution and [Mg/Fe]−[Fe/H] diagram. It has metallicity properties very similar to the full sample, but perhaps with a few more metal-rich stars. Based on the analysis of SN/BSN and D/TD sub-samples in Fig. 8, Wolf 630 appears to be a thin disk structure belonging to the nearby sample. It could have a resonant origin, again considering the uncertainties of the RAVE abundances that render the disk separation less reliable.

*Dehnen98* (9): This structure is detected inside box 9 in Fig. 8. It is a small kinematic group that was first discovered by Dehnen (1998) and was later confirmed by other studies (e.g. Antoja et al. 2012; Bobylev & Bajkova 2016). Antoja et al. (2008) found a group with the same $(U, V)$ coordinates, but after the analysis of the branch structure using modified equations, as was first proposed by Skuljan et al. (1999) to fit four branches of groups based on its motion, they concluded that the group could belong to the Coma Berenices stream. Antoja et al. (2012) subsequently detected a kinematic over-density which they associated with the Dehnen98 structure. This result is marked by a blue cross on the right-hand side of the box 9 in Fig. 7. Table 9 gives positions of this structure found in this work and from the literature.

Our detection of the Dehnen98 structure is in agreement with previous works. Dehnen98 has a very high percentage of detection in the MC simulations compared to other groups that we have detected: ∼168% MC repeats and it contains 1777 stars. The metallicity distribution and the [Mg/Fe] – [Fe/H] diagram of Dehnen98 are given in plot 9 in Fig. 9. Dehnen98 has similar metallicity properties to the total sample, with but more thin disk stars. From the analysis of Fig. 8, we can see that Dehnen98

**Table 9.** Dehnen98 positions.

| $(U, V)$ [km s$^{-1}$] | Reference |
|---|---|
| $(43, -22)$ | group 9 |
| $(50, -25)$ | Dehnen (1998) |
| $(48, -24)$ | Antoja et al. (2012) |
| $(43, -24)$ | Bobylev & Bajkova (2016) |

**Table 10.** $\gamma$Leo positions.

| $(U, V)$ [km s$^{-1}$] | Reference |
|---|---|
| $(52, 0)$ | group 12 |
| $(50, 0)$ | Dehnen (1998) |
| $(56, 2)_I$ | Antoja et al. (2012) |
| $(68, 1)_{II}$ | Antoja et al. (2012) |
| $(65, 1)$ | Bobylev & Bajkova (2016) |

**Notes.** *I* and *II* mark sub-streams found in the structure.

contains stars of different populations and belongs to the nearby sample. Concerning the assumption stated in Antoja et al. (2008) that Dehnen98 is part of a Coma Berenices branch, we can say that this group has similar properties with Wolf 630 and Coma Berenices streams, and they all could form to one large-scale structure that has a dynamical origin. A detailed chemical tagging of stars that belong to these groups is required to properly speculate on their origin.

*$\gamma$Leo* (12): This structure is shown as group 12 in Fig. 8, and has a relatively low detection percentage of 27% in the Monte Carlo simulations. It is rather small with only 96 stars from our sample. Figure 7 shows two blue crosses for this group from Antoja et al. (2012). Table 10 gives velocity positions of our detection of $\gamma$Leo together with those from the literature.

Group 12 is consistent with Dehnen (1998) and Antoja et al. (2012) peak *I*, while Bobylev & Bajkova (2016) is in agreement with structure II from Antoja et al. (2012). All the groups have similar $V$-velocities. Plot 12 in Fig. 9 shows the [Mg/Fe] – [Fe/H] diagram and the [Fe/H] distribution for group 12. The $\gamma$Leo stream shows metallicity properties similar to the total sample and it appears to be a nearby thin disk structure (see Fig. 8) with only a few stars in the TD sample. Thus, it could have formed via a dynamical mechanism.

*New* (13): Group 13 at $(37, 8)$ km s$^{-1}$ in Fig. 8 has 201 stars and a high detection level of 74% Monte Carlo repeats. We cannot find any previous detections in the literature of a structure at these coordinates, and we therefore identify this as a new structure. It appears to be a nearby structure and is detected in both the thin and the thick disk sub-samples. It is, however, not detected in the more distant BSN sample, which could be due to the smaller number of stars in the BSN sample compared to the SN sample. The metallicity distribution and [Mg/Fe] – [Fe/H] diagram for this new group 13 are shown in plot 13 in Fig. 9. This group contains stars of both disk populations. It could be an elongation of larger nearby streams such as Sirius or $\gamma$Leo, as their properties are similar. A more precise detailed chemical analysis of stars associated with these groups is required to more precisely probe the origin of the new group 13.

**Table 11.** Position of the new structure detected in this work.

| $(U, V)$ [km s$^{-1}$] | Reference |
|---|---|
| $(37, 8)$ | group 13 |

**Table 12.** Antoja12(15) positions.

| $(U, V)$ [km s$^{-1}$] | Reference |
|---|---|
| $(48, -68)$ | group 14 |
| $(60, -72)$ | Antoja et al. (2012) |
| $(72, -64)$ | Bobylev & Bajkova (2016) |

**Table 13.** Antoja12(12) positions.

| $(U, V)$ [km s$^{-1}$] | Reference |
|---|---|
| $(94, -13)$ | group 15 |
| $(92, -23)$ | Antoja et al. (2012) |
| $(91, -35)$ | Bobylev & Bajkova (2016) |

*Antoja12(15)* (14): This structure was first reported in Antoja et al. (2012) but was detected only at $2\sigma$ confidence level and needed further confirmation. In Fig. 7 it is shown as a blue cross close to the box 14. We received a $3\sigma$-significant group 14 which is 10 km s$^{-1}$ higher in $U$, but could be associated with the one detected in (Antoja et al. 2012). It has only 6% of Monte Carlo detection and accounts for eight stars. In Table 12 we show a list of positions we found in the literature for this structure and included our results.

This group appears clearly in the nearby and the thin disk sub-samples (see Fig. 9). Taking into account the low number of stars associated with this group it could not be observed in the BSN and TD samples as they consist of less stars than SN and D samples. The metallicity distribution and the [Mg/Fe] – [Fe/H] diagram for group 14 are shown in plot 14 in Fig. 8 and both point towards the thin disk population, which is coherent with the result from Fig. 9. The *Gaia* DR2 data will provide astrometric data for more stars, thus, one could verify whether this group is observed in the BSN and TD samples too. With the current results a dynamical origin seems favoured.

*Antoja12(12)* (15): This group was stated as new in (Antoja et al. 2012) and is marked by a cross in Fig. 7 close to structure 15. In this study, as in (Antoja et al. 2012), structure 15 was detected with a $3\sigma$-significance. Table 13 gives the positions for this group obtained in this work and from the literature.

Our group 15 shares the same $U$ velocity as in the other studies, but differs in $V$ direction by $-10$ km s$^{-1}$ compared to (Antoja et al. 2012). Interestingly, Bobylev & Bajkova (2016) obtained a structure which also differs by 10 km s$^{-1}$ in the $V$ direction, but in the negative direction. It could be the same structure as it is located in the low-density region of the $U - V$ map, so it cannot be affected by other stronger streams. Antoja12(12) has a 38% detection in the Monte Carlo simulations and includes only ten stars. Group 15 appears to be a thin disk structure mainly present in the nearby sample (see Fig. 8). The

**Table 14.** Bobylev16 positions.

| $(U, V)$ [km s$^{-1}$] | Reference |
|---|---|
| $(-94, -5)$ | group 16 |
| $(-96, -10)$ | Bobylev & Bajkova (2016) |

**Table 15.** $\epsilon$Ind positions.

| $(U, V)$ [km s$^{-1}$] | Reference |
|---|---|
| $(-88, -48)$ | group 17 |
| $(-81, -42)$ | Antoja et al. (2012) |
| $(-90, -49)$ | Bobylev & Bajkova (2016) |

metallicity distribution and [Mg/Fe] – [Fe/H] diagram for group 15 are shown in plot 15 in Fig. 9 and its properties are similar to the full sample. We suppose that this group is an independent one, but has to be confirmed in later studies that contain more stars. The *Gaia* DR2 data release may help to resolve this case.

*Bobylev16* (16): This group has 14 stars and 17% of Monte Carlo detection. It was first discovered in Bobylev & Bajkova (2016) and is shown with a blue cross on the left-hand side of structure 16 in Fig. 8. We confirm this group and add that it belongs to both nearby and distant, thin and thick disk samples, suggesting that it is a mixture of different types of stars.

The same as group 15, structure 16 is observed far away from the majority of kinematic groups. This supports the group's independence from other structures, but unlike group 15, structure 16 is present in all samples. The metallicity distribution and [Mg/Fe]-[Fe/H] diagram for group 16 are shown in pattern 16 (see Fig. 9) and it appears to have more thin disk stars. We propose its dynamical origin similar to the Sirius group since the sample properties are alike.

*$\epsilon$Ind* (17): The closest blue cross to group 17 in Fig. 7 is the one previously found at $2\sigma$ confidence level by Antoja et al. (2012) that is listed in Table 15. Although the structure is detected at the $3\sigma$-significane level, it has a low percentage of detection, only 12%, and contains only 24 stars. This group appears to be detected only in the nearby sample, but this could be due to the fact that this group contains very few stars.

Group 17 is a small group and is thus easier to detect in the larger SN sample. However, it is not detected in the larger thin disk sample that has 5000 more stars than the SN sample. The metallicity distribution and [Mg/Fe] – [Fe/H] diagram for group 17 are shown in plot 17 in Fig. 9; it appears to mainly be a thin disk structure. To speculate on the origin of this kinematic feature *Gaia* DR2 data should be used to gain a larger stellar sample.

*Two possibly new structures* (18–19), $J = 2$: these two groups have a low structure count in Monte Carlo simulations and contain 12 and 70 stars respectively. Group 19 can be associated with HR1614 peak detected at $(15, -60)$ km s$^{-1}$ by Dehnen (1998; marked by a blue cross in Fig. 7), but none of the groups have similar velocities. Tentatively we define them as new structures, but require further confirmation with larger data samples.

**Table 16.** Position of two possibly new structures.

| $(U, V)$ [km s$^{-1}$] | Reference |
|---|---|
| $(-88, -76)$ | group 18 |
| $(-18, -67)$ | group 19 |

The metallicity distributions and [Mg/Fe] – [Fe/H] diagrams for groups 18 and 19 are shown in plots 18 and 19 in Fig. 9. Structure 19 appears to be a thin disk structure, and structures 18 is seen only in SN sample, which could be a consequence of the group's small size. *Gaia* DR2 will help us to further investigate the existence and origin of these two structures.

## 6. Summary and discussion

We have analysed the velocity distribution of 55 831 *Gaia* DR1/TGAS stars in the solar neighbourhood and sample properties relative to distance and metallicity using wavelet analyses. Nineteen kinematic structures were detected at scales of 8–16 km s$^{-1}$, 32 at 4–8 km s$^{-1}$ and 4 structures at 16–32 km s$^{-1}$ in the $U - V$ plane. Our analysis offers several advantages compared to previous works as it is the first ever analysis of *Gaia* DR1 data in such a kinematical context, and the most important benefit is the precision of astrometry provided by TGAS itself. The high precision of the input data allow us to apply the analysis to a larger sample of stars than in previous works, and even after cutting the sample based on $\sigma_U$ and $\sigma_V < 4$ km s$^{-1}$ we still have a competitive number of stars. This limit on velocity uncertainties is important to obtain robust measurements of positions of kinematic structures. In previous works velocity uncertainties were either not regarded at all or were were established to be too high to retain more stars in the sample, possibly leading to uncertain results in both cases.

A set of $3\sigma$-significant (99.8%) wavelet coefficients that indicate kinematic structures were received after applying the wavelet analysis and filtering the data. Although the output data were already smoothed with the auto-convolution histogram method, the question of whether obtained structures are real remained due to the existence of velocity uncertainties. We then run Monte Carlo simulations and applied the same analysis to them as for the real sample. This step is beneficial for the procedure in general as it allows us to calculate the percentage of detection which indicates whether or not the structures are likely to be real.

To investigate properties of obtained structures with respect to distance and chemical composition four sub-samples were defined: a solar neighbourhood sample with stars closer than 300 pc (SN), a sample with more distant stars (BSN), and, based on [Mg/Fe] enhancement (from RAVE abundances), a thick disk sample (TD) and a thin disk sample (D). As shown is Sects. 5.2 and 5.3, some structures are SN/BSN and/or D/TD structures. For example, group 10 (Hercules) is obviously a SN/D structure, while group 4 (Coma B part) is a BSN/TD structure. Most of the moving groups are observed at close distances $d < 300$ pc and at higher metallicities. This could be a repercussion of the selection effect since SN and D samples contain more stars compared to the BSN and TD samples. Some groups change their positions and shapes when considering distance and metallicity (e.g. group 7 (Hyades), and group 2 (Sirius)). These variations could be a consequence of how the sample is split, where the SN and D samples contain more stars than BSN and TD samples, but

could also possibly prove the dynamical origin of these groups since shifts in the velocity plane were also found in Antoja et al. (2012) when analysing nearby and distant samples of stars. They found that the observed shifts were consistent with the dynamical models of spiral arm effects discussed in Antoja et al. (2011). *Gaia* DR2 data will cover more stars and can possibly resolve the question of shifted positions.

With a high probability we observe major peaks like Sirius, Coma B, Hyades, Pleiades, Hercules and Wolf 630. We confirm group 9 (Dehnen98), which was recently discovered in Dehnen (1998) and discuss the possibility of being a part of the Coma Berenices stream together with Wolf 630, since these groups share similar metallicity properties (see Figs. 9, 8). Groups 14 and 15 (Antoja12(15) and Antoja12(12)) were first reported in Antoja et al. (2012) at 2 and 3$\sigma$ confidence level. We confirm both of them at the 3$\sigma$ level. Structure 16, which was first discovered in Bobylev & Bajkova (2016), is also confirmed.

We report on a new group (number 13) which has not been discussed in the literature before. It appeared in 74% of the MC runs and contains around 201 stars. This group belongs to the nearby sample and unites stars of both disks. Group 13 is located in the proximity to Sirius and $\gamma$Leo streams. The latest one, group 12, has rather low percentage of detection, but shares similar properties to group 13. This new group could be an independent structure, but could also be an elongation of the Sirius or $\gamma$Leo streams, because the metallicity properties are similar for all three groups (see Figs. 9, 8). To claim if this structure is independent, this case should be further investigated, possibly through a detailed chemical analysis of stars that belong to the structures. The $\epsilon$Ind and another two possibly new structures have weak detection percentages in the Monte Carlo simulations (less than about 25%). Hence, the possibly new structures, 18 and 19, require further confirmation.

We discuss a possible origin of stellar streams 1–19 based on our results and previous findings form the literature. If the groups found showed metallicity homogeneity it would point towards an origin in remnants of open clusters. Most of the structures do not show any particular properties inherent to thin or thick disk populations and thus we consider them to be a mixture of different types of stars caused through dynamical resonances. Those groups that are more likely thick or thin disk structures are either large-scale structures (e.g. Hercules), or are small-scale groups located far from the most dense regions in the $U - V$ plane, and thus, should be independent structures possibly also caused by resonances. Our conclusions on the origin of kinematic structures are consistent with previous works, but should be verified with better data including more stars with high-precision abundances and astrometry.

We also want to discuss a few groups which are not observed in our work, but that were in the centre of discussions in a couple of recent works. Among them is a debatable structure at (35, −20) km s$^{-1}$ which was first reported in (Antoja et al. 2008). Taking into account its proximity to Wolf 630, Dehnen98 and bigger stream such as Sirius or Coma Berenices, authors of the same paper claim that the structure at (35, −20) km s$^{-1}$ could be en elongation of these bigger groups. At the same time (Zhao et al. 2009) detected a distinct structure at (38, −20) km s$^{-1}$ with probability 98% (~3$\sigma$) and suggested that it is an independent group. However, in our analysis we detected all of the above streams except the one at (35, −20) km s$^{-1}$, while Wolf 630 and Dehnen98 share similar metallicity properties to the Coma Berenices stream. Groups NGC 1901 & IC 2391 were detected by Dehnen (1998) and Eggen (1996) at (−25, −10) and (−20.8, −15.9) km s$^{-1}$ respectively. Interestingly, later works with larger stellar samples like Antoja et al. (2012), did not detect these structures. Antoja et al. (2008) make the assumption that these groups are weak compared to super-streams like Sirius, Coma Berenices, Hyades and Pleiades, as they did not detect them. We do not observe these groups either. We note that while the $J = 2$ scale (see Fig. 5) is almost two times more rich with kinematic structure detections than the scale $J = 3$, all these smaller-scale $J = 2$ structures could be associated with some of the $J = 3$ streams (see Table 2). Questions remain regarding groups 21 (part of $\gamma$Leo?), and groups 25–30 (parts of Antoja(12) and Antoja(15)?) detected on the $J = 2$ scale. These structures could be also independent and new; the answers may be provided later when *Gaia* DR2 data are available.

The next step should be a deeper investigation of the origin of these moving groups through a better detailed analysis of chemical composition and ages of stars associated with each group to better understand the Milky Way formation. This can be done on small scales for individual structures, but ongoing and upcoming large spectroscopic surveys such as, for example, the *Gaia*-ESO (Gilmore et al. 2012), WEAVE (Dalton et al. 2014), and 4MOST (de Jong et al. 2016) surveys will provide precise elemental abundances for millions of stars, that together with astrometry from *Gaia* will allow us to probe the kinematic structures at greater detail throughout the Galactic disk.

*Acknowledgements.* T.B. was funded by the "The New Milky Way" project grant from the Knut and Alice Wallenberg Foundation. We thank Prof. F. Murtagh for making available for us the MR software packages and for valuable and helpful comments.

## References

Adibekyan, V. Z., Sousa, S. G., Santos, N. C., et al. 2012, A&A, 545, A32
Antoja, T., Figueras, F., Fernández, D., & Torra, J. 2008, A&A, 490, 135
Antoja, T., Figueras, F., Romero-Gómez, M., et al. 2011, MNRAS, 418, 1423
Antoja, T., Helmi, A., Bienayme, O., et al. 2012, MNRAS, 426, L1
Antoja, T., Helmi, A., Dehnen, W., et al. 2014, A&A, 563, A60
Arifyanto, M. I., & Fuchs, B. 2006, A&A, 449, 533
Baranne, A., Mayor, M., & Poncet, J. L. 1979, Vist. Astron., 23, 279
Bensby, T., Oey, M. S., Feltzing, S., & Gustafsson, B. 2007, ApJ, 655, L89
Bensby, T., Alves-Brito, A., Oey, M. S., Yong, D., & Meléndez, J. 2011, ApJ, 735, L46
Bensby, T., Feltzing, S., & Oey, M. S. 2014, A&A, 562, A71
Bobylev, V. V., & Bajkova, A. T. 2016, Astron. Lett., 42, 90
Bovy, J., & Hogg, D. W. 2010, ApJ, 717, 617
Bubar, E. J., & King, J. R. 2010, AJ, 140, 293
Chakrabarty, D. 2007, A&A, 467, 145
Chereul, E., Creze, M., & Bienayme, O. 1998, A&A, 340, 384
Dalton, G., Trager, S., Abrams, D. C., et al. 2014, in SPIE Conf. Ser., 9147, 91470L
de Jong, R. S., Barden, S. C., Bellido-Tirado, O., et al. 2016, in Ground-based and Airborne Instrumentation for Astronomy VI, Proc. SPIE, 9908, 99081O
Dehnen, W. 1998, AJ, 115, 2384
Dehnen, W. 2000, AJ, 119, 800
Dekker, E. 1976, Phys. Rep., 24, 315
Eggen, O. J. 1965, The Observatory, 85, 191
Eggen, O. J. 1992, AJ, 104, 1493
Eggen, O. J. 1996, AJ, 112, 1595
ESA. 1997, The HIPPARCOS and TYCHO catalogues, ESA SP, 1200, Noordwijk, Netherlands
Famaey, B., Jorissen, A., Luri, X., et al. 2005, A&A, 430, 165
Famaey, B., Pont, F., Luri, X., et al. 2007, A&A, 461, 957
Famaey, B., Siebert, A., & Jorissen, A. 2008, A&A, 483, 453
Freeman, K., & Bland-Hawthorn, J. 2002, ARA&A, 40, 487
Fuhrmann, K. 2008, MNRAS, 384, 173
Gaia Collaboration (Brown, A. G. A., et al.) 2016, A&A, 595, A2
Gilmore, G., Randich, S., Asplund, M., et al. 2012, The Messenger, 147, 25
Hayden, M. R., Bovy, J., Holtzman, J. A., et al. 2015, ApJ, 808, 132
Haywood, M., Di Matteo, P., Lehnert, M. D., Katz, D., & Gómez, A. 2013, A&A, 560, A109

Helmi, A., White, S. D. M., de Zeeuw, P. T., & Zhao, H. 1999, Nature, 402, 53
Helmi, A., Veljanoski, J., Breddels, M. A., Tian, H., & Sales, L. V. 2017, A&A, 598, A58
Holmberg, J., Nordström, B., & Andersen, J. 2009, A&A, 501, 941
Johnson, D. R. H., & Soderblom, D. R. 1987, AJ, 93, 864
Klement, R., Fuchs, B., & Rix, H.-W. 2008, ApJ, 685, 261
Kunder, A., Kordopatis, G., Steinmetz, M., et al. 2017, AJ, 153, 75
Liang, X. L., Zhao, J. K., Oswalt, T. D., et al. 2017, ApJ, 844, 152
Lindegren, L. 2017, Proc. IAU Symp., 330, in press
Lindegren, L., Lammers, U., Bastian, U., et al. 2016, A&A, 595, A4
Luo, A.-L., Zhao, Y.-H., Zhao, G., et al. 2015, RA&A, 15, 1095
Mädler, J. H. 1846, Astron. Nachr., 24, 213
McMillan, P. J. 2017, MNRAS, 465, 76
Michalik, D., Lindegren, L., & Hobbs, D. 2015, A&A, 574, A115
Minchev, I., Boily, C., Siebert, A., & Bienayme, O. 2010, MNRAS, 407, 2122
Myeong, G. C., Evans, N. W., Belokurov, V., Koposov, S. E., & Sanders, J. L. 2017, MNRAS, 469, L78
Nordström, B., Mayor, M., Andersen, J., et al. 2004, A&A, 418, 989
Odenkirchen, M., Soubiran, C., & Colin, J. 1998, New Astron., 3, 583
Pérez-Villegas, A., Portail, M., Wegg, C., & Gerhard, O. 2017, ApJ, 840, L2
Pompéia, L., Masseron, T., Famaey, B., et al. 2011, MNRAS, 415, 1138
Proctor, R. A. 1869, Proc. Royal Society of London Series I, 18, 169
Ramya, P., Reddy, B. E., Lambert, D. L., & Musthafa, M. M. 2016, MNRAS, 460, 1356
Reddy, B. E., Lambert, D. L., & Allende Prieto, C. 2006, MNRAS, 367, 1329
Schönrich, R. 2012, MNRAS, 427, 274
Schönrich, R., & Aumer, M. 2017, MNRAS, 472, 3979
Skuljan, J., Hearnshaw, J. B., & Cottrell, P. L. 1999, MNRAS, 308, 731
Slezak, E., de Lapparent, V., & Bijaoui, A. 1993, ApJ, 409, 517
Starck, J.-L., & Murtagh, F. 2002, Astronomical image and data analysis (Berlin; New York: Springer), oCLC: 679368657
Starck, J.-L., & Pierre, M. 1998, A&AS, 128, 397
Starck, J.-L., Murtagh, F. D., & Bijaoui, A. 1998, Image Processing and Data Analysis, 297
Steinmetz, M. 2003, in Gaia Spectroscopy: Science and Technology, ed. U. Munari, ASP Conf. Ser., 298, 381
Tabernero, H. M., Montes, D., & González Hernández, J. I. 2012, A&A, 547, A13
Tian, H.-J., Liu, C., Carlin, J. L., et al. 2015, ApJ, 809, 145
Turon, C., Crézé, M., Egret, D., et al. 1992, Bulletin d'Information du Centre de Données Stellaires, 41, 9
Wojno, J., Kordopatis, G., Steinmetz, M., et al. 2016, MNRAS, 461, 4246
Zhao, J., Zhao, G., & Chen, Y. 2009, ApJ, 692, L113
Zhao, G., Zhao, Y.-H., Chu, Y.-Q., Jing, Y.-P., & Deng, L.-C. 2012, RA&A, 12, 723
Zhao, J. K., Zhao, G., Chen, Y. Q., et al. 2014, ApJ, 787, 31

# Paper II

A&A 631, A47 (2019)
https://doi.org/10.1051/0004-6361/201935234


Astronomy & Astrophysics

# Disentangling the Arcturus stream

Iryna Kushniruk and Thomas Bensby

Lund Observatory, Department of Astronomy and Theoretical Physics, Box 43, 221 00 Lund, Sweden
e-mail: iryna@astro.lu.se, tbensby@astro.lu.se

Received 8 February 2019 / Accepted 9 September 2019

**ABSTRACT**

*Context.* The Arcturus stream is an over-density of stars in velocity space and its origin has been much debated recently without any clear conclusion. The (classical) dissolved open cluster origin is essentially refuted; instead the discussions try to distinguish between an accretion, a resonant, or an external-perturbation origin for the stream. As kinematic structures are observational footprints of ongoing and past dynamical processes in disc galaxies, resolving the nature of the Arcturus stream may provide clues to the formation history of the Milky Way and its stellar populations.
*Aims.* We aim to characterise the kinematical and chemical properties of the Arcturus stream in order to resolve its origin.
*Methods.* The space velocities, angular momenta, and actions for a sample of more than 5.8 million stars, composed from *Gaia* DR2 were analysed with a wavelet transform method to characterise kinematic over-densities in the Galactic disc. The kinematic characteristics of each identified group is used to select possible members of the groups from the GALAH and APOGEE spectroscopic surveys to further study and constrain their chemical properties.
*Results.* In the velocity and angular momentum spaces the already known Sirius, Pleiades, Hyades, Hercules, AF06, Arcturus and KFR08 streams are clearly identified. The Hercules stream appears to be a mixture of thin and thick disc stars. The Arcturus stream, as well as the AF06 and KFR08 streams, are high-velocity and low-angular momentum structures with chemical compositions similar to the thick disc. These three groups extend further from the Galactic plane compared to the Hercules stream. The detections of all the groups were spaced by approximately 20−30 km s$^{-1}$ in azimuthal velocity.
*Conclusions.* A wide spread of chemical abundances within the Arcturus stream indicates that the group is not a dissolved open cluster. Instead the Arcturus stream, together with the AF06 and KFR08 streams, are more likely to be part of a phase-space wave, that could have been caused by a merger event. This conclusion is based on that the different structures are detected in steps of 20−30 km s$^{-1}$ in azimuthal velocity, that the kinematic and chemical features are different from what is expected for bar-originated structures, and that the higher-velocity streams extend further from the disc than bar-originated structures.

**Key words.** stars: kinematics and dynamics – Galaxy: formation – galaxies: kinematics and dynamics – galaxies: evolution

## 1. Introduction

The process by which large spiral galaxies form and evolve into the complicated structures that are observed today is an active area of research, and presents many challenges, both theoretically and observationally. As the Milky Way is the only galaxy where stars and structures can be studied in great detail, it serves as a benchmark galaxy when constraining models of galaxy formation. It is therefore of utmost importance to obtain a detailed map of the Milky Way looks like, and to decipher where the observed stellar populations and structures come from. Currently, the Milky Way contains a plethora of structures, both physical and kinematic, whose nature and origins are unclear.

Many studies have shown that the velocity distribution of stars in the Milky Way disc is clumpy (e.g. Dehnen 1998; Skuljan et al. 1999; Famaey et al. 2005; Antoja et al. 2008, 2012; Kushniruk et al. 2017; Ramos et al. 2018). The kinematic and chemical properties of such structures can be used to constrain the properties and the formation history of the Milky Way. For example, the Hercules stream has been widely used to probe the pattern speed and the length of the Galactic bar (e.g. Dehnen 2000; Minchev et al. 2007; Antoja et al. 2014; Wegg et al. 2015; Pérez-Villegas et al. 2017). Kinematic structures can be used to study the spiral structure of the Milky Way (e.g. Quillen & Minchev 2005; Chakrabarty 2007; Sellwood et al. 2019; Quillen et al. 2018). Studies of kinematic streams especially in the Galactic halo can tell us about the merger history of the Milky Way (e.g. Navarro et al. 2004; Helmi et al. 2006, 2017, 2018; Koppelman et al. 2018). The analysis of the *Gaia* DR2 (Gaia Collaboration 2018a,b) revealed that the kinematic over-densities are a part of a much more complicated structure that is seen as arches and ridges across velocity space and as clumps in action space (Trick et al. 2019). This structure is possibly caused by spiral arms (Quillen et al. 2018) or is a result of the phase-mixing due to a past merger event (e.g. Katz et al. 2019; Antoja et al. 2018; Ramos et al. 2018; Laporte et al. 2019), as first proposed by Minchev et al. (2009).

This structure is possibly caused by spiral arms or is a result of phase-mixing due to a past merger event (e.g. Antoja et al. 2018; Ramos et al. 2018; Quillen et al. 2018). As these studies have shown, learning more about the nature of kinematic structures can improve our understanding of the evolution of the Milky Way. In this paper we investigate the properties and origin of the Arcturus stream.

A set of about 50 stars, including the star Arcturus ($\alpha$ Bootis), was discovered by Eggen (1971) to have a very similar V space velocity component of $V \simeq -100$ km s$^{-1}$. Eggen (1971) proposed that this over-density in velocity space is composed of stars that escaped from an open cluster and it was therefore named the Arcturus moving group. Nowadays the hypothesis of the Arcturus over-density being a moving group is refuted as there is no chemical homogeneity within the group (e.g. Williams et al. 2009; Ramya et al. 2012; Bensby et al. 2014),

which there should be if the stars originate from the same open cluster (e.g. De Silva et al. 2007; Bovy 2016). We have therefore chosen to adopt the "stream" nomenclature when referring to this Arcturus over-density of stars in velocity space.

Two other possible origins of the Arcturus stream are now favoured and are widely discussed. The first is an accretion event scenario, where a small satellite galaxy merged with the Milky Way and caused this dynamical structure (e.g. Navarro et al. 2004; Helmi et al. 2006; Minchev et al. 2009). The second possibility is that it has originated due to resonances with the Galactic bar or spiral arms that cause kinematic over-densities (e.g. Gardner & Flynn 2010; Monari et al. 2013). The chemical properties of the stream do not show any chemical peculiarities, which would be expected in the case of an extra-Galactic origin (e.g. Ramya et al. 2012; Bensby et al. 2014). At the same time the low angular momentum and the low velocity of the stream indicate that it could be another substructure of tidal debris in the Galactic halo (e.g. Arifyanto & Fuchs 2006; Klement et al. 2008; Zhao et al. 2014). Despite numerous approaches to study the origin of the Arcturus stream (e.g., numerical simulations, kinematic analysis, and studies of elemental abundances), there is no consensus on its origin.

The aim of this paper is to characterise the nature of the Arcturus stream and constrain its origin. We start by detecting and characterising the velocities of the Arcturus stream using a large stellar sample constructed from the *Gaia* DR2 catalogue (see Sect. 2). We then search for over-densities in the velocity, angular momentum, and action spaces to obtain the kinematic characteristics of the stream (see Sects. 3–5). Subsequently, we investigate the chemical characteristics of the group using the data from the GALAH (Buder et al. 2018) and APOGEE (Holtzman et al. 2018) spectroscopic surveys (see Sect. 6). We conclude by discussing the possible origins for the Arcturus stream based on the kinematic and spectroscopic findings (see Sects. 7 and 8).

## 2. Stellar sample

To search for the Arcturus stream, a wavelet analysis was applied for a stellar sample defined by velocities, angular momentum, and action components. To calculate these parameters positions on the sky, proper motions, parallaxes, radial velocities, and the corresponding uncertainties for these properties are needed.

The size of the stellar sample and the quality of the astrometric data play a key role when hunting for kinematic structures. As the size of the samples of stars with available high-precision astrometric data increases, so does the level of detail with which it is possible to study kinematical structures of the Galaxy. The currently best data source is the *Gaia* satellite, which is an ongoing full-sky mission that aims to provide high-precision astrometric parameters for more than a billion targets over the whole sky. The most recent data release, *Gaia* DR2 (Gaia Collaboration 2018a), contains astrometric data for almost 1.7 billion targets, and radial velocities for a small subsample of about 7 million targets.

A stellar sample of 5 844 487 stars was constructed from the *Gaia* DR2 catalogue in the following way:

– 7 173 615 stars were obtained from McMillan (2018), who estimated distances for *Gaia* DR2 stars with measured radial velocities.

– Stars with bad fits of *Gaia* DR2 astrometric parameters were filtered out to avoid possible systematic errors in the stellar sample. Following the procedure suggested in Lindegren (2018) a re-normalised unit weight error (RUWE) was used to estimate goodness of astrometric fits. Selecting those targets with RUWE < 1.4 leaves us with 6 692 285 targets. Photometric filtering that rids the sample of stars with poor astrometric solutions (see Eq. (2) in Arenou et al. (2018)) was also applied. This cut leaves us with 6 683 408 stars.

– Space velocities $U, V, W$[1] together with angular momenta and actions that are used below were computed using the *galpy*[2] package (Bovy 2015). For action estimates we used a MWPotential2014 axisymmetric gravitational potential model pre-defined in *galpy*. Velocity uncertainties $\sigma_U, \sigma_V, \sigma_W$ were computed following equations from Johnson & Soderblom (1987). The velocities are given relative to the Local Standard of Rest: $(U_\odot, V_\odot, W_\odot) = (11.1, 12.24, 7.25)$ km s$^{-1}$ (Schönrich et al. 2010).

Taking into account the results from, for example, Zhao et al. (2014), the typical size of kinematical structures is around 20 km s$^{-1}$. Therefore we need to cut stars with $\sigma_U, \sigma_V > 20$ km s$^{-1}$, because such large velocity uncertainties will influence the precision of the results, that is the position in velocity space of the structures. This leaves us with 6 002 514 stars.

– Next, the sample was constrained to stars that are located within a distance of 5 kpc from the Sun. This filters out stars that are located in the outskirts or in the very inner parts of the Galaxy, and thus, cannot be a part of any of the local kinematic structures. The limit of 5 kpc was chosen to avoid regions in direct contact with for example the Galactic bar, whose half-length is about 3 kpc (e.g. Dehnen 2000; Minchev et al. 2010; Monari et al. 2017). According to Bailer-Jones (2015), distance estimates should not be dominated by using pre-*Gaia* information or so-called priors if fractional parallax uncertainty does not exceed 20%. Typical parallax uncertainty for bright sources in *Gaia* DR2 is about 0.4 $\mu$as (Lindegren 2018). Converting the 5 kpc cut into $\mu$as and calculating fractional parallax uncertainty we obtain 20% meaning that distance estimates in the sample should not be effected by priors. This cut leaves 5 844 487 that are used in our analysis.

Since kinematic structures are local phenomena (e.g. Antoja et al. 2012; Ramos et al. 2018; Trick et al. 2019) and the stellar sample covers a wide range in $X$ and $Y$, it was divided into 66 smaller volumes that were investigated separately. Each box is 0.4 kpc in radial coordinates and 3° in azimuthal angle[3]. The top plot in Fig. 1 shows the distribution of the 5 844 487 stars in the Galactic Cartesian $X-Y$ plane and how it is divided into small volumes. The name of each region, the number of stars, the median distance from the Sun, and median distance uncertainty are given in Table A.1 for each of the 65 volumes. The bottom plot in Fig. 1 shows the sample in Cartesian $X$ and $Z$ coordinates, where $Z$ is a vertical component of Galactocentric coordinate system (points towards the north Galactic pole).

## 3. Method

Our current knowledge of the Arcturus stream is based on observations within a small region of about 500 pc around the Sun. Its origin is unknown, mainly due to the fact that there are only rough estimates of its kinematic characteristics and its chemical properties are not well studied. Our strategy is therefore to search for streams in four different planes defined by

[1] $U$ points towards Galactic centre, $V$ velocity defines the direction of the Galactic rotation, $W$ points at the North Galactic Pole.
[2] Available at `http://github.com/jobovy/galpy`
[3] $R$ is the radial coordinate pointing towards the Galactic anti-centre, and $\phi$ is the azimuthal angle following the direction opposite to the Galactic rotation.

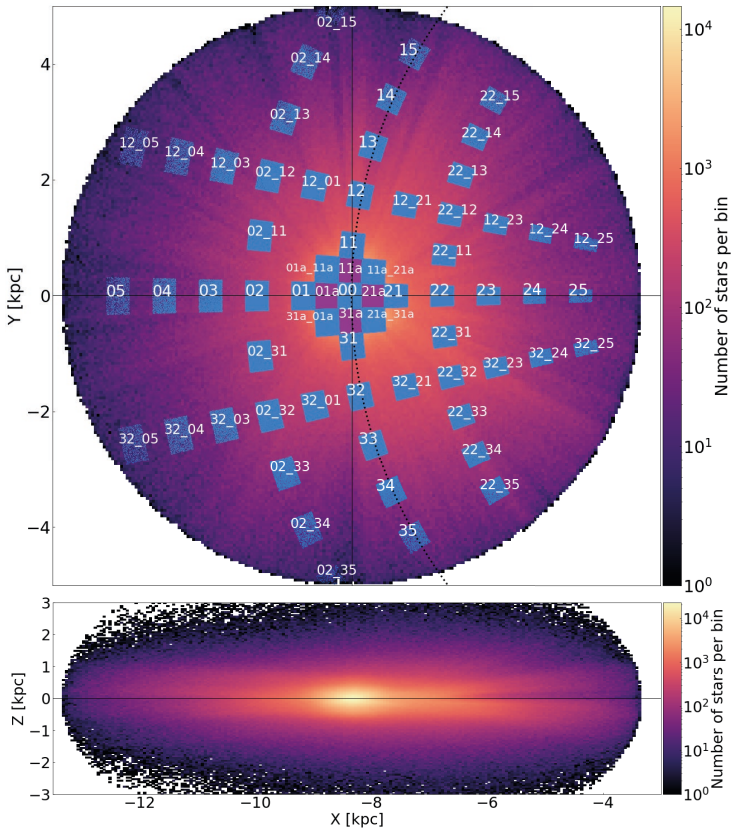


**Fig. 1.** Distribution of 5 844 487 stars with $\sigma_U$ and $\sigma_V$ < 20 km s$^{-1}$ and $R \leq 5$ kpc in $X$ and $Y$ (*top*), and $X$ and $Z$ (*bottom*) Cartesian Galactic coordinates. Blue and magenta boxes show 66 small regions investigated in this work and their names are written at the top in white. The dashed line in the top plot shows the solar circle. The black line in the bottom plot shows $Z = 0$ kpc. The bin size is 0.05 kpc for both plots.

combinations of velocity, angular momentum and action components respectively: the $U-V$ plane, the $V-\sqrt{U^2+2V^2}$ plane, the $L_z-\sqrt{L_x^2+L_y^2}$ plane, and the $L_z-\sqrt{J_r}$ plane. This will allows to characterise structures in terms of velocities, angular momenta, and actions, and obtain stronger criteria on how to select star members of kinematic structures.

### 3.1. Investigated planes

The distributions of stars in all four planes are shown in Fig. 2. The majority of the stars in our sample have negative $V$ velocities between $V \simeq 0$ and $-200$ km s$^{-1}$ and angular momentum $L_z$ between 0 and 2500 kpc km s$^{-1}$. The disc stars are located at $L_z \simeq 1800$ kpc km s$^{-1}$, the halo stars are expected at $L_z \simeq 0$ kpc km s$^{-1}$.

#### 3.1.1. The $U-V$ plane

The $U-V$ plane is widely used to search for kinematic structures (e.g. Dehnen 1998; Antoja et al. 2008, 2012, 2018; Kushniruk et al. 2017; Ramos et al. 2018; Katz et al. 2019). It allows to trace kinematic over-densities of different origin without making any assumptions on orbital parameters of stars or on the Galactic potential. The only limitation of this method is that stellar volumes must be relatively small (around 0.1−0.5 pc in $X$ and $Y$; see Trick et al. 2019), since kinematic structures in the $U-V$ plane are local. On the other hand, this limitation is an advantage, since it allows us to follow how the structures move in physical space (Ramos et al. 2018). The Arcturus stream is expected to be one of the arches in the $U-V$ plane localised around $V \simeq -100$ km s$^{-1}$ in the nearby sample. The stream is likely to cover a wide range of $U$ velocities (Williams et al. 2009).

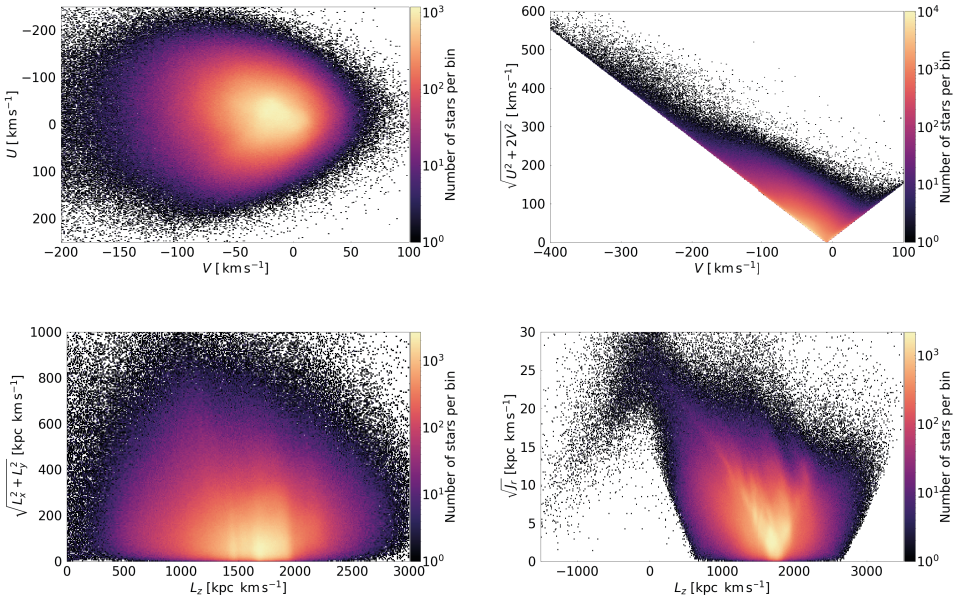


**Fig. 2.** Density map of the selected sample of 5 844 487 stars in $U-V$ space (*top left*), in $V-\sqrt{U^2+2V^2}$ space (*top right*), in $L_z-\sqrt{L_x^2+L_y^2}$ space (*bottom left*), and in $L_z-\sqrt{J_R}$ space (*bottom right*). The bin sizes are 1 km s$^{-1}$, 1 km s$^{-1}$, 10 kpc km s$^{-1}$, and $10\times0.1$ kpc km s$^{-1}$, respectively.

#### 3.1.2. The $V-\sqrt{U^2+2V^2}$ plane

Examining the distribution of stars in the $V-\sqrt{U^2+2V^2}$ plane was proposed by Arifyanto & Fuchs (2006). Here, $V$ is proportional to $L_z$, a vertical component of the angular momentum, and is an integral of motion in axisymmetric potentials. $\sqrt{U^2+2V^2}$ is a measure of eccentricity in Dekker's approximation (Dekker 1976). This means that we search for structures that share similar orbital eccentricity. This approach is applicable only for planar orbits in axisymmetric potentials. The method shows reliable results for nearby stars with eccentricities up to 0.5 (Arifyanto & Fuchs 2006). The $V-\sqrt{U^2+2V^2}$ plane was used by Klement et al. (2008) and Zhao et al. (2014) to search for kinematic structures and allowed to reveal several structures including the Arcturus stream. We expect to detect the Arcturus stream at the velocities around $V\simeq-100$ km s$^{-1}$ in the solar neighbourhood (e.g. Williams et al. 2009).

#### 3.1.3. The $L_z-\sqrt{L_x^2+L_y^2}$ plane

Another approach to search for kinematic groups was proposed by Helmi et al. (1999) who suggested to examine the distribution of stars in the plane characterised by the $L_z$ and $\sqrt{L_x^2+L_y^2}$ integrals of motion, where $L_x$, $L_y$, and $L_z$ are angular momentum components in $X$, $Y$, and $Z$ directions. The method is used to search for phase-mixed stars on similar orbits. The disadvantage of this method is that $\sqrt{L_x^2+L_y^2}$ is not fully conserved in axisymmetric potentials, but still allows dynamical structures to be revealed (e.g. Helmi et al. 1999; Klement et al. 2008; Zhao et al. 2014). The Arcturus stream is expected at $L_z$ in the range between 700 and 1100 km s$^{-1}$ kpc (e.g. Navarro et al. 2004).

#### 3.1.4. The $L_z-\sqrt{J_r}$ plane

The most general method to search for kinematic structures is to investigate action space. Actions are conserved quantities that characterise stellar orbits. In this work we use radial and azimuthal actions $J_r$ and $L_z$ that are a measure of orbital eccentricity and orbital angular momentum. As suggested in Trick et al. (2019) taking the square root of radial action will make the final plots more clear. The action space was investigated by, for example, Sellwood (2010) and Trick et al. (2019) and is rich in kinematic over-densities. We expect to detect the Arcturus stream at $L_z$ in the range between 700 and 1100 kpc km s$^{-1}$ (e.g. Navarro et al. 2004).

### 3.2. Wavelet transform

To search for kinematic structures, the methodology described in Kushniruk et al. (2017) was used with some additions. To detect over-densities, a wavelet transform was applied to the stellar sample in the $U-V$, $V-\sqrt{U^2+2V^2}$, $L_z-\sqrt{L_x^2+L_y^2}$, and $L_z-\sqrt{J_r}$ planes. The noise from the wavelet maps was then filtered and Monte Carlo simulations were used to verify whether the detected structures are real or not.

The data were analysed by the wavelet transform with the "*a trous*" algorithm (Starck & Murtagh 1998) applied to the stars in all 65 regions in the four different planes separately. The input data are in the form of a binned stellar density map in the velocity, angular momentum, and action planes. The bin sizes $\Delta$ were set to 1 km s$^{-1}$ for the $U-V$, and the $V-\sqrt{U^2+2V^2}$ planes, to 2 km s$^{-1}$ kpc for the $\sqrt{L_x^2+L_y^2}-L_z$ plane, and to $0.1\times 10$ kpc km s$^{-1}$ for the $L_z-\sqrt{J_r}$ plane. Due to the limitations of the usage of the $V-\sqrt{U^2+2V^2}$ plane, as discussed in Sect. 3.1.2, the stars that have orbits with eccentricities $e > 0.5$ were cut out. The output data are a set of wavelet coefficients at different scales that contain information about the presence of substructures. A higher wavelet coefficient means a higher probability that the structure is real. The scale $J$ is proportional to the size of the detectable structures $s$. Scales $J = 1$, 2, 3 and 4 were investigated for all maps. The relation between scale and bin size $s_J = 2^J\Delta$ characterises the typical sizes of detectable structures. The wavelet coefficient maps were then filtered for Poisson noise. The wavelet transform part as well as noise filtering from the output wavelet maps were performed in The multiresolution analysis software (MR software)[4] developed by CEA (Saclay, France) and the Nice Observatory. More details on the algorithm itself can be found in Starck & Murtagh (2002), and more details on the methods used to search for over-densities and structures can be found in Kushniruk et al. (2017).

### 3.3. Acquiring positions of the detected peaks

Monte Carlo (MC) simulations were performed to obtain the precise positions of the peaks. Monte Carlo samples were created assuming that each star can be represented as a Gaussian velocity distribution with $\mu = (U, V)$ and $\sigma = (\sigma_U, \sigma_V)$ for the two velocity components. To generate MC samples in angular momentum and action space, the orbits of stars were computed assuming that positions, proper motions, and radial velocities can be represented as Gaussians in a similar way to velocities. Here it is assumed that Gaussians are independent and do not consider correlations between astrometric parameters. These MC samples are then analysed in the same manner as the original data. Convergence is reached when the number of structures and their positions do not change as more simulations are added. Typically, results converge after about 30 simulations, but to be sure of convergence, 100 MC samples were created for all regions. Subsequently, MC wavelet maps for different scales were over-plotted and used to search for peaks by applying the *peak_local_max* feature from the *scikit-image*[5] Python package (van der Walt et al. 2014). In this work we focus on the $J = 2$ and $J = 3$ scales as they allow us to detect most structures.

## 4. Results

### 4.1. Stellar streams in the nearby sample

Figures 3 and 4 show 100 over-plotted wavelet maps for the central region 00 in four different planes for scales 2 and 3, respectively. Both scales show richness of kinematic structures for the nearby sample. The list of the centres of the peaks and the corresponding uncertainties are given in Table A.2 for scale $J = 2$ and in Table A.3 for scale $J = 3$. The fact that well-known groups like Sirius, Coma Berenices, Hyades, Pleiades, and Hercules were identified at the expected positions shows that our method is sound (see Tables 3–7 in Kushniruk et al. 2017 that summarise literature values for the $U$ and $V$ velocities of Sirius, Coma Berenices, Hyades, Pleiades, and Hercules). These groups are detected in all four planes. The detection of other groups varies between the planes. Figure 3 for scale $J = 2$ shows the same structures as in Fig. 4 for scale $J = 3$ but in greater detail. We decided to focus on scale $J = 2$ since it is more sensitive to smaller structures. By comparing our results in the nearby region "00" (centred around the Sun; see Fig. 2) for scale $J = 2$ with what has previously been found in the literature (e.g. Eggen 1998; Navarro et al. 2004; Arifyanto & Fuchs 2006; Klement et al. 2008; Williams et al. 2009; Antoja et al. 2012, 2018; Zhao et al. 2014; Kushniruk et al. 2017; Trick et al. 2019; Ramos et al. 2018) we assign names to the structures. Curved lines and boxes of different colours in Figs. 3 and 4 correspond to the names of the groups listed in the legend of Fig. 3. The structures found in the nearby region are discussed below:

– A1/A2: Groups with $V > 15$ km s$^{-1}$ and $L_z > 2000$ kpc km s$^{-1}$ we link to arches A1 and A2 detected by Ramos et al. (2018, see their Table 2). Groups A1 and A2 is shown with yellow lines and boxes on the plots.

– Sirius: The blue line and boxes correspond to the Sirius stream. Group 13 in the $U - V$ space is potentially Bobylev16 (see Bobylev & Bajkova 2016) and could be a continuation of Sirius.

– $\gamma$Leo: The pink line slightly above Sirius in $V$ is $\gamma$Leo stream (see Antoja et al. 2012). Unlike the majority of the groups, $\gamma$Leo is located at positive $U$ velocities. The stream could be a continuation of Sirius arch since both have similar angular momenta.

– Coma Berenices: The magenta line just below Sirius is Coma Berenices stream. Unlike arch-like neighbouring Sirius and Pleiades/Hyades, Coma Berenices is a clump in the $U-V$ plane and is consequently a shorter line in the angular momentum space.

– Dehnen98/Wolf630: Wolf630 and Dehnen98 (see Antoja et al. 2012; Dehnen 1998) are two small groups in between Coma Berenices and Pleiades/Hyades streams. They are shown in brown colour and could be a continuation of Coma Berenices.

– Pleiades/Hyades: A grey arch in the $U-V$ plane is associated with the Pleiades/Hyades stream. Group 29 in the $U-V$ space linked to Antoja12(15) (see Antoja et al. 2012) could be a continuation of stream.

– Hercules: Orange lines and boxes correspond to the Hercules stream, which is likely to be composed of a few substructures that are visible in the angular momenta and action spaces.

– HR1614: The HR1614 moving group (see Feltzing & Holmberg 2000; De Silva et al. 2007) we connect to the clumps just below Hercules in $V$. The group is shown in lime green.

– $\epsilon$ Ind: Groups g34 and g35 in the $U-V$ plane are linked to a group called $\epsilon$Ind (see Antoja et al. 2012). The structure is marked in black.

– AF06: The AF06 stream was first found by Arifyanto & Fuchs (2006) in the range between $V \simeq -70$ and $-100$ km s$^{-1}$. We did not find it in the $U-V$ space, but the group is detected in the other three spaces and is shown with red boxes.

– Arcturus: Group g36 in the $U-V$ plane could be the Arcturus stream. Median $V$ velocity and angular momentum of g36 are $V \simeq -92$ km s$^{-1}$ and $L_z \sim 1118$ kpc km s$^{-1}$. These values are a bit higher compared to for example values from Navarro et al. (2004), but are within the uncertainties. In the $V-\sqrt{U^2+2V^2}$ plane the nearest to Arcturus are groups g1 and g2 which have

[4] Available at http://www.multiresolutions.com/mr/
[5] https://scikit-image.org/

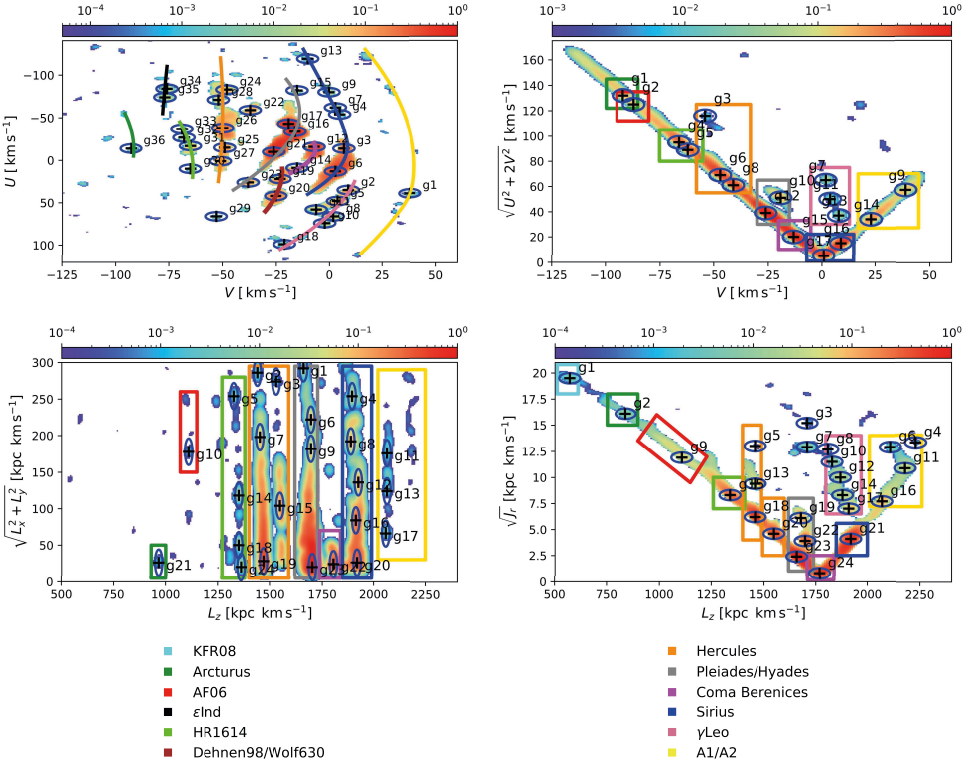


**Fig. 3.** Wavelet coefficient maps of central region 00 retrieved in $U-V$ (*top left*), $V-\sqrt{U^2+2V^2}$ (*top right*), $L_z-\sqrt{L_x^2+L_y^2}$ (*bottom left*), and $L_z-\sqrt{J_R}$ (*bottom right*) space for scale $J=2$. Colour bars show normalised wavelet coefficients. Kinematic structures are shown as blue circles with radius 5 km s$^{-1}$ or 5 kpc km s$^{-1}$ and their centres are shown with black crosses. Lines and boxes of different colours correspond to the group names as listed in the legend. We note that numbers assigned to the groups do not match between the planes.

the same angular momentum and radial action as g36 in the $U-V$ plane. In the angular momentum space g21 has the parameters closest to Arcturus. In action space there are two candidates: g9 and g2. The first group is consistent with the groups detected in velocity spaces, the second one has lower angular momentum and higher $V$ velocity. Taking into account works by for example Klement et al. (2008) and Zhao et al. (2014) we link g2 to the Arcturus stream and group g9 to the AF06 stream. Arcturus is shown as green lines and boxes on the wavelet maps.

– KFR08: Among the detected groups we assign one weak over-density in action space at $L_z \simeq 575$ kpc km s$^{-1}$ to the group called KFR08. The structure was first detected by Klement et al. (2008) at $V \simeq -160$ kpc km s$^{-1}$. Group g1 detected in action space has exactly the same median $V$ velocity. KFR08 is shown in cyan on the wavelet maps.

Overall, 36 groups at scale $J = 2$ and 16 groups at scale $J = 3$ were discovered in the $U-V$ plane that form larger-scale arches as discussed in Ramos et al. (2018), Antoja et al. (2018), and Gaia Collaboration (2018b). We also conclude that these arches correspond to the lines in the $L_z-\sqrt{L_x^2+L_y^2}$ plane and to clumps in the $V-\sqrt{U^2+2V^2}$ and $L_z-\sqrt{J_r}$ due to the very similar properties of the groups (see Tables A.2 and A.3). In the $V-\sqrt{U^2+2V^2}$, 17 and 8 groups were detected. Action space very closely mimics the $V-\sqrt{U^2+2V^2}$ plane very much but allows the structures to be detected in greater detail. In the angular momentum and action spaces, 24 groups were found in each space at scale $J = 2$ and 9 and 10 groups at scale $J = 3$, respectively.

### 4.2. Stellar streams outside the solar neighbourhood

The solar neighbourhood volume is well-studied and thus it is relatively easy to match the detected groups with groups that have been identified by other studies in the literature. The behaviour of the groups outside the solar volume was studied by for example Antoja et al. (2012) and Ramos et al. (2018). Both of these latter studies found a decreasing trend for $V$ velocity when moving to the volumes at larger $R$. In this work we also investigated the trends of the structures depending on the position in the Galaxy with a focus on the Arcturus stream.

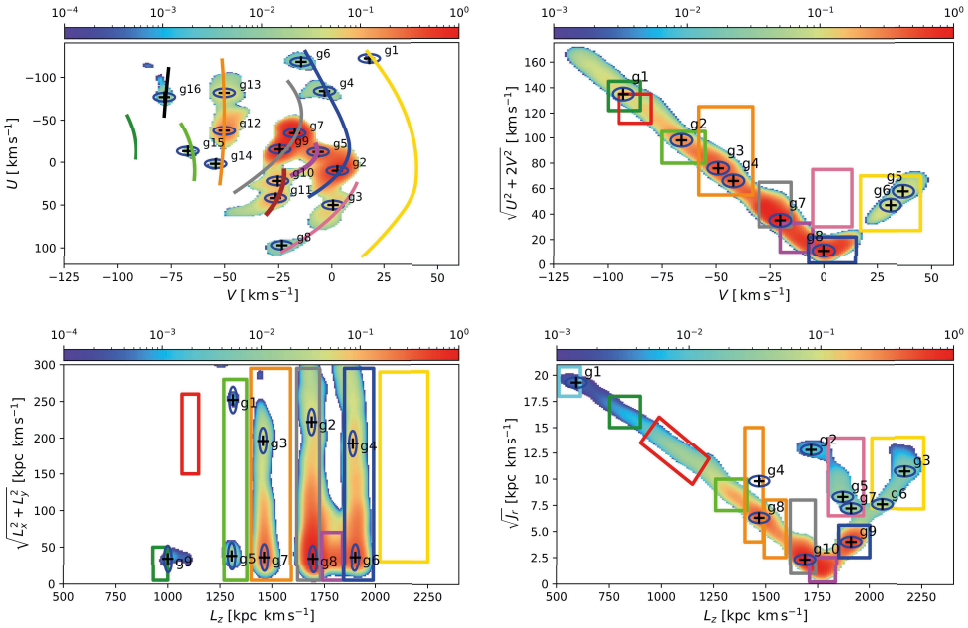


**Fig. 4.** Same as Fig. 3 but for scale $J = 3$. Lines and boxes correspond to the structures detected at scale $J = 2$. We note that numbers assigned to the groups do not match between the planes.

If one looks at the small volumes from the left-hand side of Fig. 2 and move towards positive $X$ values an increase in $V$ velocity can be observed. As an example of this trend, Fig. 5 shows how the $V$ velocity of the groups evolves with Galactocentric distance $R$ in regions 01, 01a, 00, 21, and 21a based on the analysis of the $U-V$ plane. For example, the Hercules stream in region 01 is detected at $V \simeq -70\,\mathrm{km\,s^{-1}}$, and for comparison, in region 21a the Hercules stream shifts towards positive $V$ and is located at $V \simeq -40\,\mathrm{km\,s^{-1}}$. Similar behaviours are observed for most of the major streams and is shown in the top plot of Fig. 5. On the wavelet maps for regions 01a and 21a that are shown in the middle and bottom plots of Fig. 5 we draw the lines from the top left plot in Fig. 3. Taking volumes at larger $R$ shifts the groups towards higher $V$ values and vice verse.

If one fixes the Galactocentric distance and starts exploring the regions at high $\phi$ moving down towards negative $\phi$ (e.g., start at region 15 and go down to region 35), the streams are observed at the same position in $V$. Major streams including Sirius, Pleiades, Hyades, and Hercules have the same angular momentum when fixing $R$ and looking at different $\phi$. This is different from results in Monari et al. (2019) who found that the Hercules angular momentum changes with azimuth at solar radius. We also do not observe this change when fixing $R$ inside and outside the solar circle.

The shape of the angular momentum and action spaces changes slightly at different $R$, but almost all main structures detected in the solar volume remain at the same positions within a box defined by volumes 02_12, 22_12, 22_32 and 02_32. Figure 6 shows wavelet transform maps for regions 01a and 21a (top and middle rows). Additionally a wavelet transform was applied to all the stars in the sample in the angular momentum and action spaces (bottom row) and was compared to results in volumes 01a and 21a. If there are any groups with constant actions detected in the total sample then it possible to observe them in smaller volumes. Boxes of different colours mark kinematic structures detected in the region 00. The same boxes are plotted on top of maps for regions 01a and 21a. There is a small shift in action space when changing $R$, but generally main groups are located at the same positions.

The kinematic structures are mainly detected in the central regions within the rectangle defined by regions 02_12, 22_12, 22_32 and 02_32. The rest of the remaining regions contain less stars and also have larger distance uncertainties. We tested whether or not the structures really exist only inside the box mentioned above or whether or the lack of the groups in the outer regions is a consequence of larger distances and smaller numbers of stars in subsamples. To investigate the latter, 10 000 stars were randomly selected in the central region 00 and the wavelet analysis was repeated. The results were then compared with Dehnen (1998) who used a sample of 14 000 stars in total. For our 10 000 sample, a similar result to that of Dehnen (1998) was received. The main conclusion of the test is that with the small samples it is possible to detect only the large main structures like Sirius, Hyades, Pleiades and Hercules. The more stars are in the volume, the higher the probability of detecting high-velocity structures. Due to this limitation, it is not possible claim that there is such a radius where some of the groups stop existing.

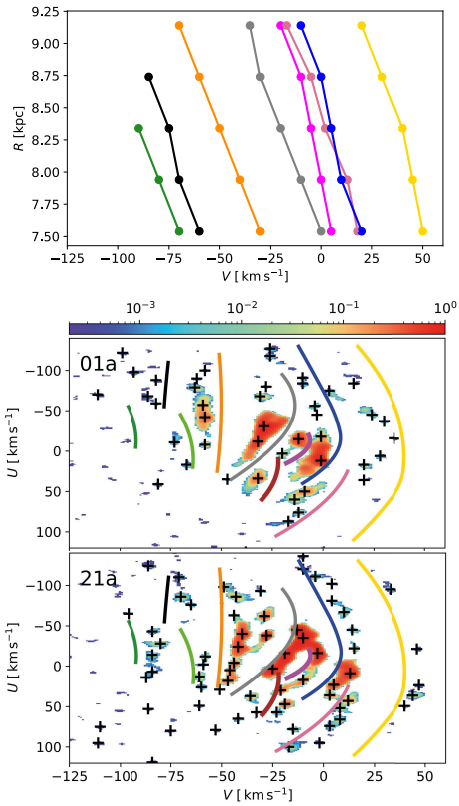


**Fig. 5.** *Top*: change of central $V$ velocities of kinematic structures as a function of Galactocentric radii $R$. Each dot corresponds to the centre of the structure determined by the wavelet transform in volumes 01, 01a, 00, 21, and 21a. Names of the groups associated with the lines are listed in the legend of Fig. 3. *Middle and bottom*: example of wavelet maps in the $U-V$ space in regions 01a and 21a. Colour bar shows normalised wavelet coefficients. Black crosses show centres of the detected structures in regions 01a and 21a. Lines show the location of kinematic structures detected in region 00 (see legend of Fig. 3).

There are many tiny groups detected in the $U-V$ plane that could potentially be a part of the Arcturus stream. We do not observe a clear arch that we can connect with the structure. Unlike the Arcturus stream, an arch at $V \simeq -80\,\mathrm{km\,s^{-1}}$ is clearly visible inside a box defined by regions 01, 11, 21, and 31 for the AF06 stream. In the $V-\sqrt{U^2+2V^2}$ plane the structures are better resolved at scale $J = 3$. In the angular momentum and action space there are strong detections of the high-velocity groups clearly visible at scale $J = 3$. The Arcturus and KFR08 streams appear stronger at the smaller Galactocentric radii. Based on the analysis of all stars in action space, the Arcturus stream is an elongated structure in $L_z$. This means it covers a wider range of orbits, unlike the Hercules stream for example.

## 5. The vertical extent of Arcturus and associated streams

We focus here on three high-velocity structures (g1, g2, and g9) detected in region 00 in action space between $V \simeq -70$ and $-160\,\mathrm{km\,s^{-1}}$. The groups that we associate with these velocities in the solar region are the AF06, Arcturus, and KFR08 streams. We would like to know whether or not they are related, whether or not they are elongations of each other, and how different they are compared to the Hercules stream. The Hercules stream is chosen as a reference as it is one of the most studied kinematic structures and is a relatively metal-rich disc structure with the dynamical origin with the Galactic bar (e.g. Bensby et al. 2007; Ramya et al. 2016; Pérez-Villegas et al. 2017). One of the main peaks of the Hercules stream is group g18 detected in action space. We study properties of this group for a comparison with the high-velocity structures.

To further distinguish the three streams we investigate how the number density of stars in the Hercules, Arcturus, AF06, and KFR08 streams varies with vertical distance from the Galactic plane. Candidate member stars of the three streams were selected from the stellar sample constructed as described in Sect. 2 using the characteristic velocities of the streams that were found for region 00 (see Table A.2). From now on, it is assumed that kinematic groups are defined as stars on similar orbits. We assume that a star belongs to a group if its radial action and angular momentum fall into an ellipse around the centre of the group as shown in Fig. 3.

The leftmost plot of Fig. 7 shows the variation of the normalised number of stars in g1, g2, g9, and g18 streams as defined in action space (see Fig. A.2) with the module of the distance from the Galactic plane $|Z|$ for region 00. The Hercules stream is slightly more concentrated towards the Galactic plane compared to the three high-velocity structures. To check if this is valid in the regions outside the solar neighbourhood, stars in regions 01, 11, 21, and 31 (see Fig. 2) that are members of groups g1, g2, g9, and g18 were selected. A star is defined as a member of a group if it has $J_r$ and $L_z$ values located within an ellipse around a group in action space as shown in Fig. 2. Since actions are conserved quantities along orbits of stars in static potentials, it is expected that the structures will show up at the same positions in $L_z$ and $J_r$. The right-hand side plot in Fig. 7 is the same as the one on the left, but for regions 01, 11, 21, and 31. The Hercules stream is strongly concentrated to the Galactic plane and becomes rapidly weaker with distance from the plane. At distances above $|Z| \gtrsim 0.7$ kpc, the density of stars in the Hercules stream drops to zero. In comparison, the g1, g2, and g9 structures reach larger heights from the plane. The disappearance of the Hercules stream after about 0.7 kpc is consistent with the results from Antoja et al. (2012) that detected the Hercules stream at a lower confidence level at higher $Z$. To further probe the origins of the detected kinematic structures and how they relate to each other we make use of the detailed elemental abundance data from recent spectroscopic surveys.

## 6. Chemical properties of the kinematic streams

In this section we investigate whether or not the detected streams show distinct elemental abundance patterns. To our aim the detailed abundance data from large spectroscopic surveys such as GALAH DR2 (Buder et al. 2018) and APOGEE DR 14 (Holtzman et al. 2018) were used. GALAH DR2 includes over 340 000 stars and APOGEE DR14 around 263 000 stars. Both GALAH and APOGEE have determined radial velocities for all

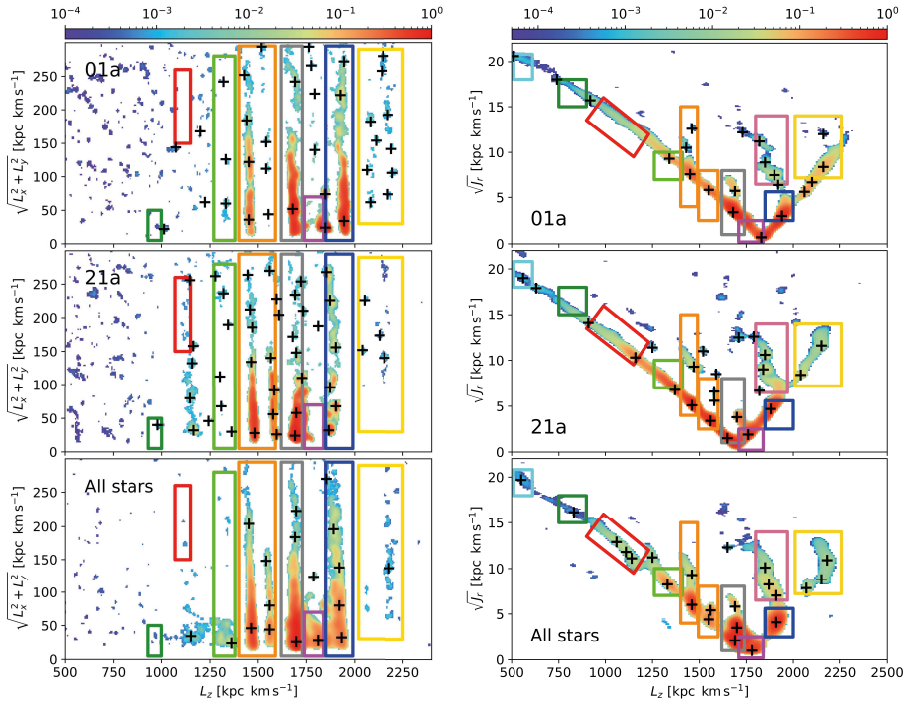


**Fig. 6.** Wavelet coefficient maps of regions 01a (*top*), 21a (*middle*) and all stars studied in this work (*bottom*) retrieved in $L_z - \sqrt{L_x^2 + L_y^2}$ (*left column*) and $L_z - \sqrt{J_R}$ (*right column*) space for scale $J = 2$. Colour bars show normalised wavelet coefficients. Black crosses show centres of the structures. Boxes around the crosses show location of kinematic structures based on the nearby sample 00 (see Fig. 3). Colours of the boxes correspond to different names of the structures listed in the legend of Fig. 3.

their targets, and those stars overlap to only a limited extent with the subsample of stars in *Gaia* that come with measured radial velocities in *Gaia* DR2. This means there will be just a few stars in each kinematic group when cross-matching GALAH and APOGEE with our sample that are constructed from *Gaia* DR2.

Therefore, to increase the number of stars that can be associated with the streams that were detected and that have elemental abundances in the GALAH and APOGEE data releases, we compute space velocities $U, V, W$, angular momenta $L_x, L_y, L_z$, and radial action $J_r$ for all APOGEE and GALAH stars using astrometric data from *Gaia* DR2 and radial velocities from GALAH and APOGEE. The stars with $\sigma_U, \sigma_V \leq 20\,\mathrm{km\,s^{-1}}$ and with good quality flags were then selected. For GALAH, stars with good data quality flags were included: $flag\_cannon = 0$ and $flag\_x\_fe = 0$, where X is a chemical element, and for APOGEE the following quality flags were used: $X\_FE\_FLAG = 0$, where $X$ is a chemical element. This left us with a sample of 101 862 and 72 517 stars for the GALAH and APOGEE surveys, respectively. To select stars that are possible members of the detected kinematic streams, we use our kinematic constraints for action space listed in Table A.2, meaning that a star must be within a specific range in $L_z$ and $J_r$ (i.e. must fall into an ellipse around the structure as shown in Fig. 2).

Figure 8 shows the $X-Y$ distributions for the constructed GALAH and APOGEE samples. It is seen that APOGEE covers more stars of the Northern sky and GALAH covers mainly the Southern part of the sky.

The top plots of Fig. 9 show the [$\alpha$/Fe]−[Fe/H] diagrams for stars in groups g1, g2, g9, and g18 selected in nine regions around the solar neighbourhood (01a_11a, 11a, 11a_21a, 01a, 00, 21a, 31a_01a, 31a, and 21a_31a) for GALAH and APOGEE samples. We over-plot results for these nine regions simply because there are not enough stars in the high-velocity streams in each region to present them separately. The stars members of the groups were selected based on the properties of the groups in region 00 listed in Table A.2. Since actions are conserved quantities, the groups are expected at the same positions after correcting $L_z$ values for the shift that arises due to differences in Galactocentric radii. The solid lines in these diagrams show the running mean for each stream. The shaded regions around each line show the corresponding $1\sigma$ dispersions around the mean value.

The bottom plots of Fig. 9 show generalised metallicity distributions for the same groups as in the upper plots. Median values of the metallicity distributions and the corresponding dispersion of groups g18, g9, g2, and g1 are presented in Table 1 for the GALAH and APOGEE samples. The high-velocity streams generally have wide metallicity distributions and reaching lower metallicities

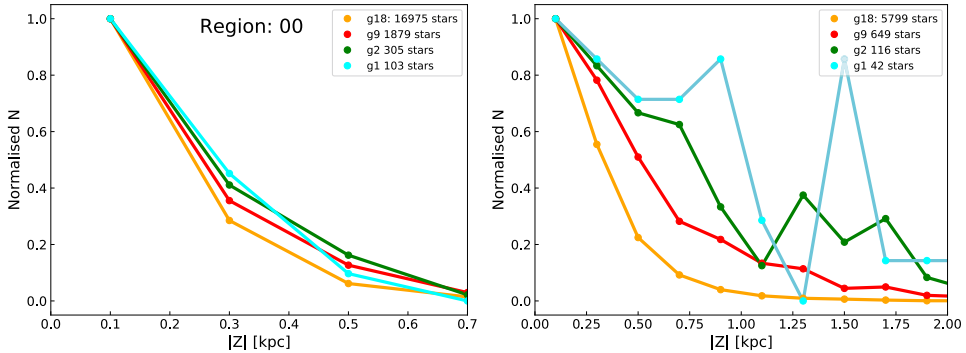


**Fig. 7.** Number of stars in Hercules, AF06, Arcturus, and KFR08 versus module of distance from the Galactic disc $|Z|$ in region 00 (*left*) and in regions 01, 11, 21, and 31 (*right*).

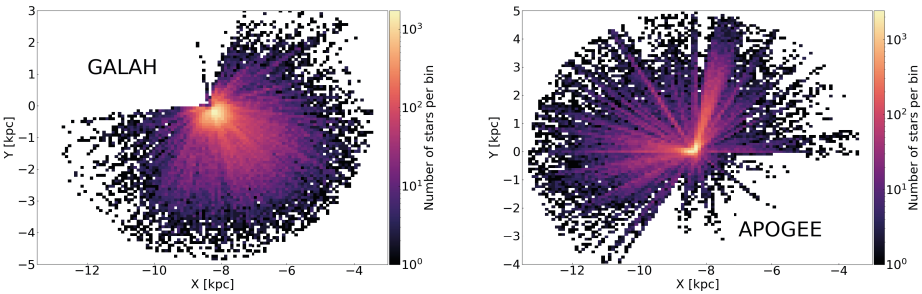


**Fig. 8.** $X-Y$ distributions for GALAH stars (*left*) and for APOGEE stars (*right*) with $\sigma_U, \sigma_V \leq 20\,\mathrm{km\,s^{-1}}$ and good quality flags. The bin size is 0.1 kpc for both plots.

down to [Fe/H] $\lesssim -1$. The Hercules stream is more metal-rich. These plots show that the high-velocity streams could be high-alpha thick-disc structures, while the Hercules stream is likely a mixture of both the thin and thick discs. Two-sided Kolmogorov–Smirnov tests were then used to check if the metallicity distribution of any of the streams come from the same distribution. In all cases the $p$-values were infinitesimally small, indicating that the null-hypothesis must be rejected, meaning that all the distributions are different. Results using APOGEE and GALAH surveys are similar: the high-velocity streams appear to be thick disc structures, while the Hercules stream is a mixture of both the thin and the thick-discs, and is a more metal-rich structure.

## 7. The origin of the Arcturus stream

In this section, we first provide a brief overview of the debates around the origin of the Arcturus stream, then summarise the kinematic and chemical characteristics of the Arcturus stream from this work, and based on that we discuss the possible origins of the stream.

### 7.1. Accretion origin: debris of a disrupted satellite

In Eggen (1996, 1998) it was shown that the Arcturus stream (then called a moving group) belongs to the old thick-disc population. It was fitted with a 10 Gyr isochrone and the metallicity of Arcturus was estimated as [Fe/H] $\simeq -0.6$. Similar properties were observed by Gilmore et al. (2002) and Wyse et al. (2006) who found a clump of stars at $V \simeq -100\,\mathrm{km\,s^{-1}}$ that were estimated to be about 10−12 Gyr old and metal-poor with $-2.5 <$ [Fe/H] $< -0.5$. This is consistent with the properties of the Galactic thick disc.

One of the first attempts to explain the phenomenon of the Arcturus stream numerically was performed by Navarro et al. (2004). Assuming a merger event that happened 10−12 Gyr ago Navarro et al. (2004) obtained a structure with similar properties to the Arcturus stream. Navarro et al. (2004) also estimated the vertical component of the angular momentum of the group to be $L_z \simeq 1000\,\mathrm{kpc\,km\,s^{-1}}$.

Further evidence for a possible debris origin for the Arcturus stream comes from Helmi et al. (2006), who found that a satellite galaxy with similar orbital properties to the Arcturus stream can produce three kinematic over-densities. One of the groups was linked to the Arcturus stream and investigated further through a detailed elemental abundance analysis by Ženovienė et al. (2014). These latter authors found that the average metallicity of the stream is [Fe/H] $\simeq -0.42$ and that its stars are about 8–12 Gyr old, which is consistent with the properties of the thick disc. Considering the results from Helmi et al. (2006), the Ženovienė et al. (2014) study supported a merger origin

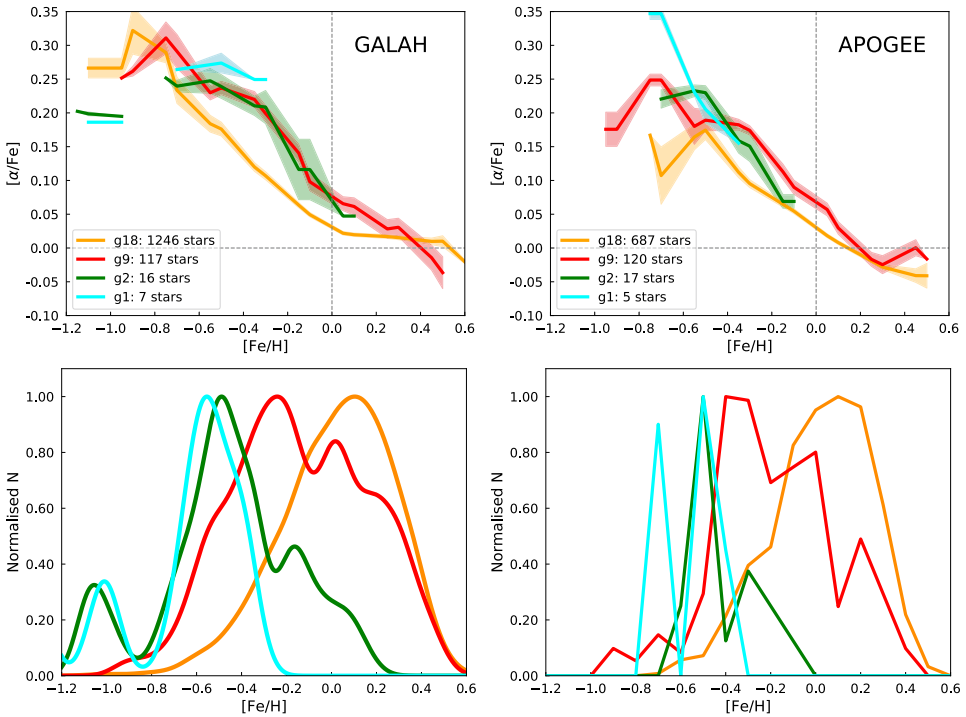


**Fig. 9.** *Top plots*: [Fe/H]−[$\alpha$/Fe] trends for the streams selected from the GALAH and APOGEE data in action space in a square of nine regions defined by regions 01a_11a, 11a_21a, 21a_31a and 31a_01a. The solid lines show the running means of the [$\alpha$/Fe] distributions in bins of [Fe/H], and the shaded regions give the 1-$\sigma$ dispersions of the data around the means. The bin width when calculating running means is 0.05 dex. *Bottom plots*: normalised generalised metallicity distributions for the stellar samples shown in the top plots. Here each star is represented by a Gaussian with a central peak at the estimated metallicity and a width given by the uncertainty of the metallicity.

**Table 1.** Median metallicities and corresponding dispersions of star members of the groups located in the square defined by nine regions around the central region 00 that were selected from APOGEE and GALAH samples.

| Group | GALAH | | APOGEE | |
|---|---|---|---|---|
| | $[Fe/H]_{median}$ | $\sigma_{[Fe/H]}$ | $[Fe/H]_{median}$ | $\sigma_{[Fe/H]}$ |
| g18 | 0.0 | 0.2 | 0.0 | 0.2 |
| g9 | −0.2 | 0.3 | −0.2 | 0.3 |
| g2 | −0.5 | 0.3 | −0.5 | 0.2 |
| g1 | −0.6 | 0.3 | −0.5 | 0.1 |

for the stream. On the other hand, a comparison with another detailed elemental abundance study by Ramya et al. (2012), who applied different selection criteria for possible Arcturus stream stars, suggested that it is different from the thick disc and the two groups studied in these works are different.

An alternative approach to search for kinematic overdensities was proposed by Arifyanto & Fuchs (2006), and then followed by Klement et al. (2008) and Zhao et al. (2014). Using wavelet transforms they searched for clumps in the plane defined by the $\sqrt{U^2 + 2V^2}$ and $V$ space velocities , where $U$ and $V$ are radial and tangential velocity components, respectively. These latter authors detected many kinematic structures in the range $-200 \leq V \leq -80\,\mathrm{km\,s^{-1}}$, including candidates for the Arcturus stream. Following the approach proposed by Helmi et al. (1999), Klement et al. (2008), and Zhao et al. (2014) studied angular momenta space defined by $\sqrt{L_x^2 + L_y^2}$ and $L_z$, the angular momenta components of the stars. They placed the Arcturus stream at $V \simeq -100\,\mathrm{km\,s^{-1}}$ and $L_z \simeq 1000\,\mathrm{kpc\,km\,s^{-1}}$. The high eccentricity and low metallicity of the high-velocity streams lead to a conclusion that the Arcturus has a merger debris origin.

The above papers provide evidence that the Arcturus stream and other high-velocity streams can be explained as debris from disrupted satellite galaxies that merged with the Milky Way in the past.

### 7.2. Galactic origin: resonances

If the debris origin for the observed streams is correct, the stars within a stream should have a distinct elemental abundance pattern different from what is observed for the disc stars of the

Milky Way. A detailed chemical analysis of possible members of the Arcturus stream and another group called the AF06 stream, first assigned by Arifyanto & Fuchs (2006), was performed by Ramya et al. (2012). No unique chemical features were found for either of the groups; their chemical compositions are similar to the background thick disc stars, being metal-poor, alpha-enriched, and have ages between 10 and 14 Gyr. This indicates that these structures are likely to have a dynamical origin within the Galaxy.

Another chemical analysis of the Arcturus stream was performed by Williams et al. (2009). The stellar sample was constructed based on results of the N-body simulations, where a satellite was accreted by the Milky Way. It was also found by these latter authors that the stream stars are chemically inhomogeneous, being similar to the thick disc, and thus, cannot be called a moving group. The authors discuss a possible origin of the group within the Milky Way, being dynamically formed due to Lindblad resonances. At the same time they do not reject the possibility of a merger origin.

Bensby et al. (2014) studied ages and chemical composition of the Galactic disc stars and briefly explored those that could potentially belong to the Arcturus stream ($-115 < V < -85\,\mathrm{km\,s^{-1}}$). These latter authors found no chemical signature of a merger event, but rather that a dynamical origin is more probable due to similarities of chemical patterns of the group with the thick disc.

If the discussed spectroscopic studies question an accretion origin for the Arcturus, can the structure be reproduced in a resonant scenario via numerical simulations? Assuming resonances with the Galactic long bar, Gardner & Flynn (2010) simulated a kinematic group which has properties similar to the Arcturus stream. Numerical simulations performed by Monari et al. (2013) show a similar result; the Galactic long bar can produce a feature that is consistent with the Arcturus stream.

All these findings lead to the question of whether the Arcturus stream formed due to resonances or due to a merger event. Simulations assuming either hypothesis are able to reproduce a phase-space structure similar to the Arcturus stream. At the same time there is no clear consensus from the detailed elemental abundance studies.

### 7.3. Other hypothesis and recent findings

An alternative opinion on the origin of the Arcturus stream was proposed by Minchev et al. (2009). Assuming the existence of a dynamically unrelaxed population which formed after a merger event, these latter authors simulated how the distribution of stars in the $U-V$ and $V-\sqrt{U^2+2V^2}$ changes with time. They found ring-like structures that represent a wave with streams appearing almost every $20\,\mathrm{km\,s^{-1}}$ in $V$, placing the Arcturus stream at $-100\,\mathrm{km\,s^{-1}}$. Based on the kinematics of the simulated structures, the authors state that the Galactic disc was perturbed about 1.9 Gyr ago and match it with the time when the Galactic bar could have formed.

Another support of the ringing hypothesis came with the *Gaia* DR2 (Gaia Collaboration 2018a) release. The analysis of *Gaia* DR2 data revealed a rich arch- and ridge-like substructure in the phase-space that is strong evidence that the disc of the Milky Way is far from being in equilibrium and undergoes phase-mixing (Antoja et al. 2018; Ramos et al. 2018; Monari et al. 2018; Tian et al. 2018). This phase-mixing could be a result of external-perturbations due to a passage of the Sagittarius dwarf galaxy (e.g. Antoja et al. 2018). Indeed, Laporte et al. (2019) demonstrated, using a state-of-the-art simulation of the Milky Way-Sagittarius interaction, that a range of complex phase-space structures discovered in *Gaia* DR2 data can be explained simultaneously by their model existing prior to the *Gaia* DR2 data release, including the disk in-plane velocity field (Katz et al. 2019), the ridges in the $V_\phi-R$ plane (Antoja et al. 2018; Kawata et al. 2018), and the spiral in the $Z-V_z$ plane (Antoja et al. 2018). Here, $V_\phi$ and $V_z$ are velocities in the Galactocentric coordinate system. At the same time, Hunt et al. (2018), Quillen et al. (2018), and Sellwood et al. (2019), show that the phase-space ridges could be a result of an impact of the Galactic spiral arms, but the simulations do not cover the high-velocity field. The Arcturus stream is one of the arch-like structures seen in Ramos et al. (2018), who performed a deeper study of the substructures with the wavelet analysis. If the Arcturus is a kinematic wave in the Galactic disc, then what triggers the formation of these structures, the bar, spiral arms or a merger event? What is the nature of the Arcturus stream and how similar is it to the other kinematic structures?

### 7.4. The origin of the Arcturus stream in this study

Before discussing possibilities for the nature and origin of the Arcturus stream (g2), we summarise the properties of the kinematic substructures associated with the Arcturus stream that we have found so far:

– The rotational velocity of the Arcturus stream is $V \simeq -127\,\mathrm{km\,s^{-1}}$, and the vertical component of the angular momentum is $L_z \simeq 840\,\mathrm{kpc\,km\,s^{-1}}$. This is in agreement with the results from Navarro et al. (2004) who found the Arcturus stream at $V \simeq -100\,\mathrm{km\,s^{-1}}$ and $L_z \simeq$ in the range between 700 and $1100\,\mathrm{kpc\,km\,s^{-1}}$, Klement et al. (2008) who found it at $V \simeq -120\,\mathrm{km\,s^{-1}}$ and $L_z \simeq 1000\,\mathrm{kpc\,km\,s^{-1}}$, and Ramya et al. (2012) who found it at $V \simeq -125\,\mathrm{km\,s^{-1}}$ and $L_z \simeq 811\,\mathrm{kpc\,km\,s^{-1}}$.

– The Arcturus stream (g2), as well as the AF06 and KFR08 streams (g1 and g9), are not only detected in the solar neighbourhood. The structures appear in a larger box defined by regions 01_12, 22_12, 22_32, and 02_32. The remaining regions contain significantly less stars and their distance uncertainties are larger (see Table A.1). Considering the fact stated above it is not possible to definitely answer whether or not there are kinematic structures in those regions, or if they are weaker, or if it is a consequence of the properties of the stellar sample.

– The Arcturus stream extends to about 2 kpc vertically from the Galactic plane. At the same time the stars of the Hercules stream appear to be disappearing at distances greater than $|Z| \gtrsim 1$ kpc. The streams detected at even higher $V$ velocities extend to even greater distances from the Galactic plane. This is consistent with the results from Antoja et al. (2012) who found that the Hercules stream has a lower detection level after $|Z| \gtrsim 0.6$ kpc.

– The Arcturus, KFR08, and AF06 streams are alpha-enhanced in the [$\alpha$/Fe]–[Fe/H] diagram, and show similarities to the Galactic thick disc. They are clearly different from the Hercules stream which appears to be a mixture of the thin and thick discs. This is in agreement with, for example Bensby et al. (2007, 2014), Williams et al. (2009), and Ramya et al. (2012).

– The Arcturus stream has a wide metallicity distribution spanning the interval $-1.2 \leq$ [Fe/H] $\leq 0.2$ and peaking at $\simeq -0.5$, which is not different from what has been found in other studies. Eggen (1996) found [Fe/H] $\simeq -0.6$, and Ramya et al. (2012) found a more metal-poor range for the Arcturus stream, $-1.4 \leq$ [Fe/H] $\leq -0.37$, peaking at [Fe/H] $\simeq -0.7$.

Considering the chemical properties of the Arcturus stream (g2) we see that it is not a chemically homogeneous structure. This indicates that the Arcturus stream is not a moving group, similarly to what was found by Williams et al. (2009), Ramya et al. (2012), and Bensby et al. (2014). Also, the metallicity distributions for the Arcturus, KFR08, and AF06 streams (g2, g1, and g9, respectively) are too wide for them to be called moving groups. At the same time, the mean metallicities are different for each stream, meaning that they appear to be independent structures, which is different from the conclusion by Zhao et al. (2014) that the Arcturus and AF06 streams should be regarded as one structure. It was also shown that a two-sided K–S tests rejected the hypothesis that any of the groups could come from the same population.

Groups g1, g2, and g9 found in this work appear, at least chemically, to be thick disc structures. Therefore, we question the debris origin for the streams. If the streams have a debris origin, their chemical compositions should be different from the thick disc stars. This is different from the Liu et al. (2015) conclusion of a merger origin for the KFR08 stream. It is clearly seen that KFR08 has a wide metallicity distribution and its kinematics and chemistry are consistent with what is seen for the stars in the Galactic thick disc.

The two remaining possibilities for the origin of the Arcturus stream and the neighbouring KFR08 and AF06 streams (g2, g1 and g9 respectively) are the external-perturbation origin or being due to the resonances with the spiral arms or the Galactic bar. The results we have present here are consistent with the results from Minchev et al. (2009), who simulated the velocity distribution in the $V-\sqrt{U^2+2V^2}$ and $U-V$ planes assuming a merger event that perturbed the Galactic disc and caused an ongoing phase-mixing, inducing kinematic over-densities to be placed on the $V$ axis every $20\,\mathrm{km\,s^{-1}}$. This is essentially what we observe in this work. Arch-like structures are easily recognisable in Fig. 3 and are similar to what was found in for example Gaia Collaboration (2018b), Antoja et al. (2018), and Ramos et al. (2018). The patterns discussed in Minchev et al. (2009) are observed at the $V-\sqrt{U^2+2V^2}$ and action space; the arches observed in the $U-V$ plane become clumps. These clumps and arches are observed as lines in the angular momentum space. Within the uncertainties these features (arches, clumps, and lines) show up 20–30 $\mathrm{km\,s^{-1}}$ apart in the $V$ velocity component. According to Minchev et al. (2009), this could be due to ongoing mixing in the disc after a merger event. The fact that the high-velocity groups extend to higher $|Z|$ than the bar-originated structures leads us to conclude on an external-perturbation (phase-mixing) origin for the Arcturus stream and its neighbour KFR08 and AF06 streams is a possible scenario.

## 8. Summary

In order to resolve the nature of the Arcturus stream we analysed the velocity and angular momenta distributions of the *Gaia* DR2 stars at different Galactocentric radii. The analysis revealed the following:

– The analysis of four spaces defined by velocity, angular momentum, and action components in 65 smaller volumes allowed us to detect the previously well-studied Sirius, Pleiades, Hyades, and Hercules streams; a few high-velocity structures that are associated with the AF06, Arcturus, and KFR08 streams; and many unknown clumps that might be a part of larger streams.

– The picture observed in the velocity space is consistent with the results from Minchev et al. (2009). Their model predicts kinematic structures to be placed every 20−30 $\mathrm{km\,s^{-1}}$ in $V$. This is similar to what was observed with the *Gaia* DR2 sample: starting with the Sirius at $0\,\mathrm{km\,s^{-1}}$ and ending with the KFR08 stream at $\simeq -160\,\mathrm{km\,s^{-1}}$ we observe kinematic structures every $V \simeq 20-30\,\mathrm{km\,s^{-1}}$ (taking into account velocity uncertainties and the sizes of the structures).

– The arches observed in the $U-V$ plane are observed as clumps in the $V-\sqrt{U^2+2V^2}$ and action space and lines in the angular momentum space. Minchev et al. (2009) as well as Antoja et al. (2018) link these arches to the ongoing phase-mixing in the disc of the Milky Way due to a strong disc perturbation, likely originating from a merger event.

– The high-velocity streams are observed at higher $|Z|$ compared to the Hercules stream which is currently considered to be a structure caused by the Galactic bar (e.g. Antoja et al. 2014; Pérez-Villegas et al. 2017). The KFR08 stream, which has the highest values of $V$ and lowest $L_z$ extends at least 2 kpc further from the Galactic disc, while the Hercules is located closer to the Galactic disc $|Z| < 0.7$ kpc.

– The majority of stars from the sample analysed in this work are within 1 kpc in $|Z|$ and according to Monari et al. (2013) the Galactic bar can influence stellar motion up to $|Z| \simeq 1$ kpc in the thin disc and up to $|Z| \simeq 2$ kpc. However, the bar-induced arches do not cover the observed range of about $\pm 100\,\mathrm{km\,s^{-1}}$ in radial Galactocentric velocity $V_r$.

– The high-velocity groups are present mainly in the nearby regions. This is consistent with Ramos et al. (2018), where one of the discovered arches, that the authors associate with the Arcturus group, is located mainly in the solar neighbourhood and within the solar circle. At the same time this result could be the consequence of the fact that nearby regions contain more stars and distance uncertainties are smaller.

– Ramos et al. (2018) discuss the negative gradients of the rotational velocity of the structures with the Galactocentric radii. This gradient should be positive for the Cartesian velocities $V$. We do observe similar gradients in the $U-V$ plane.

– The analysis of the chemical abundances of stars that are members of the groups taken from the APOGEE and GALAH spectroscopic surveys confirmed that the AF06, Arcturus, and KFR08 groups have chemical patterns that resemble that of the thick disc. The groups cover wider metallicity ranges compared to Hercules, which appears to be a mixture of the thin and thick disc stars, which is in agreement with the literature (e.g. Bensby et al. 2014; Ramya et al. 2016). The estimated median metallicity of Hercules in this work is $[\mathrm{Fe/H}] \simeq 0.0$. In comparison, Ramya et al. (2016), for example, obtained $[\mathrm{Fe/H}] \simeq 0.15$.

– The two-sided K–S test performed for different combinations of the groups (Hercules, AF06, Arcturus, KFR08) rejected the possibility for all of them to be drawn from the same distribution.

Arcturus, KFR08, and AF06 are kinematic structures that have rotational $V$ velocities separated with a fixed step, extend farther from the Galactic plane compared to other over-densities such as the Hercules stream, and have chemical compositions consistent with the properties of the Galactic thick disc. Collectively, this points towards an origin for the structures related to the ongoing kinematic mixing or ringing in the disc, as was suggested in Minchev et al. (2009). The recently discovered ridges and arches in the phase-space (Antoja et al. 2018; Ramos et al. 2018) found with the *Gaia* DR2, including the Arcturus arch, represent further evidence that the high-velocity kinematic structures such as the Arcturus stream could be a result of the external-perturbation process and were formed inside the Milky Way.

Though a great amount of effort has been made to understand the nature of these phase-space waves with the *Gaia* DR2 data, we are still far from an unambiguous answer. Do these waves have a merger origin as was originally proposed by Minchev et al. (2009), or are they caused by the spiral arms as suggested, for example, by Quillen et al. (2018), Hunt et al. (2018), and Sellwood et al. (2019)? Numerical simulations together with the chemical abundances from spectroscopic surveys like the *Gaia*-ESO survey (Gilmore et al. 2012), WEAVE (Dalton et al. 2014), and 4MOST (de Jong et al. 2019), in combination with upcoming *Gaia* data releases, will broaden the opportunities for us to better understand the formation of the phase-space warps and might provide a definitive answer about the origin of kinematic structures like the Arcturus stream. Current observational evidence however points towards a phase-space mixing origin.

*Acknowledgements.* We thank Prof. F. Murtagh for making available for us the MR software packages and Dr. P. J. McMillan for a valuable help when needed. T. B. was funded by the project grant "The New Milky Way" from the Knut and Alice Wallenberg foundation.

## References

Antoja, T., Figueras, F., Fernández, D., & Torra, J. 2008, A&A, 490, 135
Antoja, T., Helmi, A., Bienayme, O., et al. 2012, MNRAS, 426, L1
Antoja, T., Helmi, A., Dehnen, W., et al. 2014, A&A, 563, A60
Antoja, T., Helmi, A., Romero-Gómez, M., et al. 2018, Nature, 561, 360
Arenou, F., Luri, X., Babusiaux, C., et al. 2018, A&A, 616, A17
Arifyanto, M. I., & Fuchs, B. 2006, A&A, 449, 533
Bailer-Jones, C. A. L. 2015, PASP, 127, 994
Bensby, T., Oey, M. S., Feltzing, S., & Gustafsson, B. 2007, ApJ, 655, L89
Bensby, T., Feltzing, S., & Oey, M. S. 2014, A&A, 562, A71
Bobylev, V. V., & Bajkova, A. T. 2016, Astron. Lett., 42, 90
Bovy, J. 2015, ApJS, 216, 29
Bovy, J. 2016, ApJ, 817, 49
Buder, S., Asplund, M., Duong, L., et al. 2018, MNRAS, 478, 4513
Chakrabarty, D. 2007, A&A, 467, 145
Dalton, G., Trager, S., Abrams, D. C., et al. 2014, Ser., 9147, 91470L
de Jong, R. S., Agertz, O., Berbel, A. A., et al. 2019, The Messenger, 175, 3
De Silva, G. M., Freeman, K. C., Bland-Hawthorn, J., Asplund, M., & Bessell, M. S. 2007, AJ, 133, 694
Dehnen, W. 1998, AJ, 115, 2384
Dehnen, W. 2000, AJ, 119, 800
Dekker, E. 1976, Phys. Rep., 24, 315
Eggen, O. J. 1971, PASP, 83, 762
Eggen, O. J. 1996, AJ, 112, 1595
Eggen, O. J. 1998, AJ, 115, 2397
Famaey, B., Jorissen, A., Luri, X., et al. 2005, A&A, 430, 165
Feltzing, S., & Holmberg, J. 2000, A&A, 357, 153
Gaia Collaboration (Brown, A. G. A., et al.) 2018a, A&A, 616, A1
Gaia Collaboration (Katz, D., et al.) 2018b, A&A, 616, A11
Gardner, E., & Flynn, C. 2010, MNRAS, 405, 545
Gilmore, G., Wyse, R. F. G., & Norris, J. E. 2002, ApJ, 574, L39
Gilmore, G., Randich, S., Asplund, M., et al. 2012, The Messenger, 147, 25
Helmi, A., White, S. D. M., de Zeeuw, P. T., & Zhao, H. 1999, Nature, 402, 53
Helmi, A., Navarro, J. F., Nordström, B., et al. 2006, MNRAS, 365, 1309
Helmi, A., Veljanoski, J., Breddels, M. A., Tian, H., & Sales, L. V. 2017, A&A, 598, A58
Helmi, A., Babusiaux, C., Koppelman, H. H., et al. 2018, Nature, 563, 85
Holtzman, J. A., Hasselquist, S., Shetrone, M., et al. 2018, AJ, 156, 125
Hunt, J. A. S., Hong, J., Bovy, J., Kawata, D., & Grand, R. J. J. 2018, MNRAS, 481, 3794
Johnson, D. R. H., & Soderblom, D. R. 1987, AJ, 93, 864
Katz, D., Sartoretti, P., Cropper, M., et al. 2019, A&A, 622, A205
Kawata, D., Baba, J., Ciucă, I., et al. 2018, MNRAS, 479, L108
Klement, R., Fuchs, B., & Rix, H.-W. 2008, ApJ, 685, 261
Koppelman, H., Helmi, A., & Veljanoski, J. 2018, ApJ, 860, L11
Kushniruk, I., Schirmer, T., & Bensby, T. 2017, A&A, 608, A73
Laporte, C. F. P., Minchev, I., Johnston, K. V., & Gómez, F. A. 2019, MNRAS, 485, 3134
Lindegren, L. 2018, Gaia Technical Note: GAIA-C3-TN-LU-LL-124-01
Liu, C., Feltzing, S., & Ruchti, G. 2015, A&A, 580, A111
McMillan, P. J. 2018, Res. Notes Am. Astron. Soc., 2, 51
Minchev, I., Nordhaus, J., & Quillen, A. C. 2007, ApJ, 664, L31
Minchev, I., Quillen, A. C., Williams, M., et al. 2009, MNRAS, 396, L56
Minchev, I., Boily, C., Siebert, A., & Bienayme, O. 2010, MNRAS, 407, 2122
Monari, G., Antoja, T., & Helmi, A. 2013, ArXiv e-prints [arXiv:1306.2632]
Monari, G., Kawata, D., Hunt, J. A. S., & Famaey, B. 2017, MNRAS, 466, L113
Monari, G., Famaey, B., Minchev, I., et al. 2018, Res. Notes Am. Astron. Soc., 2, 32
Monari, G., Famaey, B., Siebert, A., et al. 2019, in press, https://doi.org/10.1051/0004-6361/201936455
Navarro, J. F., Helmi, A., & Freeman, K. C. 2004, ApJ, 601, L43
Pérez-Villegas, A., Portail, M., Wegg, C., & Gerhard, O. 2017, ApJ, 840, L2
Quillen, A. C., & Minchev, I. 2005, AJ, 130, 576
Quillen, A. C., Carrillo, I., Anders, F., et al. 2018, MNRAS, 480, 3132
Ramos, P., Antoja, T., & Figueras, F. 2018, A&A, 619, A72
Ramya, P., Reddy, B. E., & Lambert, D. L. 2012, MNRAS, 425, 3188
Ramya, P., Reddy, B. E., Lambert, D. L., & Musthafa, M. M. 2016, MNRAS, 460, 1356
Schönrich, R., Binney, J., & Dehnen, W. 2010, MNRAS, 403, 1829
Sellwood, J. A. 2010, MNRAS, 409, 145
Sellwood, J. A., Trick, W. H., Carlberg, R. G., Coronado, J., & Rix, H.-W. 2019, MNRAS, 484, 3154
Skuljan, J., Hearnshaw, J. B., & Cottrell, P. L. 1999, MNRAS, 308, 731
Starck, J.-L., & Murtagh, F. 2002, Astronomical Image and Data Analysis (Berlin: Springer)
Starck, J. L., & Murtagh, F. D. 1998, Image Processing and Data Analysis (Cambridge: Cambridge University Press), 297
Tian, H.-J., Liu, C., Wu, Y., Xiang, M.-S., & Zhang, Y. 2018, ApJ, 865, L19
Trick, W. H., Coronado, J., & Rix, H.-W. 2019, MNRAS, 484, 3291
van der Walt, S., Schönberger, J. L., Nunez-Iglesias, J., et al. 2014, PeerJ, 2, e453
Wegg, C., Gerhard, O., & Portail, M. 2015, MNRAS, 450, 4050
Williams, M. E. K., Freeman, K. C., Helmi, A., & RAVE Collaboration 2009, in The Galaxy Disk in Cosmological Context, eds. J. Andersen, B. M. Nordströara, & J. Bland-Hawthorn, IAU Symp., 254, 139
Wyse, R. F. G., Gilmore, G., Norris, J. E., et al. 2006, ApJ, 639, L13
Ženovienė, R., Tautvaišienė, G., Nordström, B., & Stonkutė, E. 2014, A&A, 563, A53
Zhao, J. K., Zhao, G., Chen, Y. Q., et al. 2014, ApJ, 787, 31

## Appendix A: Additional tables

**Table A.1.** Number of stars, median distance, and median distance uncertainty for the stars located in the 65 regions (as defined in Fig. 1).

| $N$ | Region | $N$ stars | $D_{\rm median}$ [pc] | $\sigma_{D_{\rm median}}$ [pc] |
|---|---|---|---|---|
| 1 | 00 | 666 505 | 212 | 2 |
| 2 | 01 | 48 759 | 851 | 45 |
| 3 | 02 | 13 647 | 1689 | 181 |
| 4 | 03 | 6332 | 2483 | 386 |
| 5 | 04 | 3041 | 3285 | 677 |
| 6 | 05 | 1621 | 4083 | 932 |
| 7 | 11 | 70 747 | 861 | 38 |
| 8 | 12 | 22 070 | 1778 | 164 |
| 9 | 13 | 8991 | 2636 | 375 |
| 10 | 14 | 3521 | 3502 | 669 |
| 11 | 15 | 1685 | 4338 | 918 |
| 12 | 21 | 81 838 | 777 | 38 |
| 13 | 22 | 24 823 | 1602 | 171 |
| 14 | 23 | 10 146 | 2392 | 410 |
| 15 | 24 | 3307 | 3204 | 803 |
| 16 | 25 | 1386 | 4011 | 1171 |
| 17 | 31 | 64 875 | 868 | 38 |
| 18 | 32 | 19 806 | 1778 | 164 |
| 19 | 33 | 10 747 | 2624 | 365 |
| 20 | 34 | 4307 | 3489 | 655 |
| 21 | 35 | 1873 | 4329 | 826 |
| 22 | 22_11 | 18 596 | 1798 | 209 |
| 23 | 22_12 | 13 098 | 2258 | 306 |
| 24 | 22_13 | 8223 | 2853 | 495 |
| 25 | 22_14 | 4132 | 3522 | 724 |
| 26 | 22_15 | 2197 | 4216 | 898 |
| 27 | 22_31 | 27 838 | 1780 | 194 |
| 28 | 22_32 | 18 135 | 2242 | 284 |
| 29 | 22_33 | 9545 | 2839 | 458 |
| 30 | 22_34 | 5646 | 3507 | 690 |
| 31 | 22_35 | 2832 | 4200 | 922 |
| 32 | 02_11 | 11 447 | 1942 | 215 |
| 33 | 02_12 | 8189 | 2546 | 349 |
| 34 | 02_13 | 3219 | 3321 | 608 |
| 35 | 02_14 | 2267 | 4145 | 852 |
| 36 | 02_15 | 308 | 4897 | 954 |
| 37 | 02_31 | 12 179 | 1939 | 232 |
| 38 | 02_32 | 9594 | 2544 | 372 |
| 39 | 02_33 | 4786 | 3306 | 602 |
| 40 | 02_34 | 1887 | 4147 | 868 |
| 41 | 02_35 | 263 | 4881 | 903 |
| 42 | 12_01 | 13 658 | 2042 | 217 |
| 43 | 12_03 | 4287 | 3177 | 589 |
| 44 | 12_04 | 1942 | 3893 | 847 |
| 45 | 12_05 | 1125 | 4605 | 1024 |
| 46 | 12_21 | 21 401 | 1864 | 189 |
| 47 | 12_23 | 6129 | 2823 | 538 |
| 48 | 12_24 | 2440 | 3500 | 896 |
| 49 | 12_25 | 1195 | 4206 | 1173 |
| 50 | 32_01 | 13 717 | 2044 | 219 |
| 51 | 32_03 | 3988 | 3176 | 609 |
| 52 | 32_04 | 2172 | 3871 | 829 |
| 53 | 32_05 | 1290 | 4592 | 1081 |
| 54 | 32_21 | 22 441 | 1856 | 186 |
| 55 | 32_23 | 3331 | 3496 | 855 |
| 56 | 32_24 | 11 387 | 2806 | 495 |
| 57 | 32_25 | 1447 | 4209 | 1166 |
| 58 | 01a | 211 846 | 453 | 12 |
| 59 | 11a | 271 059 | 444 | 10 |
| 60 | 21a | 317 397 | 387 | 9 |
| 61 | 31a | 256 489 | 448 | 10 |
| 62 | 01a_11a | 127 033 | 630 | 22 |
| 63 | 11a_21a | 175 045 | 568 | 18 |
| 64 | 21a_31a | 184 213 | 574 | 18 |
| 65 | 31a_01a | 127 733 | 636 | 22 |

**Table A.2.** Kinematic structures found in region 00 in the $U-V$ (Plane 1), $V-\sqrt{U^2+2V^2}$ (Plane 2), $L_z-\sqrt{L_x^2+L_y^2}$ (Plane 3) and $L_z-\sqrt{J_r}$ (Plane 4) planes at scale $J=2$.

| $N$ | Plane | Group | Name | $N$ stars | $U$ [km s$^{-1}$] | $V$ [km s$^{-1}$] | $L_z$ [kpc km s$^{-1}$] | $\sqrt{J_r}$ [kpc km s$^{-1}$] | $\sigma_U$ [km s$^{-1}$] | $\sigma_V$ [km s$^{-1}$] | $\sigma_{L_z}$ [kpc km s$^{-1}$] | $\sigma_{\sqrt{J_r}}$ [kpc km s$^{-1}$] |
|---|---|---|---|---|---|---|---|---|---|---|---|---|
| 1 | 1 | g1 | A1/A2 | 173 | 39 | 37 | 2158 | 12 | 2 | 2 | 30 | 0.6 |
| 2 | 1 | g2 | $\gamma$Leo | 2643 | 34 | 8 | 1926 | 7 | 2 | 2 | 28 | 0.5 |
| 3 | 1 | g3 | Sirius | 6966 | −13 | 6 | 1918 | 3.6 | 2 | 2 | 31 | 0.5 |
| 4 | 1 | g4 | Sirius | 1659 | −53 | 4 | 1900 | 6.3 | 2 | 2 | 30 | 0.5 |
| 5 | 1 | g5 | $\gamma$Leo | 2277 | 47 | 3 | 1894 | 7.9 | 2 | 2 | 31 | 0.5 |
| 6 | 1 | g6 | Sirius | 10 303 | 12 | 2 | 1888 | 4.1 | 2 | 2 | 30 | 0.5 |
| 7 | 1 | g7 | Sirius | 1416 | −61 | 2 | 1887 | 6.9 | 2 | 2 | 30 | 0.5 |
| 8 | 1 | g8 | $\gamma$Leo | 1080 | 65 | 1 | 1872 | 9.9 | 2 | 2 | 27 | 0.5 |
| 9 | 1 | g9 | Sirius | 871 | −79 | 0 | 1858 | 8.8 | 2 | 2 | 31 | 0.5 |
| 10 | 1 | g10 | $\gamma$Leo | 785 | 73 | −2 | 1844 | 10.6 | 2 | 2 | 28 | 0.5 |
| 11 | 1 | g11 | $\gamma$Leo | 1881 | 57 | −5 | 1819 | 8.5 | 2 | 2 | 32 | 0.5 |
| 12 | 1 | g12 | Coma Berenices | 12 046 | −15 | −7 | 1808 | 1.3 | 2 | 2 | 29 | 0.5 |
| 13 | 1 | g13 | Bobylev16 | 180 | −118 | −10 | 1776 | 13.1 | 2 | 2 | 31 | 0.5 |
| 14 | 1 | g14 | Coma Berenices | 8439 | 8 | −14 | 1745 | 2.4 | 2 | 2 | 30 | 0.5 |
| 15 | 1 | g15 | Pleiades/Hyades | 960 | −81 | −14 | 1744 | 8.3 | 2 | 2 | 29 | 0.5 |
| 16 | 1 | g16 | Pleiades/Hyades | 14 380 | −33 | −16 | 1733 | 2.7 | 2 | 2 | 28 | 0.5 |
| 17 | 1 | g17 | Pleiades/Hyades | 11 749 | −42 | −19 | 1710 | 3.8 | 2 | 2 | 25 | 0.4 |
| 18 | 1 | g18 | Antoja12(12) | 302 | 98 | −21 | 1695 | 13 | 2 | 2 | 29 | 0.5 |
| 19 | 1 | g19 | Wolf 630 | 6104 | 21 | −22 | 1678 | 4.1 | 2 | 2 | 29 | 0.5 |
| 20 | 1 | g20 | Dehnen98 | 4129 | 41 | −25 | 1664 | 6.3 | 2 | 2 | 26 | 0.4 |
| 21 | 1 | g21 | Pleiades/Hyades | 13 084 | −10 | −25 | 1657 | 2.2 | 2 | 2 | 26 | 0.4 |
| 22 | 1 | g22 | Hercules | 2604 | −58 | −37 | 1562 | 6.5 | 2 | 2 | 24 | 0.4 |
| 23 | 1 | g23 | Pleiades/Hyades | 3428 | 25 | −37 | 1561 | 5.7 | 2 | 2 | 27 | 0.4 |
| 24 | 1 | g24 | Hercules | 1380 | −82 | −47 | 1473 | 9.5 | 2 | 2 | 27 | 0.4 |
| 25 | 1 | g25 | Hercules | 3529 | −15 | −48 | 1468 | 5.8 | 2 | 2 | 25 | 0.4 |
| 26 | 1 | g26 | Hercules | 4626 | −37 | −49 | 1463 | 6.6 | 2 | 2 | 22 | 0.4 |
| 27 | 1 | g27 | Hercules | 2816 | 0 | −50 | 1455 | 6.2 | 2 | 2 | 24 | 0.5 |
| 28 | 1 | g28 | Hercules | 1593 | −70 | −51 | 1450 | 8.9 | 2 | 2 | 25 | 0.5 |
| 29 | 1 | g29 | Antoja12(15) | 633 | 65 | −52 | 1441 | 10.2 | 2 | 2 | 27 | 0.4 |
| 30 | 1 | g30 | HR1614 | 1286 | 9 | −64 | 1342 | 8.2 | 2 | 2 | 25 | 0.5 |
| 31 | 1 | g31 | HR1614 | 1989 | −16 | −64 | 1343 | 8.1 | 2 | 2 | 25 | 0.4 |
| 32 | 1 | g32 | HR1614 | 1619 | −26 | −67 | 1321 | 8.5 | 2 | 2 | 24 | 0.5 |
| 33 | 1 | g33 | HR1614 | 1345 | −36 | −68 | 1313 | 8.9 | 2 | 2 | 25 | 0.5 |
| 34 | 1 | g34 | $\epsilon$Ind | 498 | −83 | −75 | 1252 | 12 | 2 | 2 | 25 | 0.4 |
| 35 | 1 | g35 | $\epsilon$Ind | 626 | −73 | −76 | 1247 | 11.5 | 2 | 2 | 24 | 0.5 |
| 36 | 1 | g36 | Arcturus | 358 | −13 | −92 | 1118 | 11.6 | 2 | 2 | 23 | 0.6 |
| 37 | 2 | g1 | Arcturus | 1840 | −11 | −91 | 1125 | 11.7 | 25 | 2 | 22 | 0.6 |
| 38 | 2 | g2 | AF06 | 2013 | −12 | −86 | 1168 | 11.1 | 26 | 2 | 24 | 0.7 |
| 39 | 2 | g3 | Hercules | 1483 | −85 | −54 | 1431 | 10.4 | 57 | 2 | 26 | 0.8 |
| 40 | 2 | g4 | HR1614 | 7629 | −10 | −65 | 1337 | 8.3 | 20 | 1 | 23 | 0.5 |
| 41 | 2 | g5 | HR1614 | 8490 | −9 | −61 | 1366 | 7.8 | 19 | 1 | 24 | 0.5 |
| 42 | 2 | g6 | Hercules | 14 860 | −10 | −46 | 1482 | 5.8 | 19 | 2 | 27 | 0.5 |
| 43 | 2 | g7 | Sirius | 2459 | −60 | 1 | 1876 | 8 | 64 | 2 | 29 | 1.4 |
| 44 | 2 | g8 | Hercules | 15 404 | −5 | −40 | 1539 | 4.9 | 21 | 2 | 25 | 0.7 |
| 45 | 2 | g9 | A1/A2 | 1129 | −5 | 38 | 2173 | 10.6 | 17 | 2 | 30 | 0.6 |
| 46 | 2 | g10 | Pleiades/Hyades | 16 788 | −41 | −19 | 1707 | 3.9 | 34 | 2 | 26 | 1.1 |
| 47 | 2 | g11 | $\gamma$Leo | 4112 | 45 | 3 | 1893 | 7.4 | 49 | 2 | 31 | 1.3 |
| 48 | 2 | g12 | Pleiades/Hyades | 38 181 | −7 | −25 | 1660 | 2.5 | 14 | 2 | 27 | 0.7 |
| 49 | 2 | g13 | $\gamma$Leo | 5460 | 30 | 7 | 1921 | 6.3 | 34 | 2 | 29 | 1.1 |
| 50 | 2 | g14 | A1/A2 | 3361 | −5 | 22 | 2044 | 7 | 13 | 1 | 32 | 0.6 |
| 51 | 2 | g15 | Coma Berenices | 26 737 | −2 | −12 | 1766 | 1.2 | 10 | 2 | 29 | 1 |
| 52 | 2 | g16 | Sirius | 19311 | 0 | 8 | 1926 | 4.3 | 9 | 2 | 27 | 0.5 |
| 53 | 2 | g17 | Sirius | 19 358 | 0 | 0 | 1872 | 2.9 | 5 | 2 | 31 | 0.5 |

**Notes.** First column is a line number in the table; the second one denotes the plane; names of the groups as in Fig. 3 are given in Col. 3 and names of the groups as in the literature are provided in Col. 4; the number of stars in each group is given in Col. 5; median $U$, $V$ velocities, median angular momentum $L_z$ and the median value of the square root of radial action per group is given in Cols. 6–9; Cols. 8–13 are standard deviations of the same quantities as in Cols. 6–9.

**Table A.2.** continued.

| $N$ | Plane | Group | Name | $N$ stars | $U$ [km s$^{-1}$] | $V$ [km s$^{-1}$] | $L_z$ [kpc km s$^{-1}$] | $\sqrt{J_r}$ [kpc km s$^{-1}$] | $\sigma_U$ [km s$^{-1}$] | $\sigma_V$ [km s$^{-1}$] | $\sigma_{L_z}$ [kpc km s$^{-1}$] | $\sigma_{\sqrt{J_r}}$ [kpc km s$^{-1}$] |
|---|---|---|---|---|---|---|---|---|---|---|---|---|
| 54 | 3 | g1 | Pleiades/Hyades | 81 | −13 | −23 | 1661 | 3.2 | 40 | 2 | 2 | 2.8 |
| 55 | 3 | g2 | Hercules | 47 | −12 | −52 | 1439 | 6.6 | 47 | 2 | 2 | 2.3 |
| 56 | 3 | g3 | Hercules | 66 | −18 | −41 | 1529 | 5.7 | 47 | 2 | 2 | 2.3 |
| 57 | 3 | g4 | Sirius | 86 | −6 | 4 | 1895 | 4.4 | 33 | 3 | 2 | 1.9 |
| 58 | 3 | g5 | HR1614 | 41 | −17 | −67 | 1325 | 8.7 | 45 | 2 | 1 | 1.9 |
| 59 | 3 | g6 | Pleiades/Hyades | 171 | −12 | −20 | 1698 | 3.5 | 34 | 2 | 2 | 2.1 |
| 60 | 3 | g7 | Hercules | 120 | −27 | −51 | 1452 | 6.7 | 34 | 2 | 2 | 1.3 |
| 61 | 3 | g8 | Sirius | 165 | −3 | 2 | 1890 | 4.2 | 35 | 3 | 2 | 2.2 |
| 62 | 3 | g9 | Pleiades/Hyades | 264 | −19 | −20 | 1698 | 2.8 | 36 | 2 | 2 | 2.5 |
| 63 | 3 | g10 | AF06 | 17 | −22 | −94 | 1109 | 12.4 | 45 | 2 | 2 | 1.5 |
| 64 | 3 | g11 | A1/A2 | 41 | −10 | 24 | 2064 | 8.1 | 38 | 3 | 2 | 2 |
| 65 | 3 | g12 | Sirius | 263 | −2 | 7 | 1926 | 4.6 | 29 | 3 | 2 | 1.7 |
| 66 | 3 | g13 | A1/A2 | 55 | −13 | 26 | 2063 | 7.9 | 30 | 3 | 2 | 1.5 |
| 67 | 3 | g14 | HR1614 | 119 | −11 | −62 | 1350 | 8.4 | 38 | 2 | 2 | 1.3 |
| 68 | 3 | g15 | Hercules | 339 | −20 | −39 | 1547 | 5.4 | 39 | 2 | 2 | 1.7 |
| 69 | 3 | g16 | Sirius | 456 | 0 | 6 | 1914 | 4.3 | 28 | 3 | 2 | 1.7 |
| 70 | 3 | g17 | A1/A2 | 54 | −16 | 24 | 2057 | 7.5 | 28 | 3 | 2 | 1.5 |
| 71 | 3 | g18 | HR1614 | 108 | −17 | −62 | 1349 | 8.4 | 39 | 2 | 2 | 1.6 |
| 72 | 3 | g19 | Hercules | 379 | −32 | −48 | 1470 | 6.5 | 31 | 2 | 2 | 1.4 |
| 73 | 3 | g20 | Sirius | 427 | 3 | 5 | 1919 | 4.2 | 23 | 3 | 2 | 1.5 |
| 74 | 3 | g21 | Arcturus | 8 | −44 | −111 | 967 | 15.4 | 60 | 1 | 3 | 0.6 |
| 75 | 3 | g22 | Coma Berenices | 644 | −9 | −7 | 1806 | 2 | 27 | 2 | 2 | 2.3 |
| 76 | 3 | g23 | Pleiades/Hyades | 865 | −21 | −19 | 1703 | 2.5 | 25 | 2 | 2 | 1.7 |
| 77 | 3 | g24 | HR1614 | 90 | −18 | −61 | 1362 | 8.3 | 39 | 2 | 2 | 1.5 |
| 78 | 4 | g1 | KFR08 | 107 | −13 | −160 | 575 | 19.5 | 49 | 2 | 23 | 0.2 |
| 79 | 4 | g2 | Arcturus | 303 | −6 | −127 | 841 | 16.1 | 40 | 3 | 23 | 0.2 |
| 80 | 4 | g3 | Antoja12(12) | 122 | 103 | −19 | 1707 | 15.1 | 125 | 3 | 22 | 0.3 |
| 81 | 4 | g4 | A1/A2 | 132 | 31 | 43 | 2223 | 13.3 | 42 | 4 | 22 | 0.2 |
| 82 | 4 | g5 | Hercules | 326 | −111 | −50 | 1460 | 13 | 103 | 3 | 22 | 0.2 |
| 83 | 4 | g6 | A1/A2 | 255 | 27 | 30 | 2110 | 12.8 | 69 | 4 | 22 | 0.2 |
| 84 | 4 | g7 | Antoja12(12) | 579 | 92 | −19 | 1710 | 12.9 | 105 | 4 | 23 | 0.3 |
| 85 | 4 | g8 | $\gamma$Leo | 405 | 84 | −7 | 1805 | 12.7 | 102 | 4 | 22 | 0.2 |
| 86 | 4 | g9 | AF06 | 1836 | −18 | −92 | 1113 | 11.9 | 27 | 2 | 21 | 0.2 |
| 87 | 4 | g10 | $\gamma$Leo | 803 | 77 | −4 | 1828 | 11.4 | 84 | 4 | 23 | 0.3 |
| 88 | 4 | g11 | A1/A2 | 1026 | −7 | 39 | 2177 | 10.9 | 26 | 3 | 20 | 0.3 |
| 89 | 4 | g12 | $\gamma$Leo | 1765 | 64 | 0 | 1867 | 10 | 70 | 4 | 23 | 0.3 |
| 90 | 4 | g13 | Hercules | 3649 | −72 | −50 | 1460 | 9.4 | 64 | 4 | 23 | 0.3 |
| 91 | 4 | g14 | $\gamma$Leo | 3393 | 48 | 1 | 1878 | 8.3 | 57 | 4 | 24 | 0.2 |
| 92 | 4 | g15 | HR1614 | 8691 | −15 | −64 | 1342 | 8.3 | 22 | 2 | 21 | 0.3 |
| 93 | 4 | g16 | A1/A2 | 2922 | −13 | 25 | 2064 | 7.7 | 20 | 3 | 20 | 0.3 |
| 94 | 4 | g17 | $\gamma$Leo | 5271 | 33 | 6 | 1910 | 7 | 44 | 4 | 23 | 0.3 |
| 95 | 4 | g18 | Hercules | 16 701 | −21 | −49 | 1463 | 6.2 | 19 | 2 | 20 | 0.3 |
| 96 | 4 | g19 | Dehnen98 | 7245 | 36 | −23 | 1679 | 6.1 | 47 | 4 | 22 | 0.3 |
| 97 | 4 | g20 | Pleiades/Hyades | 15 246 | −15 | −38 | 1551 | 4.6 | 19 | 3 | 22 | 0.3 |
| 98 | 4 | g21 | Sirius | 22 970 | 0 | 6 | 1916 | 4.1 | 15 | 3 | 22 | 0.3 |
| 99 | 4 | g22 | Pleiades/Hyades | 21 418 | −39 | −20 | 1699 | 3.9 | 29 | 4 | 22 | 0.3 |
| 100 | 4 | g23 | Pleiades/Hyades | 32 987 | −13 | −25 | 1664 | 2.4 | 11 | 3 | 22 | 0.2 |
| 101 | 4 | g24 | Coma Berenices | 21 624 | −11 | −11 | 1769 | 0.9 | 6 | 3 | 23 | 0.2 |

**Table A.3.** Kinematic structures found in region 00 in the $U - V$ (Plane 1), $V - \sqrt{U^2 + 2V^2}$ (Plane 2), $L_z - \sqrt{L_x^2 + L_y^2}$ (Plane 3) and $L_z - \sqrt{J_r}$ (Plane 4) planes at scale $J = 3$.

| $N$ | Plane | Group | Name | $N$ stars | $U$ [km s$^{-1}$] | $V$ [km s$^{-1}$] | $L_z$ [kpc km s$^{-1}$] | $\sqrt{J_r}$ [kpc km s$^{-1}$] | $\sigma_U$ [km s$^{-1}$] | $\sigma_V$ [km s$^{-1}$] | $\sigma_{L_z}$ [kpc km s$^{-1}$] | $\sigma_{\sqrt{J_r}}$ [kpc km s$^{-1}$] |
|---|---|---|---|---|---|---|---|---|---|---|---|---|
| 1 | 1 | g1 | A1/A2 | 44 | −122 | 17 | 2003 | 15.9 | 2 | 2 | 34 | 0.5 |
| 2 | 1 | g2 | Sirius | 10 806 | 9 | 2 | 1890 | 3.9 | 2 | 2 | 30 | 0.5 |
| 3 | 1 | g3 | $\gamma$Leo | 2325 | 49 | 0 | 1872 | 7.9 | 2 | 2 | 32 | 0.5 |
| 4 | 1 | g4 | Bobylev16 | 824 | −83 | −3 | 1840 | 9.1 | 2 | 2 | 30 | 0.5 |
| 5 | 1 | g5 | Coma Berenices | 12 027 | −11 | −6 | 1814 | 1.3 | 2 | 2 | 29 | 0.5 |
| 6 | 1 | g6 | Bobylev16 | 194 | −118 | −13 | 1750 | 12.9 | 2 | 2 | 29 | 0.4 |
| 7 | 1 | g7 | Pleiades/Hyades | 14 437 | −33 | −17 | 1726 | 2.7 | 2 | 2 | 28 | 0.5 |
| 8 | 1 | g8 | Antoja12(12) | 332 | 96 | −22 | 1686 | 12.8 | 2 | 2 | 30 | 0.5 |
| 9 | 1 | g9 | Pleiades/Hyades | 14 069 | −14 | −23 | 1672 | 2 | 2 | 2 | 28 | 0.4 |
| 10 | 1 | g10 | Wolf 630 | 5913 | 21 | −24 | 1665 | 4.2 | 2 | 2 | 28 | 0.5 |
| 11 | 1 | g11 | Dehnen98 | 4086 | 41 | −25 | 1659 | 6.4 | 2 | 2 | 26 | 0.5 |
| 12 | 1 | g12 | Hercules | 4670 | −37 | −49 | 1463 | 6.5 | 2 | 2 | 22 | 0.4 |
| 13 | 1 | g13 | Hercules | 1394 | −81 | −49 | 1464 | 9.6 | 2 | 2 | 25 | 0.4 |
| 14 | 1 | g14 | Hercules | 2400 | 1 | −53 | 1438 | 6.5 | 2 | 2 | 26 | 0.5 |
| 15 | 1 | g15 | HR1614 | 1769 | −13 | −66 | 1331 | 8.2 | 2 | 2 | 25 | 0.5 |
| 16 | 1 | g16 | $\epsilon$Ind | 544 | −76 | −77 | 1239 | 11.7 | 2 | 2 | 23 | 0.5 |
| 17 | 2 | g1 | Arcturus | 1837 | −13 | −92 | 1113 | 11.9 | 28 | 2 | 22 | 0.7 |
| 18 | 2 | g2 | HR1614 | 7724 | −14 | −66 | 1330 | 8.5 | 24 | 2 | 24 | 0.5 |
| 19 | 2 | g3 | Hercules | 15 998 | −20 | −49 | 1463 | 6.3 | 24 | 2 | 25 | 0.5 |
| 20 | 2 | g4 | Hercules | 15 702 | −12 | −42 | 1524 | 5.4 | 25 | 2 | 29 | 0.7 |
| 21 | 2 | g5 | A1/A2 | 1270 | −6 | 37 | 2167 | 10.5 | 21 | 2 | 32 | 0.6 |
| 22 | 2 | g6 | A1/A2 | 1835 | −7 | 30 | 2108 | 8.8 | 17 | 2 | 36 | 0.6 |
| 23 | 2 | g7 | Pleiades/Hyades | 40 542 | −11 | −21 | 1696 | 2 | 17 | 2 | 29 | 0.9 |
| 24 | 2 | g8 | Sirius | 21 306 | 6 | 0 | 1865 | 3 | 10 | 2 | 33 | 0.8 |
| 25 | 3 | g1 | HR1614 | 35 | −16 | −68 | 1315 | 8.7 | 40 | 2 | 2 | 1.7 |
| 26 | 3 | g2 | Pleiades/Hyades | 190 | −11 | −21 | 1692 | 3.3 | 39 | 2 | 2 | 2.6 |
| 27 | 3 | g3 | Hercules | 125 | −26 | −50 | 1457 | 6.6 | 42 | 2 | 2 | 1.8 |
| 28 | 3 | g4 | Sirius | 165 | −3 | 2 | 1890 | 4.2 | 35 | 3 | 2 | 2.2 |
| 29 | 3 | g5 | HR1614 | 85 | −33 | −68 | 1308 | 9.2 | 37 | 2 | 2 | 1.5 |
| 30 | 3 | g6 | Sirius | 522 | 6 | 4 | 1901 | 4.1 | 27 | 3 | 2 | 1.7 |
| 31 | 3 | g7 | Hercules | 383 | −31 | −49 | 1464 | 6.6 | 33 | 2 | 2 | 1.4 |
| 32 | 3 | g8 | Pleiades/Hyades | 939 | −20 | −20 | 1697 | 2.8 | 28 | 2 | 2 | 1.8 |
| 33 | 3 | g9 | Arcturus | 8 | −49 | −106 | 1000 | 14.2 | 38 | 1 | 2 | 0.8 |
| 34 | 4 | g1 | KFR08 | 94 | −14 | −159 | 586 | 19.3 | 51 | 2 | 21 | 0.2 |
| 35 | 4 | g2 | Antoja12(12) | 585 | 91 | −18 | 1718 | 12.8 | 104 | 4 | 23 | 0.3 |
| 36 | 4 | g3 | A1/A2 | 1081 | −6 | 38 | 2172 | 10.8 | 27 | 3 | 22 | 0.3 |
| 37 | 4 | g4 | Hercules | 2939 | −77 | −49 | 1463 | 9.7 | 70 | 4 | 23 | 0.2 |
| 38 | 4 | g5 | $\gamma$Leo | 3455 | 49 | 0 | 1869 | 8.3 | 58 | 4 | 24 | 0.2 |
| 39 | 4 | g6 | A1/A2 | 3076 | −14 | 24 | 2058 | 7.6 | 21 | 3 | 21 | 0.3 |
| 40 | 4 | g7 | $\gamma$Leo | 4959 | 35 | 6 | 1910 | 7.2 | 45 | 4 | 24 | 0.2 |
| 41 | 4 | g8 | Hercules | 17 305 | −24 | −49 | 1466 | 6.3 | 21 | 3 | 21 | 0.3 |
| 42 | 4 | g9 | Sirius | 23 880 | 0 | 5 | 1909 | 4 | 15 | 3 | 22 | 0.3 |
| 43 | 4 | g10 | Pleiades/Hyades | 35 424 | −17 | −22 | 1687 | 2.3 | 13 | 3 | 24 | 0.2 |

**Notes.** First column is a line number in the table; the second one denotes the plane; names of the groups as in Fig. 4 are given in Col. 3 and names of the groups as in the literature are provided in column 4; number of stars in each group is given in Col. 5; median $U$, $V$ velocities, median angular momentum $L_z$ and the median value of the square root of radial action per group is given in Cols. 6–9; Cols. 8–13 are standard deviations of the same quantities as in Cols. 6–9.

# Paper III

A&A 638, A154 (2020)
https://doi.org/10.1051/0004-6361/202037923


Astronomy & Astrophysics

# The HR 1614 moving group is not a dissolving cluster

Iryna Kushniruk[1], Thomas Bensby[1], Sofia Feltzing[1], Christian L. Sahlholdt[1], Diane Feuillet[1], and Luca Casagrande[2]

[1] Lund Observatory, Department of Astronomy and Theoretical Physics, Box 43, 221 00 Lund, Sweden
e-mail: iryna@astro.lu.se, tbensby@astro.lu.se
[2] Research School of Astronomy & Astrophysics, Mount Stromlo Observatory, The Australian National University, Canberra, ACT 2611, Australia

Received 11 March 2020 / Accepted 8 May 2020

**ABSTRACT**

*Context.* The HR 1614 is an overdensity in velocity space and has for a long time been known as an old (∼2 Gyr) and metal-rich ([Fe/H] ≈ +0.2) nearby moving group that has a dissolving open cluster origin. The existence of such old and metal-rich groups in the solar vicinity is quite unexpected since the vast majority of nearby moving groups are known to be young.
*Aims.* In the light of new and significantly larger data sets than ever before (astrometric, photometric, and spectroscopic), we aim to re-investigate the properties and origin of the HR 1614 moving group. If the HR 1614 overdensity is a dissolving cluster, its stars should represent a single-age and single-elemental abundance population.
*Methods.* To identify and characterise the HR 1614 moving group we use astrometric data from *Gaia* DR2; distances, extinction, and reddening corrections from the StarHorse code; elemental abundances from the GALAH and APOGEE spectroscopic surveys; and photometric metallicities from the SkyMapper survey. Bayesian ages were estimated for the SkyMapper stars. Since the Hercules stream is the closest kinematical structure to the HR 1614 moving group in velocity space and as its origin is believed to be well-understood, we use the Hercules stream for comparison purposes. Stars that are likely to be members of the two groups were selected based on their space velocities.
*Results.* The HR 1614 moving group is located mainly at negative $U$ velocities, does not form an arch of constant energy in the $U-V$ space, and is tilted in $V$. We find that the HR 1614 overdensity is not chemically homogeneous, but that its stars exist at a wide range of metallicities, ages, and elemental abundance ratios. They are essentially similar to what is observed in the Galactic thin and thick discs, a younger population (around 3 Gyr) that is metal-rich ($-0.2 \leq$ [Fe/H] $\leq 0.4$) and alpha-poor. These findings are very similar to what is seen for the Hercules stream, which is believed to have a dynamical origin and consists of regular stars from the Galactic discs.
*Conclusions.* The HR 1614 overdensity has a wide spread in metallicity, [Mg/Fe], and age distributions resembling the general properties of the Galactic disc. It should therefore not be considered a dissolving open cluster, or an accreted population. Based on the kinematic and chemical properties of the HR 1614 overdensity we suggest that it has a complex origin that could be explained by combining several different mechanisms such as resonances with the Galactic bar and spiral structure, phase mixing of dissolving spiral structure, and phase mixing due to an external perturbation.

**Key words.** stars: kinematics and dynamics – Galaxy: kinematics and dynamics – Galaxy: formation – Galaxy: evolution

## 1. Introduction

The Milky Way has a complex structure (e.g. Bland-Hawthorn & Gerhard 2016). By studying how stars move in the Galaxy we can trace the formation history of the Milky Way (e.g. Freeman & Bland-Hawthorn 2002). Stars that share a common motion are usually called kinematic structures, and studying their origin is one of the ways of obtaining more information about the formation and evolution of the Galactic disc. The analysis of data from the Hipparcos mission (Perryman et al. 1997) revealed a rich structure of the local velocity distribution (e.g. Dehnen 2000; Arifyanto & Fuchs 2006). Later, an even more complex picture was discovered by the *Gaia* mission (Gaia Collaboration 2016). The local velocity field is composed of dozens of kinematic structures that together form arches and ridges in different velocity projections (e.g. Antoja et al. 2018; Gaia Collaboration 2018c; Ramos et al. 2018; Khanna et al. 2019; Kushniruk & Bensby 2019). The origin of the non-smooth local velocity distribution is directly linked to major formation processes of the Milky Way. For example, kinematic structures can have different origins, including resonances with the Galactic bar (e.g. Dehnen 2000; Monari et al. 2018), resonances with the spiral arms (e.g. Quillen et al. 2018a), phase mixing as a result of a dynamical interaction with a merging dwarf galaxy (e.g. Minchev et al. 2009; Antoja et al. 2018; Laporte et al. 2019), phase mixing as a result of transient spiral arms and a perturbation with a dwarf satellite (e.g. Khanna et al. 2019), and phase mixing due to transient spiral structure (e.g. Hunt et al. 2019).

Another explanation for some kinematic structures is that open clusters dissolve with time and form moving groups. This idea was first introduced by Olin Eggen (Eggen 1965). Since stars in a moving group originate from the same cluster, they share similar chemical composition, ages, and motion. Two well-known moving groups are the Pleiades and the Hyades, which are visible to the naked eye. More contended examples of moving groups are the Arcturus and the HR 1614 moving groups that were discovered in Eggen (1971, 1978). The groups were later confirmed with Hipparcos and *Gaia* data (e.g. Dehnen 1998; Feltzing & Holmberg 2000; Ramos et al. 2018; Kushniruk & Bensby 2019). For a long time the Arcturus structure was considered a dissolving open cluster, later an accreted stellar population. However, Kushniruk & Bensby (2019) used the *Gaia* Data Release 2 (DR2) data and found no signatures of it being a dissolving cluster or an accreted

population. Instead, the group was likely caused by phase mixing induced by a merger, as was proposed by Minchev et al. (2009).

A discovery of a group of stars with mean radial velocity component $U \simeq 0\,\mathrm{km\,s^{-1}}$ and mean rotational velocity component $V \simeq -60\,\mathrm{km\,s^{-1}}$ and higher than solar metallicity was first reported in Eggen (1978). The group was named after the star HR 1614[1] which is one of its member stars. It was proposed that the overdensity is a dissolving old open cluster. Later Eggen (1992) estimated that the HR 1614 moving group is about 5 Gyr old. The origin of the group was re-investigated in Feltzing & Holmberg (2000) using HIPPARCOS data. Candidate member stars of the group were carefully selected by examining Hertzsprung–Russell diagrams (HR diagram) for different slices of the $U - V$ space velocity distribution. A slice with younger and more metal-rich stars was found. From dynamical simulations of a disrupting open cluster they could explain the tilt of the group in the $U - V$ space. They also found the group to be about 2 Gyr old, and that its metallicity is [Fe/H] $\simeq 0.19$. Later, De Silva et al. (2007) performed a spectroscopic study of stars that were assigned as members of the group by Feltzing & Holmberg (2000) and confirmed that HR 1614 is a 2 Gyr metal-rich group with [Fe/H] $\geq 0.25$. It was also found to be chemically homogeneous with a scatter of only about 0.01 dex in various chemical elements. So, from the literature we know that HR 1614 is a metal-rich, 2 Gyr moving group that is scattered around the Sun.

When searching for the Arcturus stream Kushniruk & Bensby (2019) were able to clearly identify the HR 1614 moving group in the velocity distribution. The question is whether HR 1614 can still be considered a dissolved open cluster if the much larger and more precise astrometric sample from *Gaia* DR2 is used to identify and characterise its properties in more detail. In this paper we aim to do just that, to analyse kinematic, chemical, and photometric properties of the 1614 moving group in order to constrain its origin using data from *Gaia* DR2 and spectroscopic surveys such as APOGEE and GALAH.

The paper is structured in the following way. The data sets used are described in Sect. 2. The selection of candidate member stars of the HR 1614 moving group is described in Sect. 3, where we also analyse the HR diagrams, and the metallicity and age distributions of the HR 1614 moving group stars. In Sect. 4 we discuss the possible origins of HR 1614, and finally our findings are summarised in Sect. 5.

## 2. Data

In this work we use proper motions, sky positions, and radial velocities from the *Gaia* DR2 (Gaia Collaboration 2018b) catalogue, Bayesian extinction corrections and distances from the `StarHorse` code (Anders et al. 2019). We cross-match the `StarHorse` and *Gaia* DR2 catalogues by *Gaia* IDs where the radial velocity is not NULL, where the internal `StarHorse` quality flag `SH_OUTFLAG` is set to `'00000'`, and where the *Gaia* quality flag `SH_GAIAFLAG` is set to `'000'`. These are recommended quality flags that are explained in detail in Anders et al. (2019). In addition, we also cut out stars with `parallax_over_error` > 10 and `visibility_periods_used` > 8 as suggested by Gaia Collaboration (2018a). The final data query is as follows:

```
SELECT s.*, g.*
FROM gdr2.gaia_source AS g,
gdr2_contrib.starhorse AS s
WHERE g.source_id = s.source_id
AND g.radial_velocity IS NOT NULL
AND s.SH_OUTFLAG LIKE '00000'
AND s.SH_GAIAFLAG LIKE '000'
AND g.parallax_over_error > 10
AND g.visibility_periods_used > 8
```

The query listed above gives us a sample of 4 790 725 stars. We use the *galpy*[2] package (Bovy 2015) to calculate: 1) space velocities $U$, $V$, and $W$[3] corrected for peculiar motion of the Sun with $(U_\odot, V_\odot, W_\odot) = (11.10, 12.24, 7.25)$ km s$^{-1}$ (Schönrich et al. 2010) and 2) Galactocentric cylindrical coordinates $R$, $\phi$, and $Z$[4] with $R_\odot = 8.34$ kpc (Reid et al. 2014), $\phi_\odot = 0°$, and $Z_\odot = 14$ pc (Binney et al. 1997).

To characterise the groups chemically, we use elemental abundances from both the APOGEE (Majewski et al. 2017) and GALAH (De Silva et al. 2015) spectroscopic surveys. APOGEE provides stellar atmospheric parameters and elemental abundances derived from near-IR ($H$-band), high-resolution ($R \sim 23\,000$) spectra. We use the abundances from APOGEE DR16 (Ahumada et al. 2019), which includes stars in both the northern and southern hemispheres. After applying the same cuts for quality assurance as in Feuillet et al. (2019) and cross-matching our sample with APOGEE by *Gaia* IDs, we have a sample of 126 690 red giants. GALAH is also a high-resolution ($R \sim 28\,000$) spectroscopic survey operating at optical wavelengths in the southern hemisphere that provides stellar atmospheric parameters and elemental abundances. We use GALAH DR2 Buder et al. (2018), setting the flag_cannon and flag_x_fe flags to zero as recommended. Cross-matching GALAH with our set of stars results in a sample of 231 725 stars. We also use data from the SkyMapper (Casagrande et al. 2019) survey, which provided photometric metallicities for 907 893 stars after cross-matching it with our sample of *Gaia* IDs. To navigate on HR diagrams presented in this paper, we use PARSEC 1.2S isochrones[5] re-derived for the *Gaia* DR2 photometric system (Maíz Apellániz & Weiler 2018).

## 3. Analysis

### 3.1. The old HR 1614 moving group

The nature of the HR 1614 overdensity was previously investigated by Feltzing & Holmberg (2000). They used HIPPARCOS data and divided the $U - V$ space into seven smaller boxes. Individual HR diagrams for each box revealed one box with a population that was younger and more metal-rich than the Sun, which was connected to the HR 1614 moving group.

In this study we repeat the same procedure, but with our much larger stellar sample. Figure 1 shows the $U - V$ distribution of 581 190 stars close to the Sun within a region defined by $R_\odot \pm 0.2$ kpc and $\phi_\odot \pm 1.5°$. This data is sliced into seven boxes, as was done in Feltzing & Holmberg (2000). The boxes are shown with dashed lines in Fig. 1. Box 5 is where the group is supposed to be located according to Feltzing & Holmberg (2000). With *Gaia* DR2/`StarHorse` we clearly see that box 5 contains two velocity overdensities, whereas in Feltzing & Holmberg (2000) two separate overdensities were not observed (probably due to a significantly smaller stellar sample). The inclined overdensity in

[1] HR1614 has a *Gaia* DR2 ID: `3211461469444773376`. ID in the Henry Draper Catalogue is HD 32147.

[2] Available at https://github.com/jobovy/galpy

[3] $U$ points at the Galactic centre, $V$ in the direction of Galactic rotation, and $W$ towards the Galactic north pole.

[4] $R$ and $\phi$ point in the opposite direction to $U$ and $V$.

[5] Available at http://stev.oapd.inaf.it/cgi-bin/cmd

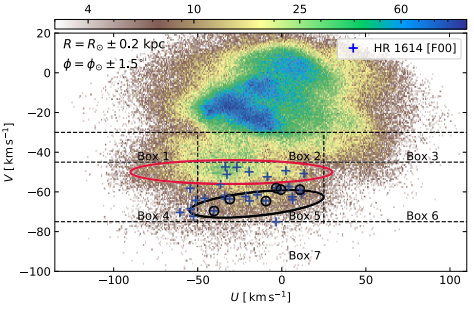


**Fig. 1.** $U - V$ distribution of 581 190 stars inside a region defined in $R_\odot \pm 0.2$ kpc and $\phi_\odot \pm 1.5°$ (see Sect. 3). The color scale is proportional to the number of stars, as indicated in the bar at the top. Stars in the HR 1614 moving group from Feltzing & Holmberg (2000) are shown as blue crosses and their best-selected candidates as black open circles. We identify stars within the red and black ellipses as members of the Hercules stream and the HR 1614 moving group, respectively (see discussion in Sect. 3). Dashed lines and numbers show the same boxes as in Feltzing & Holmberg (2000).

box 5 in Fig. 1 is what we link to the HR 1614 moving group (marked by a black ellipse). The horizontal overdensity in box 5 is known as the Hercules stream (marked by a red ellipse). The identification of the groups is based on results of the wavelet transform performed in Kushniruk & Bensby (2019).

The Hercules stream has been studied in many works: it is likely caused by resonances with the bar (e.g. Dehnen 2000; Bensby et al. 2007; Wegg et al. 2015), and thus, will be used as a benchmark group in this study. Due to its resonant origin, the Hercules stream mainly consists of stars from the Galactic disk. Fig. 1 show stars that are potential members of the HR 1614 group taken from Table 1 in Feltzing & Holmberg (2000). These are the same stars as the ones shown as filled black circles in Table 1 in Feltzing & Holmberg (2000). Interestingly, although Feltzing & Holmberg (2000) did not see HR 1614 as a separate overdensity in their box 5, the circled crosses that show stars from their paper and our black ellipse are tilted at similar angles.

Figure 2 shows individual HR diagrams for boxes 1–7 using extinction corrected colours and absolute magnitudes from the `StarHorse` catalogue. Two sets of isochrones are shown: one with an age of 2 Gyr and metallicity [M/H] = +0.2 and one with an age of 8 Gyr and [M/H] = +0.0. It is clear that none of the HR diagrams can be fitted with only one isochrone. This probably means that the stars in all boxes represent an underlying population of stars with a wide range in metallicity and/or age. Similarly to what was seen in Feltzing & Holmberg (2000), boxes 2 and 5 appear to contain younger stars compared to the other boxes. These are also the boxes with the largest number of stars. As was shown in Fig. 1, in our larger data set we clearly see that box 5 consists of two different groups, Hercules and HR 1614, that were not observed as separate overdensities with the HIPPARCOS data (Feltzing & Holmberg 2000).

### 3.2. The new HR 1614 moving group

A more robust way to select candidate member stars in the HR 1614 moving group is to apply the results of the wavelet transform analysis presented in Kushniruk & Bensby (2019). They analysed the *Gaia* DR2 radial velocity sample in the $U - V$ space by individually exploring smaller sub-samples at different $R$ and $\phi$. Their analysis is based on the discrete wavelet transform, an algorithm that decomposes data into a set of wavelet coefficients. These coefficients contain information about the location and significance of velocity overdensities present in the data. More details on the wavelet transform can be found in Starck & Murtagh (2002), and about the procedure in Kushniruk et al. (2017) and Kushniruk & Bensby (2019).

The locations of the sub-samples (regions 00, 01a, 11a, 21a, and 31a) from Kushniruk & Bensby (2019) in Cartesian Galactic $X$ and $Y$ coordinate system are shown in the top left plot of Fig. 3. The other plots in Fig. 3 show wavelet transform maps for the corresponding regions. The HR 1614 moving group is observed as four overdensities with mean $U = -18\,\mathrm{km\,s^{-1}}$ and $V = -65\,\mathrm{km\,s^{-1}}$ in region 00. The group is also visible in regions 11a and 31a at the same location and is slightly shifted downwards in $V$ in region 01a and shifted upwards in region 21a. The shift occurs due to the location of the regions at different Galacticentric radii.

The $U - V$ distribution of stars in Fig. 1 is shown for region 00. A black ellipse drawn around the HR 1614 moving group is centred at $U = -18\,\mathrm{km\,s^{-1}}$ and $V = -65\,\mathrm{km\,s^{-1}}$, and a red ellipse around the Hercules stream is centred at $U = -37\,\mathrm{km\,s^{-1}}$ and $V = -49\,\mathrm{km\,s^{-1}}$. The positions of the two groups were taken from Kushniruk & Bensby (2019), and the height and width of the ellipse were arbitrarily selected to fit the $U - V$ distribution.

Figure 4 shows HR diagrams for the stars inside the black and red ellipses that we link to the HR 1614 moving group and the Hercules stream. The red circles show stars from Feltzing & Holmberg (2000) that we also could identify in our `StarHorse` sample. Most of these stars follow an [M/H] = 0.2 and 2 Gyr isochrone, the parameters of HR 1614 that were found by Feltzing & Holmberg (2000) and De Silva et al. (2007). At the same time it is clearly seen that stars from ellipses around Hercules and HR 1614 are also composed of multiple stellar populations and cannot be fitted with only one isochrone. From now on we refer to stars inside the black and red ellipses in Fig. 1 as the HR 1614 moving group and the Hercules stream, respectively.

#### 3.2.1. HR diagrams

Figures 5 and 6 show HR diagrams of the HR 1614 moving group and the Hercules stream, respectively, for six metallicity bins in the range $-0.6 <$ [Fe/H] $< 0.6$. The top panels in each figure show the APOGEE and GALAH data (red and blue dots, respectively), and the bottom panels show stars with SkyMapper data (green dots). We plot isochrones with a metallicity corresponding to the mean metallicity of the stars in each bin. The HR diagrams show that the HR 1614 moving group and the Hercules stream cover a wide range of metallicities and ages. An age–metallicity gradient appears to be present in both groups. Metal-poor stars tend to be older and metal-rich stars seem to be younger, based on a visual inspection of the HR diagrams. It is worth noting that stars in the most metal-poor and metal-rich bins do not perfectly match the isochrones. Therefore, in Fig. 7 we compare metallicities for stars in common between the GALAH and SkyMapper, and the APOGEE and SkyMapper surveys. The difference between SkyMapper and GALAH or APOGEE metallicities increases for metal-rich SkyMapper targets. As the SkyMapper metallicities are estimated based on photometric parameters and calibrated on data from the GALAH survey. The SkyMapper metallicities are overestimated for

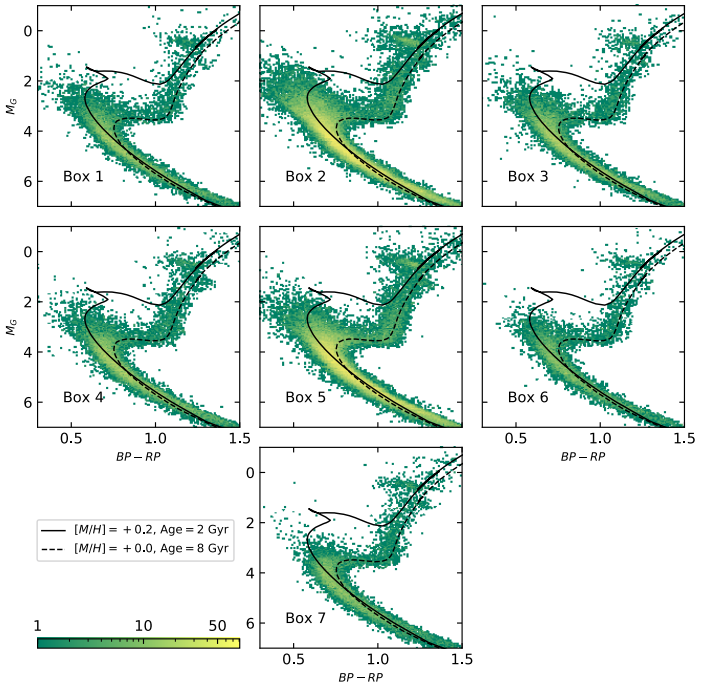


**Fig. 2.** Hertzsprung–Russel diagrams for stars inside the seven boxes as shown in Fig. 1. The dashed line is an isochrone for [M/H] = 0 and 8 Gyr, the solid line shows an isochrone for [M/H] = +0.2 and 8 Gyr. The Colour bar shows the number of stars in each bin.

targets more metal-rich than ≃0.5 dex, where the GALAH survey does not provide any stars (see Fig. 11 in Casagrande et al. (2019) for more details).

Overall, the HR diagrams presented in Figs. 4–6 show that the HR 1614 moving group is a more complex structure than previously thought, and that it does not consist of single-age and single-elemental abundance population of stars, similarly to the Hercules stream. This finding contradicts the hypothesis that the HR 1614 overdensity has a moving group origin, in which case its stars would show homogeneity in age and elemental abundance.

### 3.2.2. Abundance trends and metallicity distribution

Figure 8 shows the [Mg/Fe] versus [Fe/H] diagrams for stars from the GALAH and APOGEE catalogues that are located in region 00. Candidate members of the HR 1614 moving group (left panels) and the Hercules stream (right panels) are shown as red dots. The GALAH data (lower panels) generally show larger uncertainties than the APOGEE data (upper panels), and therefore we only show a single error bar representing the mean uncertainty for the GALAH stars. Background distributions as well as stars from the groups are composed of two sequences, low- and high-alpha stellar populations, that can be recognised as the chemically defined Galactic thin and thick discs (e.g. Bensby et al. 2011).

The metallicity distributions for the HR 1614 moving group and the Hercules stream with GALAH, APOGEE, and SkyMapper data are shown in Fig. 9. The distributions for the HR 1614 moving group look more spiky due to lower number of stars in the group compared to the Hercules stream. Again, both groups cover a wide range of metallicities and are likely composed of stars that come from different stellar populations. We do not observe the overdensity around [Fe/H] = 0.2 in the metallicity distribution of the HR 1614 moving group. These findings question the existence of a single metal-rich population of stars reported in Feltzing & Holmberg (2000) and De Silva et al. (2007) as well as the dissolving cluster origin of the HR 1614 overdensity.

### 3.2.3. Age distribution

Figure 10 shows the age–metallicity probability distributions for the HR 1614 moving group and the Hercules streams. To determine these distributions, we first calculated the two-dimensional probability distributions in age and metallicity, $\mathcal{G}_i(\tau, [\mathrm{Fe/H}])$, for each star $i$ following the method by Howes et al. (2019). In short, the $\mathcal{G}$ function of a star is calculated by fitting a grid of isochrones (PARSEC) to the observed $G$ magnitude, $G_{BP} - G_{RP}$ colour, metallicity, and distance. Then the age–metallicity distribution of the sample as a whole, $\phi(\tau, [\mathrm{Fe/H}])$, is estimated by maximising the likelihood

$$L(\phi) = \prod_i \int \mathcal{G}_i(\tau, [\mathrm{Fe/H}]) \phi(\tau, [\mathrm{Fe/H}])\, \mathrm{d}\tau\, \mathrm{d}[\mathrm{Fe/H}]\,, \qquad (1)$$

using an inversion algorithm. The inversion is subject to regularisation which means there is a single free parameter governing

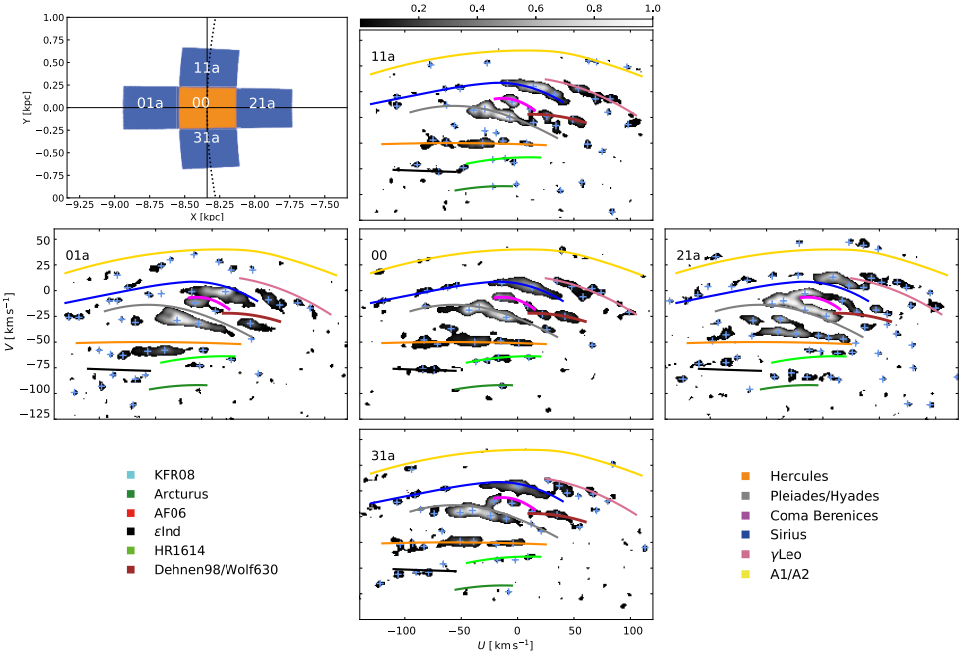


**Fig. 3.** *Top left*: location of five regions (00, 01a, 11a, 21a, and 31a) in the $X - Y$ space explored in this work. *Other plots*: wavelet transform maps that show location of the kinematic overdensities in the $U - V$ space. Their centres are shown with blue crosses. Lines connect eponymous overdensities into structures. The names of the structures are listed in the legend. The colour bar shows the normalised wavelet coefficients in each bin.

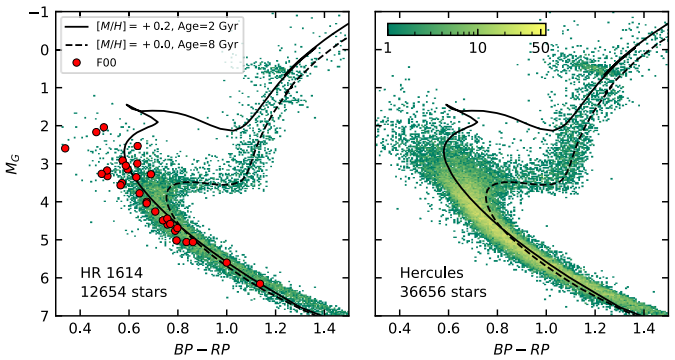


**Fig. 4.** Hertzsprung–Russel diagrams for 12 654 stars from the HR 1614 moving group (*left*) and 36 656 stars from Hercules (*right*) selected from the black and red ellipses shown in Fig. 1. An isochrone with [M/H] = +0.2 and 2 Gyr is shown as a black solid line, and one with [M/H] = 0 and 8 Gyr is shown as a dashed line. Red dots in the *top left plot* show all the stars from Table 1 in Feltzing & Holmberg (2000). The colour bar shows the number of stars in each bin for both plots.

the smoothness of $\phi$. Figure 10 shows the results for one choice of this parameter, but we have tested a wide range of values and find that the results are similar enough to not affect our conclusions. This method will be described in detail in an upcoming publication (Sahlholdt & Lindegren, in prep.).

Both groups are composed of at least two stellar populations. The first population is metal-poor and old with the centre at [Fe/H] $\approx -0.2$ and an age of about 8 Gyr. The second population is metal-rich and young with the centre at [Fe/H] $\approx +0.1$ and an age of about 3 Gyr. These two populations can most likely be associated with the Galactic thin and thick discs. There is also a third clump at a very young age, less than about 1 Gyr. These are stars with ages that are located at the edge of the grid and are artefacts of the age estimation procedure.

From this analysis it is clear that the HR 1614 overdensity is not a 2 Gyr old stellar population, but rather is composed of a

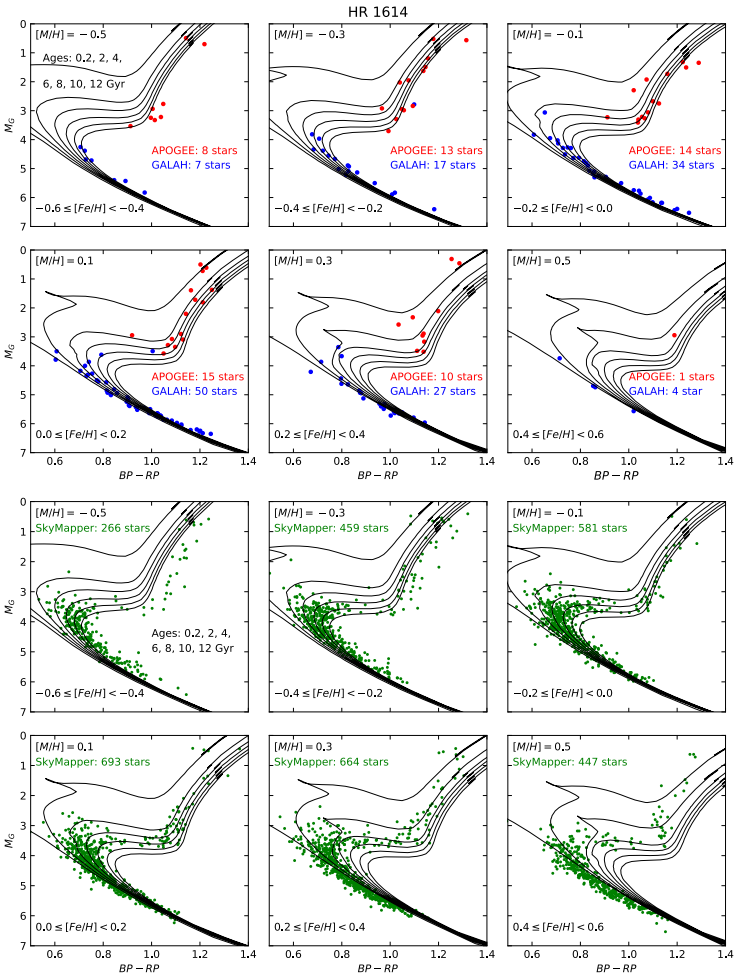


**Fig. 5.** Hertzsprung–Russel diagrams for the stars in the HR 1614 moving group selected from the cross-matched samples between `StarHorse` and APOGEE (red), and StarHorse and GALAH (blue), and `StarHorse` and SkyMapper for different metallicity bins. Black lines show isochrones for a mean metallicity of each bin and cover ages 0.2 Gyr and from 2 to 12 Gyr with the steps of 2 Gyr.

mix of stars from the Galactic disc. The presence of an age bimodality in the HR 1614 overdensity also contradicts the idea of its dissolving cluster origin.

## 4. Origin of the HR 1614 overdensity

### 4.1. Dissolving open cluster origin

Stars that originate from a dissolving open cluster were formed from the same molecular cloud, and thus, retain similar chemical compositions and ages (Freeman & Bland-Hawthorn 2002). As was proposed in Eggen (1971, 1992, 1998), for a long time HR 1614 was considered a classical moving group. The analysis of HIPPARCOS stars accompanied by photometric and spectroscopic data by Feltzing & Holmberg (2000) and De Silva et al. (2007) showed that HR 1614 was a unique stellar population with a metallicity [Fe/H] ≈ 0.2, and age of about 2 Gyr with a very small scatter in abundances in other elements. However, we do not see any evidence that the HR 1614 overdensity is a mono-age and mono-abundance stellar population in our study. The analysis of HR diagrams, metallicity, and age distributions presented in Sect. 3 clearly shows that HR 1614 is a mix of two stellar populations that resemble properties of the Galactic thin and thick discs. A small scatter in abundances observed in

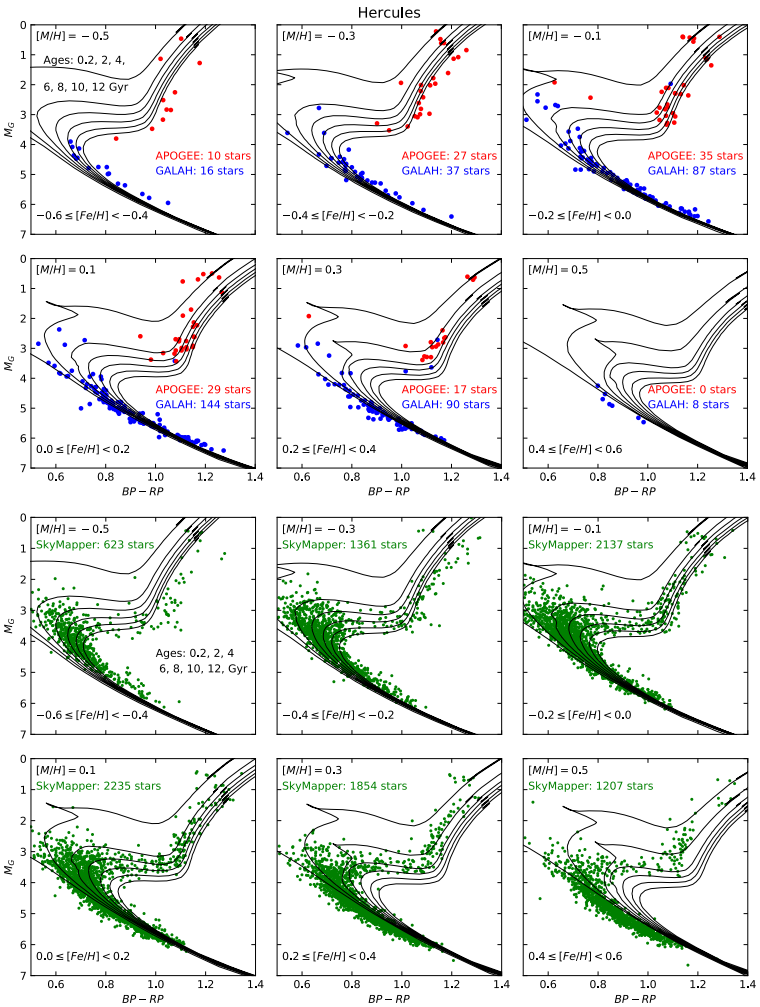


**Fig. 6.** Same as Fig. 5, but for the Hercules stream.

De Silva et al. (2007) is, possibly, a result of the stellar sample analysed in their work. It is mainly composed of stars from Feltzing & Holmberg (2000), who selected metal-rich stars from their Box 5 as possible members of the HR 1614 moving group. This selection effect can potentially explain the small scatter in abundances reported in De Silva et al. (2007).

In this work we selected 12 654 targets in the HR 1614 moving group from our data sample. This is a significantly larger number of stars-members of the group than ever analysed before. Pre-*Gaia* works studied stars that are located roughly within 100 pc around the Sun and found that the HR 1614 overdensity is a single age and abundance population (e.g. Feltzing & Holmberg 2000; De Silva et al. 2007). Since our stellar sample covers a larger volume around the Sun, we check if young stars with higher than solar metallicities are located closer to the Sun in Fig. 11. We do not observe any peculiarities in distributions shown for SkyMapper stars in Fig. 11. Both distributions look similar to younger stars in the metal-rich part of the diagram and older stars in the metal-poor part. It also shows that most of the stars are located within a 500 pc radius around the Sun. There is no unique, young, and nearby stellar population with higher-than-solar metallicity neither in the HR 1614 nor in the Hercules velocity overdensities. This means that HR 1614 should not be considered a dissolving open cluster any longer.

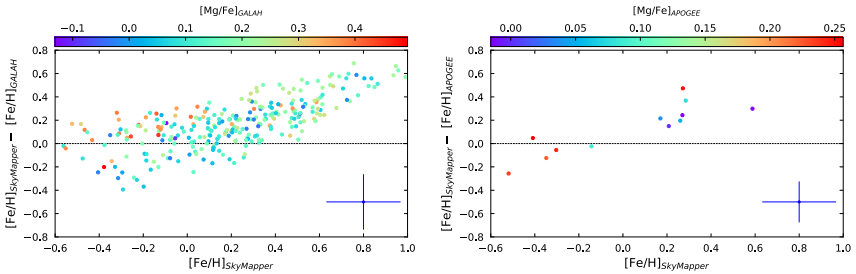


**Fig. 7.** Difference between GALAH and SkyMapper metallicities as a function of SkyMapper metallicity (*left*). Difference between APOGEE and SkyMapper metallicities as a function of SkyMapper metallicity (*right*). Both plots are colour-coded by [Mg/Fe] values taken from the GALAH and APOGEE samples, respectively, and are shown for stars in the HR 1614 moving group and the Hercules stream. Blue crosses show typical (mean) error.

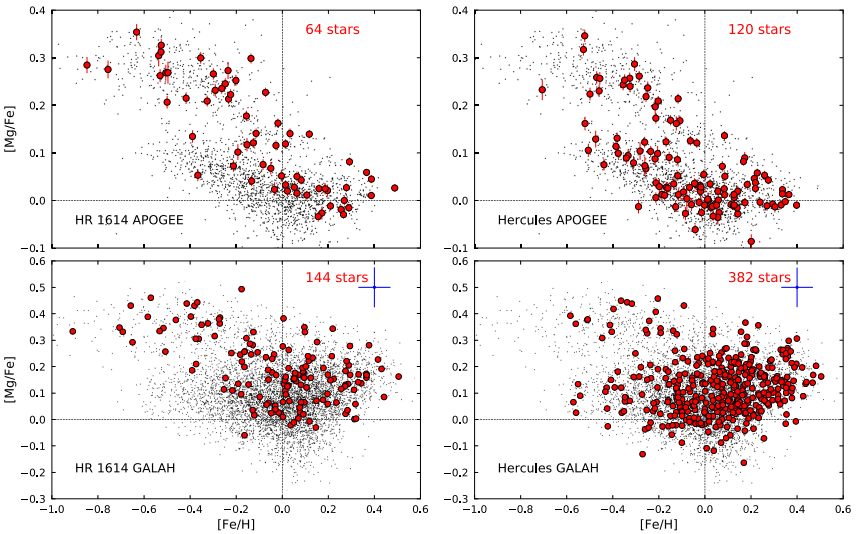


**Fig. 8.** [Mg/Fe]–[Fe/H] diagrams for HR 1614 (*left*) and Hercules (*right*) selected from the APOGEE (*top*) and GALAH (*bottom*) surveys are shown as red dots. The corresponding uncertainties are shown as error bars for APOGEE distributions and a typical (mean) error is shown for GALAH stars. Background black distributions show stars from APOGEE and GALAH in region 00.

### 4.2. Accretion origin

Stars that originate from a dwarf galaxy or satellite and were accreted to the Milky Way retain unique chemical composition, ages, and velocities that are usually different from the background Milky Way stars (e.g. Tolstoy et al. 2009; Ruchti et al. 2015; Helmi 2020). Recent examples of such populations are *Gaia*-Sequoia (e.g. Myeong et al. 2019), *Gaia*-Sausage/*Gaia*-Enceladus (e.g. Belokurov et al. 2018; Helmi et al. 2018). Based on the metallicity, velocity, and age distributions discussed in Sect. 3, it is clear that the HR 1614 and Hercules overdensities are not accreted stellar populations. The dynamical and chemical properties of the groups are similar to the vast majority of the Milky Way disc stars. It is unlikely that HR 1614 is an accreted stellar population.

### 4.3. Resonant origin

Stars that were influenced by resonances with the bar and/or spiral arms can be observed as kinematic structures that consist of mixed stellar populations. Hercules is a group that is widely discussed in the context of resonances. As was first proposed in Dehnen (2000), the Hercules stream is possibly caused by the outer Lindblad resonance (OLR) of the Galactic bar. Later it was proposed that the Hercules stream is likely a result of a corotation resonance (CR) with the bar (e.g. Pérez-Villegas et al. 2017; Binney 2020). Recent results from Hunt et al. (2019) show that it is possible to reproduce the Hercules stream in simulations by combining bar and multiple spiral structures. In their Fig. 2 Hunt et al. (2019) call the bottom-most structure a part of the Hercules stream. If we convert $V$ velocity of the HR 1614 group

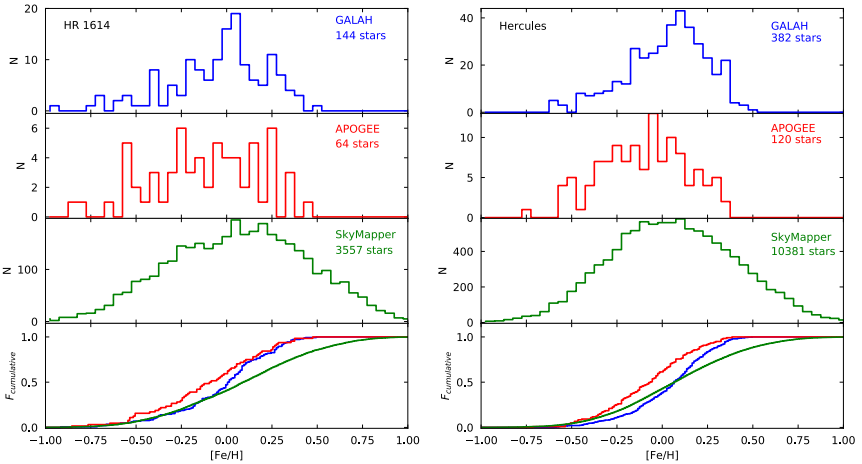


**Fig. 9.** Metallicity distributions for HR 1614 (*left*) and Hercules (*right*) from the GALAH (blue), APOGEE (red), and SkyMapper (green) surveys. Both regular histograms (*upper three panels*) and normalised cumulative histograms (*bottom panel*) are shown.

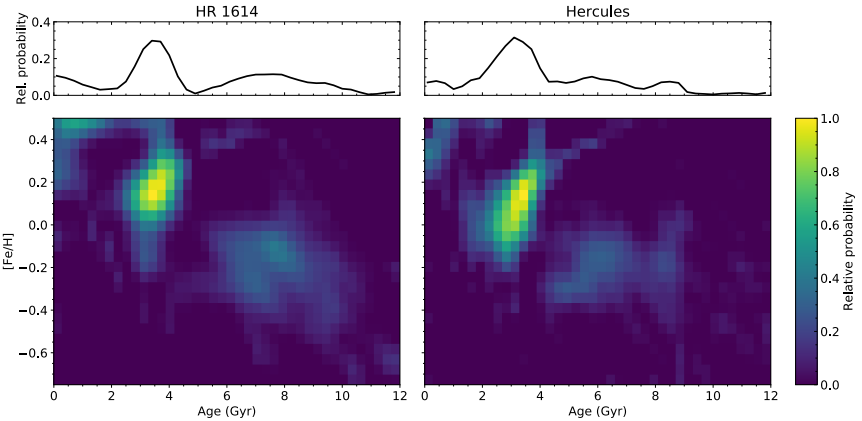


**Fig. 10.** Age–metallicity probability distributions for the HR 1614 moving group (*left*) and Hercules stream (*right*) for stars from the SkyMapper survey. The *upper panels* show the normalised age distributions after summing over the metallicity dimension.

to the vertical component of the angular momentum $L_z$, assuming that the Sun is located at 8.34 kpc from the Galactic centre, we get $\sim$1340 kpc km s$^{-1}$. This is similar to the value found in Hunt et al. (2019). Hunt et al. (2019) and we use the same values that we do for the peculiar motion of the Sun. It is exactly the same position in the distribution where the HR 1614 overdensity is supposed to be located, and thus, should be called the HR 1614 moving group instead.

Many studies show that the Hercules stream conserves a vertical component of angular momentum with Galactocentric radii which is a signature of a resonant origin (e.g. Ramos et al. 2018; Hunt et al. 2019; Kushniruk & Bensby 2019). In Figs. 1 and 3 we clearly see that the Hercules stream is not tilted in the $U - V$ space. It covers a wide range of negative $U$ velocities, but its $V$ velocity is $-50$ km s$^{-1}$ and is almost constant. This means that the vertical component of angular momentum $L_z$ is conserved (taking into account that $V$ is proportional to $L_z$). Unlike the Hercules stream, the HR 1614 overdensity is tilted in the $U - V$ space. This tilt was explained in Feltzing & Holmberg (2000) in dynamical simulations of a dissolving open cluster. At the same time Feltzing & Holmberg (2000) found that the HR 1614 overdensity is homogeneous in age and metallicity, which we do not observe in our work. The HR 1614 overdensity is also present in other four regions shown in Fig. 3. It almost retain $L_z$ with $R$. Taking into account that the HR 1614 overdensity is mainly located at negative $U$ and its proximity to the Hercules stream,

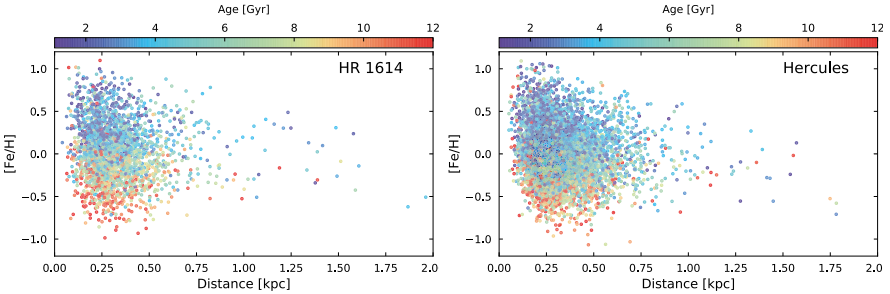


**Fig. 11.** Distance relative to the Sun vs. metallicity diagram colour-cored by age for SkyMapper stars in the HR 1614 moving group (*left*) and the Hercules stream (*right*).

the resonant origin of the HR 1614 overdensity should not be excluded.

### 4.4. Phase mixing origin

The concept of phase mixing implies that a phase-space (position and momentum variables) full of overdensities will evolve with time to a stationary state (Tremaine 1999). A moving groups is one example of a phase mixing process. In the recent literature, phase mixing is mainly discussed in the context of internal or external perturbation mechanisms that can induce the process on large scales (e.g. Laporte et al. 2019; Hunt et al. 2019). This discussion is especially pertinent after the discovery of a phase spiral by Antoja et al. (2018), which is strong evidence of an ongoing phase mixing in the Galactic disc.

Symmetric arches of constant energy around $U = 0\,\mathrm{km\,s^{-1}}$ with $20\,\mathrm{km\,s^{-1}}$ separation in $V$ were predicted in the model that was first proposed by Minchev et al. (2009), where a perturbation with a dwarf galaxy, that took place roughly 2 Gyr ago, leads to a phase wrapping. This external perturbation event could have contributed to a velocity distribution and can be observed as overdensities aligned across lines of constant energy. Minchev et al. (2009) discuss the HR 1614 overdensity in the context of a dissolving cluster and try to fit it into their ringing theory. They state that the HR 1614 moving group is elongated in $U$ and curved in $V$ in their Figure 3, which makes is consistent with a wrapping origin. The fact that the moving group is not symmetric and is elongated towards negative $U$ is explained by Minchev et al. (2009) as being due to the proximity to the Hercules stream, which is most likely caused by the Galactic bar. In summary, Minchev et al. (2009) suggest that the HR 1614 overdensity is a dissolving open cluster that formed earlier than an external perturbation event took place and was distorted by phase wrapping, forming almost an arch of constant energy, and by resonances with the bar, causing elongation towards negative $U$.

Since the arches predicted by Minchev et al. (2009) are symmetrical and the observed velocity distribution has non-asymmetries, Quillen et al. (2018b) proposed another explanation, where asymmetric arches are formed due to stars crossing spiral arms. At the same time their theory cannot explain vertical velocity distribution, and thus external perturbation is not excluded. Hunt et al. (2019) explored various combinations of spirals and bar resonances, and stars crossing dissolving transient spirals and found that there are many models that can successfully explain the main velocity overdensities. Some simulations reproduce a velocity overdensity at the place where the HR 1614 moving group is supposed to be. Khanna et al. (2019) showed that phase mixing of disrupting spiral arms and phase mixing due to external perturbation can generate arches and ridges, but they do not talk specifically about the HR 1614 moving group in their work.

In our work we clearly see that the HR 1614 overdensity is not a dissolving open cluster due to chemical and age spread in the group of stars. We also observe that the HR 1614 overdensity is located mainly at negative $U$. At the same time the group is tilted in $V$, but does not form a complete arch of constant energy. This points towards a complex origin of the HR 1614 overdensity. The stars could be influenced by transiting spirals and bar that would shift it towards negative $U$. Phase mixing due to disrupting spiral structure or ringing due to external perturbation could have contributed to the tilt in $V$.

## 5. Conclusions

In this paper we revised the origin of the HR 1614 moving group. We analysed a combination of *Gaia* and `StarHorse` catalogues and investigated kinematic and photometric properties of stars in a small volume near to the Sun. To study chemical properties of the group we accompanied kinematic data with elemental abundances from the APOGEE and GALAH surveys and photometric metallicities SkyMapper survey. For SkyMapper stars Bayesian ages were calculated for stellar populations. Combining these surveys allowed us to analyse a significantly larger data set with higher precision in the astrometric, photometric, and spectroscopic measurements compared to previous studies. Using the methods developed in Kushniruk & Bensby (2019) we have improved the selection of potential members. These two advances allowed us to better explore the possibility that HR 1614 is or is not a dissolving open cluster. We also compared the properties of the HR 1614 moving group with the Hercules stream which is the nearest velocity overdensity to the HR 1614 moving group. The Hercules stream is most likely of resonant origin, making it a valuable comparison to determine whether HR 1614 is a single stellar population. The main results of the paper are the following:

– The HR 1614 overdensity is clearly present in the $U - V$ velocity distribution at $U \simeq -20$, $V \simeq -60\,\mathrm{km\,s^{-1}}$. This location is consistent with the results from previous studies (e.g. Eggen 1998; Feltzing & Holmberg 2000; Ramos et al. 2018; Kushniruk & Bensby 2019).

– The HR diagrams, metallicity, and age distributions show that HR 1614 consists of two stellar populations that have properties similar to the thin and thick discs.
– The HR 1614 overdensity is mainly present at negative $U$ velocities, which could point towards a resonant origin similarly to the Hercules stream. At the same time the HR 1614 overdensity is slightly tilted in $V$, which means that the group has a variation in its vertical angular momentum distribution.
– The HR 1614 overdensity does not form a complete arch of constant energy in the $U - V$ space, which would be an indication of a phase mixing origin.

Based on the above, it is clear that the HR 1614 overdensity is neither a dissolving open cluster nor an accreted stellar population. We conclude that the HR 1614 overdensity has a complex origin which is a combination of various dynamical mechanisms. As in the case of the Hercules stream, the HR 1614 overdensity could have formed due to different types of resonances such as the CR or OLR with the Galactic bar. This together with phase mixing due to disrupting spiral arms could explain the shape and location of the group in the $U - V$ space. Phase mixing due to external perturbation with a dwarf galaxy or a satellite that happened 2 Gyr ago, as proposed in Minchev et al. (2009), is also possible. The mixed populations that we observe in the HR 1614 overdensity and the Hercules stream are older than a potential perturbation event. Also in Kushniruk & Bensby (2019) we observed kinematic structures with roughly 20 km s$^{-1}$ separation in $V$, especially at lower $V$, which is consistent with a ringing event proposed in Minchev et al. (2009).

In order to disentangle how many different dynamical mechanisms have actually contributed to the formation of velocity structures like the HR 1614 overdensity, further studies are required. Numerical simulations combined with detailed investigation of elemental abundances from spectroscopic surveys like WEAVE (Dalton et al. 2014), 4MOST (de Jong et al. 2019), and the *Gaia*-ESO survey (Gilmore et al. 2012), and kinematics from upcoming *Gaia* data releases will provide more information about the origin of kinematic structures.

*Acknowledgements.* T.B. was funded by grant No. 2018-04857 from the Swedish Research Council. L.C. acknowledges support from the Australian Research Council Future Fellowship FT160100402. C.L.S., D.F., and S.F. were supported by the project grant The New Milky Way from the Knut and Alice Wallenberg foundation and by the grant 2016-03412 from the Swedish Research Council.

## References

Ahumada, R., Allende Prieto, C., Almeida, A., et al. 2019, ArXiv e-prints [arXiv:1912.02905]
Anders, F., Khalatyan, A., Chiappini, C., et al. 2019, A&A, 628, A94
Antoja, T., Helmi, A., Romero-Gómez, M., et al. 2018, Nature, 561, 360
Arifyanto, M. I., & Fuchs, B. 2006, A&A, 449, 533
Belokurov, V., Erkal, D., Evans, N. W., Koposov, S. E., & Deason, A. J. 2018, MNRAS, 478, 611
Bensby, T., Oey, M. S., Feltzing, S., & Gustafsson, B. 2007, ApJ, 655, L89
Bensby, T., Alves-Brito, A., Oey, M. S., Yong, D., & Meléndez, J. 2011, ApJ, 735, L46
Binney, J. 2020, MNRAS, 495, 895
Binney, J., Gerhard, O., & Spergel, D. 1997, MNRAS, 288, 365
Bland-Hawthorn, J., & Gerhard, O. 2016, Ann. Rev. Astron. Astrophys., 54, 529
Bovy, J. 2015, ApJS, 216, 29
Buder, S., Asplund, M., Duong, L., et al. 2018, MNRAS, 478, 4513
Casagrande, L., Wolf, C., Mackey, A. D., et al. 2019, MNRAS, 482, 2770
Dalton, G., Trager, S., Abrams, D. C., et al. 2014, in SPIE Conf. Ser., 9147, 91470L
de Jong, R. S., Agertz, O., Berbel, A. A., et al. 2019, Messenger, 175, 3
De Silva, G. M., Freeman, K. C., Bland-Hawthorn, J., et al. 2015, MNRAS, 449, 2604
De Silva, G. M., Freeman, K. C., Bland-Hawthorn, J., Asplund, M., & Bessell, M. S. 2007, AJ, 133, 694
Dehnen, W. 1998, AJ, 115, 2384
Dehnen, W. 2000, AJ, 119, 800
Eggen, O. J. 1965, Moving Groups of Stars (University of Chicago Press), 111
Eggen, O. J. 1971, PASP, 83, 762
Eggen, O. J. 1978, ApJ, 222, 203
Eggen, O. J. 1992, AJ, 104, 1493
Eggen, O. J. 1998, AJ, 115, 2397
Feltzing, S., & Holmberg, J. 2000, A&A, 357, 153
Feuillet, D. K., Frankel, N., Lind, K., et al. 2019, MNRAS, 489, 1742
Freeman, K., & Bland-Hawthorn, J. 2002, ARA&A, 40, 487
Gaia Collaboration (Prusti, T., et al.) 2016, A&A, 595, A1
Gaia Collaboration (Katz, D., et al.) 2018a, A&A, 616, A11
Gaia Collaboration (Brown, A. G. A., et al.) 2018b, A&A, 616, A1
Gaia Collaboration (Babusiaux, C., et al.) 2018c, A&A, 616, A10
Gilmore, G., Randich, S., Asplund, M., et al. 2012, Messenger, 147, 25
Helmi, A. 2020, ARA&A, submitted
Helmi, A., Babusiaux, C., Koppelman, H. H., et al. 2018, Nature, 563, 85
Howes, L. M., Lindegren, L., Feltzing, S., Church, R. P., & Bensby, T. 2019, A&A, 622, A27
Hunt, J. A. S., Bub, M. W., Bovy, J., et al. 2019, MNRAS, 490, 1026
Khanna, S., Sharma, S., Tepper-Garcia, T., et al. 2019, MNRAS, 489, 4962
Kushniruk, I., & Bensby, T. 2019, A&A, 631, A47
Kushniruk, I., Schirmer, T., & Bensby, T. 2017, A&A, 608, A73
Laporte, C. F. P., Minchev, I., Johnston, K. V., & Gómez, F. A. 2019, MNRAS, 485, 3134
Maíz Apellániz, J., & Weiler, M. 2018, A&A, 619, A180
Majewski, S. R., Schiavon, R. P., Frinchaboy, P. M., et al. 2017, AJ, 154, 94
Minchev, I., Quillen, A. C., Williams, M., et al. 2009, MNRAS, 396, L56
Monari, G., Famaey, B., Minchev, I., et al. 2018, Res. Notes Am. Astron. Soc., 2, 32
Myeong, G. C., Vasiliev, E., Iorio, G., Evans, N. W., & Belokurov, V. 2019, MNRAS, 488, 1235
Pérez-Villegas, A., Portail, M., Wegg, C., & Gerhard, O. 2017, ApJ, 840, L2
Perryman, M. A. C., Lindegren, L., Kovalevsky, J., et al. 1997, A&A, 500, 501
Quillen, A. C., Carrillo, I., Anders, F., et al. 2018a, MNRAS, 480, 3132
Quillen, A. C., De Silva, G., Sharma, S., et al. 2018b, MNRAS, 478, 228
Ramos, P., Antoja, T., & Figueras, F. 2018, A&A, 619, A72
Reid, M. J., Menten, K. M., Brunthaler, A., et al. 2014, ApJ, 783, 130
Ruchti, G. R., Read, J. I., Feltzing, S., et al. 2015, MNRAS, 450, 2874
Schönrich, R., Binney, J., & Dehnen, W. 2010, MNRAS, 403, 1829
Starck, J.-L., & Murtagh, F. 2002, Astronomical Image and Data Analysis, (Berlin; New York: Springer), oCLC: 679368657
Tolstoy, E., Hill, V., & Tosi, M. 2009, ARA&A, 47, 371
Tremaine, S. 1999, MNRAS, 307, 877
Wegg, C., Gerhard, O., & Portail, M. 2015, MNRAS, 450, 4050